Technical Report 5

DISCRETE ECHOES IN IONOSPHERICALLY PROPAGATED GROUND BACKSCATTER

By: TAYLOR W. WASHBURN

Prepared for:

OFFICE OF NAVAL RESEARCH
FIELD PROJECTS PROGRAMS, CODE 418
ARLINGTON, VIRGINIA 22217

CONTRACT N00014-70-C-0413

Sponsored by

ADVANCED RESEARCH PROJECTS AGENCY
ARPA ORDER 1656

STANFORD RESEARCH INSTITUTE
Menlo Park, California 94025 · U.S.A.

Security Classification

DOCUMENT CONTROL DATA - R & D

Security classification of title, body of abstract and indexing annotation must be entered when the overall report is classified)

1. ORIGINATING ACTIVITY (Corporate author) Stanford Research Institute Menlo Park, California 94025	2a. REPORT SECURITY CLASSIFICATION Unclassified 2b. GROUP N/A

3. REPORT TITLE

DISCRETE ECHOES IN IONOSPHERICALLY PROPAGATED GROUND BACKSCATTER

4. DESCRIPTIVE NOTES (Type of report and inclusive dates)

Technical Report Covering the period May 1968 to December 1970

5. AUTHOR(S) (First name, middle initial, last name)

Taylor W. Washburn

6. REPORT DATE	7a. TOTAL NO. OF PAGES	7b. NO. OF REFS
August 1971	140	39

8a. CONTRACT OR GRANT NO.	9a. ORIGINATOR'S REPORT NUMBER(S)
N00014-70-C-0413 b. PROJECT NO. ARPA Order No. 1656 c. d.	Technical Report 5 SRI Project 8727 9b. OTHER REPORT NO(S) (Any other numbers that may be assigned this report)

10. DISTRIBUTION STATEMENT

Approved for public release; distribution unlimited.

11. SUPPLEMENTARY NOTES	12. SPONSORING MILITARY ACTIVITY
	Office of Naval Research Field Projects Programs, Code 418 Arlington, Virginia 22217

13. ABSTRACT

Ionospherically propagated ground-backscatter signals in the 10-to-30-MHz frequency band have been used for decades as a means for studying the earth's ionosphere. Long pulse lengths and wide antenna beamwidths have resulted in backscatter echoes that were spatially averaged enough to give ambiguous information about the ionosphere. The purpose of this research is to explore experimentally how a backscatter sounder having high resolution in time delay (3 μs) and in azimuth (1/2 deg) could be used to better measure ionospheric effects in backscatter signals.

A pulse-compression waveform commonly referred to as sweep-frequency, continuous-wave (SFCW) modulation was used to achieve very short effective pulse lengths while allowing the transmitter to use a unity duty cycle. This waveform is very resistant to the effects of interference. A receiving-antenna azimuthal beamwidth of 1/2 deg was obtained through the use of an existing 2.5-km filled-aperture array of vertical monopoles.

It is found that with a backscatter sounder having these characteristics, the spatial variations in ground-scatter coefficient are remarkably prominent in backscatter data. While it is possible to observe large areas (typically a few hundred km on a side) where the average reflectivity varies considerably from adjacent areas of comparable size, this research explores the use of bright, point-like echoes that are now clearly visible with the equipment described above. These echoes are a manifestation of very

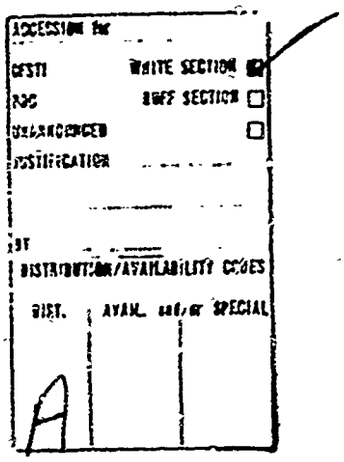

The views and conclusions contained in this document are those of the authors and should not be interpreted as necessarily representing the official policies, either expressed or implied, of the Advanced Research Projects Agency or the U.S. Government.

14. KEY-WORDS	LINK A		LINK B		LINK C	
	ROLE	WT	ROLE	WT	ROLE	WT
HF propagation						
Ground backscatter						
High resolution						
Ionospheric propagation						

ABSTRACT (concluded)

localized increases in the ground-scatter coefficient. Over a 600-by-700-km area principally in Colorado and New Mexico, 70 such echoes were recorded. Ten percent of these were visible more than 80 percent of the time. Some of these echoes have intensities relative to the background greater than 20 dB. No location and identification of their sources was attempted, and it is shown here that for ionospheric-sounding purposes it is not necessary to do so.

These localized scatterers produce multicomponent echoes on backscatter ionograms, which are explained as time-delay-separated, two-way combinations of upper and lower rays and ordinary and extraordinary modes. A raytracing simulation shows that a linearly polarized point scatterer adequately simulates the observed echoes.

It is found that Faraday rotation with signal frequency and with time of day is now discernible on a single echo at a time. Magnetoionic splitting in backscatter focusing lines is observed distinctly and frequently for the first time; the presence of discrete echoes provides firm verification of this interpretation.

Processing for delay resolution as small as 3 μs showed that the discrete echoes had delay widths varying from the minimum observable up to about 50 μs. Delay-resolvable echoes generally showed point-like components in their delay profiles. It was found that the 1/2-deg receiving beam was not adequate to clearly resolve the discrete echoes in azimuth.

It is concluded that the degree of resolution attained is adequate to discern detailed scattering characteristics of the ground. For ionospheric-sounding purposes, it is now possible to crudely characterize these discrete echoing regions as linearly polarized, isotropic, broadband, point scatterers. This fortuitous circumstance allows a far better separation of ground-scatter effects from ionospheric-propagation effects than has been previously possible. The increased complexity of the type of sounder used is offset by the advantage of not having to perform expensive simulations in order to interpret backscatter signals.

STANFORD RESEARCH INSTITUTE
Menlo Park, California 94025 · U.S.A.

Technical Report 5 *August 1971*

DISCRETE ECHOES IN IONOSPHERICALLY PROPAGATED GROUND BACKSCATTER

By: TAYLOR W. WASHBURN

Prepared for:

OFFICE OF NAVAL RESEARCH
FIELD PROJECTS PROGRAMS, CODE 418
ARLINGTON, VIRGINIA 22217

CONTRACT N00014-70-C-0413
ARPA Order No. 1656
Program Code No. OE30

SRI Project 8727

This research was supported by the Advanced Research Projects Agency of the Department of Defense and was monitored by the Office of Naval Research under Contract N00014-70-C-0413.

Approved by:

O. G. VILLARD, Jr., *Director*
Ionospheric Dynamics Laboratory

RAY L. LEADABRAND, *Executive Director*
Electronics and Radio Sciences Division

Copy No. 118

ABSTRACT

Ionospherically propagated ground-backscatter signals in the 10-to-30-MHz frequency band have been used for decades as a means for studying the earth's ionosphere. Long pulse lengths and wide antenna beamwidths have resulted in backscatter echoes that were spatially averaged enough to give ambiguous information about the ionosphere. The purpose of this research is to explore experimentally how a backscatter sounder having high resolution in time delay (3 μs) and in azimuth (1/2 deg) could be used to better measure ionospheric effects in backscatter signals.

A pulse-compression waveform commonly referred to as sweep-frequency, continuous-wave (SFCW) modulation was used to achieve very short effective pulse lengths while allowing the transmitter to use a unity duty cycle. This waveform is very resistant to the effects of interference. A receiving-antenna azimuthal beamwidth of 1/2 deg was obtained through the use of an existing 2.5-km filled-aperture array of vertical monopoles.

It is found that with a backscatter sounder having these characteristics, the spatial variations in ground-scatter coefficient are remarkably prominent in backscatter data. While it is possible to observe large areas (typically a few hundred km on a side) where the average reflectivity varies considerably from adjacent areas of comparable size, this research explores the use of bright, point-like echoes that are now clearly visible with the equipment described above. These echoes are a manifestation of very localized increases in the ground-scatter coefficient. Over a 600-by-700-km area principally in Colorado and New Mexico, 70 such echoes were recorded. Ten percent of these were visible more than 80 percent of the time. Some of these echoes have intensities

relative to the background greater than 20 dB. No location and identification of their sources was attempted, and it is shown here that for ionospheric-sounding purposes it is not necessary to do so.

These localized scatterers produce multicomponent echoes on backscatter ionograms, which are explained as time-delay-separated, two-way combinations of upper and lower rays and ordinary and extraordinary modes. A raytracing simulation shows that a linearly polarized point scatterer adequately simulates the observed echoes.

It is found that Faraday rotation with signal frequency and with time of day is now discernible on a single echo at a time. Magnetoionic splitting in backscatter focusing lines is observed distinctly and frequently for the first time; the presence of discrete echoes provides firm verification of this interpretation.

Processing for delay resolution as small as 3 μs showed that the discrete echoes had delay widths varying from the minimum observable up to about 50 μs. Delay-resolvable echoes generally showed point-like components in their delay profiles. It was found that the 1/2-deg receiving beam was not adequate to clearly resolve the discrete echoes in azimuth.

It is concluded that the degree of resolution attained is adequate to discern detailed scattering characteristics of the ground. For ionospheric-sounding purposes, it is now possible to crudely characterize these discrete echoing regions as linearly polarized, isotropic, broadband, point scatterers. This fortuitous circumstance allows a far better separation of ground-scatter effects from ionospheric-propagation effects than has been previously possible. The increased complexity of the type of sounder used is offset by the advantage of not having to perform expensive simulations in order to interpret backscatter signals.

CONTENTS

ILLUSTRATIONS

TABLE

ACKNOWLEDGMENTS

I would like to thank Prof. O. G. Villard, Jr. for his unfailing encouragement and for providing a constant source of novel ideas. Prof. L. A. Manning and Prof. T. R. Rambo made suggestions that improved the quality of the presentation. Thanks go to the staff of the Ionospheric Dynamics Laboratory who contributed crucially in planning and running experiments, in data reduction, and in report preparation. Without their help this research would not have been possible.

This work was funded by the Advanced Research Projects Agency, through the Office of Naval Research, initially under Contract Nonr-225(64) at Stanford University and now under Contract N00014-70-C-0413 at Stanford Research Institute. I am grateful for the privilege of using the fine research facility made possible by their support.

I INTRODUCTION

A. Purpose

The purpose of this research was to investigate experimentally certain properties of ionospherically propagated, ground-backscattered radio signals over the 9-to-27-MHz frequency band. It has been known for decades that ground-scattered skywave energy could return to its originating location on the earth, and this circumstance has been frequently employed as a means for studying ionospheric effects on radio propagation. Very little knowledge has been available concerning the scattering properties of the earth at these frequencies. Furthermore, the level of equipmental sophistication has been such that the influence of the ground in backscatter sounding has been only occasionally discernible. The present work takes advantage of recent improvements in equipment to separate out characteristics of the ground-scatter process and to explore their use for sounding purposes.

Most of the difficulties in drawing meaningful inferences about the ionosphere with the backscatter sounding technique lie in the inability to separate ground-scatter effects from ionospheric propagation effects. Conventional backscatter sounders record only a spatially averaged indication of the return from the earth-ionosphere combination, further hindering such a separation. In addition, ionospheric phenomena of interest vary with azimuth, elevation, and slant range (only two of these three variables are independent). In the extreme, this state of affairs means that very little more can be learned about the ionosphere from backscatter sounding than can be determined from an ionospheric predictions journal.

A logical way to reduce this uncertainty is to increase the spatial-discrimination characteristics of a backscatter sounder to the point where the detailed scattering behavior of the ground is observable. While such a high-resolution device might complicate interpretation of measurements, it might nevertheless be useful for making more precise inferences about the ionosphere.

In the work described here, very short effective pulses and very narrow azimuthal beamwidths are employed to achieve a high degree of spatial resolution in backscatter sounding. The ultimate goal is to be able to study the ionosphere more effectively through the use of back-scatter sounding; but the immediate goal, pursued here, is to explore in what manner the improved spatial discrimination may be used to separate ground backscatter effects from ionosphere effects.

As a result of the improved discrimination now available, it is shown in what way spatial variations in the ground-backscatter coefficient can be of first importance in backscatter sounding. This work especially explores measurements of backscatter echoes produced by numerous localized increases in ground reflectivity. Such measurements are seen to allow a far better separation of the earth/ionosphere combination than has been previously possible. It is important to note at the outset that most of the results obtained here are normally not of use over the sea, where the scattering surface is relatively uniform from place to place.

B. Background

Verification that the rough surface of the earth could actually scatter ionospherically propagated radio waves back to their points of origin was first provided by Peterson[1] and Dieminger.[2] Indeed, many experiments have been undertaken for ionospheric study using this two-way mode of propagation through the ionosphere.

Until recently, data interpretation and subsequent inferences were based on assuming that the ground-backscatter coefficient was constant from place to place but varied with elevation angle, ψ. This assumption was used in the only two procedures now in existence for simulating backscatter returns via digital computation. Croft[2,4] constructed a two-dimensional (slant-range-vs.-elevation-angle) approximation for the radar equation involving ditital raytracing techniques; while Georges and Stephenson[5] generalized this procedure to include the third dimension (azimuth). When these procedures were developed, it was concluded that available data could be adequately simulated by (1) neglecting magnetic field effects, (2) neglecting variations in the earth's backscatter cross section from place to place, and (3) assuming two-way propagation over the same ionospheric path (mode). It will be shown here that the availability of techniques giving high resolution in delay and azimuth, plus the decided advantages of a modulation scheme known as SFCW (sweep-frequency, continuous-wave), allows the observation of backscatter features that invalidate one or several of the above approximations.

The foremost advantage that can be claimed for backscatter sounding of the ionosphere is that with this technique one may investigate phenomena at all azimuths and over a large increment of ranges from a single location. Unfortunately there is the formidable problem of sorting out wanted signals from unwanted signals, principally because it is difficult to determine exactly where the scattering occurs. With complete knowledge of the ionosphere, this problem would be essentially circumvented, but then there would be no reason to study the ionosphere. One other difficulty that must be surmounted is that the signal energy scattered from the earth's surface is not very large, especially relative to background interference and noise.

In spite of these difficulties, the backscatter technique, even with its ambiguities and weak signal environment, is useful for exploring the spatial and temporal variation of such phenomena as sporadic-E patches (variable clouds of ionization at 100 km altitude that strongly affect radio propagation). The backscatter technique is also used for detection of and measurements on traveling ionospheric disturbances (TID's).[4-7] However, Georges and Stephenson[5] point out very well that backscatter indications of disturbance phenomena cannot be simply interpreted. Backscatter sounders may also be employed for mapping ionospheric plasma frequencies over a sizable region of the ionosphere.[7]

Other than using backscatter to study ionospheric phenomena for their own sake, a useful practical application exists as well. If the detailed properties of radio-wave propagation can be determined over a particular path via backscatter soundings, a convenient means of accurate prediction of communication quality over that path will be available.

The several general topics listed here have usually been investigated with little knowledge of the ground-scatter process. For example, the location of the "leading edge" or minimum-time-delay focusing line in the time-delay-vs.-signal-frequency domain is determined by ionospheric propagation factors alone.[1] The behavior of the leading edge has been studied extensively; however, uncertainty as to where the backscatter echo comes from (in the ionosphere or on the ground) limits the usefulness of the leading edge for ionospheric study.

Several workers have attempted to measure or deduce the variation of terrain scatter with elevation angle.[2,8-12] Many include some treatment of the effects of polarization on ground-backscatter coefficients. A few have studied the ways in which the cross section σ can vary from place to place. σ is defined as the reflected power per unit solid angle in the direction of the source, per unit power density incident upon the scatterer.

Virtually all measurements have been made with line-of-sight geometry between transmitter/receiver and scattering region. Scatter sources studied include different types of terrain,[12] trees,[9,11] buildings,[9,10] powerlines,[11] and of course mountains.[2,11,12] For several reasons (discussed in Section II) it has proven difficult to observe any place-to-place variations in scatter from the earth as seen by a backscatter sounder. A long-time controversy has raged as to whether sea or land scatters more efficiently at HF frequencies (the most recent discussion is by Barnum).[10]

C. Approach Used in the Present Study

A straightforward approach using existing equipmental facilities has been developed by Stanford Electronics Laboratories at Los Banos, California and elsewhere for determining the effects of variable scattering from the ground on ionospherically propagated backscatter signals. Particular use has been made of a capability to generate very short effective "pulses." The time-delay resolution thus obtained has bordered on the maximum supportable value for the dispersive, birefringent ionosphere having numerous sources of inhomogeneity. It was also possible to take advantage of a very large (2.5-km) linear array developed by Sweeney,[13] which was the narrowest filled-aperture, easily-steerable antenna beam available for use in the high-frequency band.

The combination of these features in the sounding system localizes the echoing regions on the ground and in the ionosphere. Thus it is now to be determined how this improved spatial resolution can be used to separate out the ground influence on backscatter sounding.

One important answer sought in this study is whether it is possible to glean useful information without specific location and identification of the scattering sources. The equipmental facilities for proceeding

along the latter path are available; but it is judged worthwhile to determine what information is attainable without locating and identifying the scattering sources.

A portable repeater was placed in the field for calibration and reference purposes. One of the inherent difficulties in ionospheric research lies in a common inability to control experiments. Therefore a means was developed whereby the repeater could serve as a control variable. Comparison of echoes from the repeater (with known characteristics) to echoes from localized regions on the earth helps verify the inferences drawn from the naturally occurring echoes. A simulation via three-dimensional raytracing further aids and supports the data interpretation.

Two types of backscatter data are analyzed here: the first is the informative and commonly used wide-sweep backscatter ionogram (a display of time delay vs. signal frequency), while the second is a display of time delay vs. azimuth. A series of experiments is performed using these data formats to build up a rudimentary model of ground-scatter effects in backscatter sounding of the ionosphere. Rather than a very narrow study in great depth, the research leading toward this stated aim is fairly broadly based. Several diverse observations are analyzed in construction of the ground-scatter model; it is shown that this approach does allow clearer inferences about the ionosphere than have previously been possible.

II BACKSCATTER SOUNDING WITH SHORT EFFECTIVE PULSES AND NARROW ANTENNA BEAMS

A. Equipment Used for This Research

In this section the essential features of the experimental facilities are described, leaving the details to Appendix A. A backscatter sounder operated by Stanford University is located in the San Joaquin Valley of California. With this sounder, the properties of narrow-beam, short-pulse HF backscatter from land could conveniently be investigated. The sounder operated bistatically, with the transmitter placed near Lost Hills, California and the receiver located 185 km to the northwest, in Los Banos, California (see Figure 1). Forward-oblique soundings for reference purposes were made over an east-west 2600-km path from Bearden, Arkansas to the receiving facility. A portable repeater operating from a station wagon was available to satisfy various calibration requirements.

At each of the transmitting sites there was a frequency standard for time synchronization with the other sites; a compressed-pulse waveform generator; a linear power amplifier operating over the HF band (10 watts at Bearden and 30 kilowatts at Lost Hills); and an antenna. The Lost Hills antenna was unusual in that it was a vertically polarized, steerable array, boresited at 90 degrees (true) and producing a beam covering 6 degrees in azimuth. (See Appendix A for details and a representative antenna pattern.)

The equipment at the Los Banos site consisted of a timing standard, a compressed-pulse generator, a receiver, data-processing and recording equipment, and an antenna. The receiving antenna was a 2.52-km linear array of 256 vertical monopoles producing a nominal 1/2-degree azimuthal

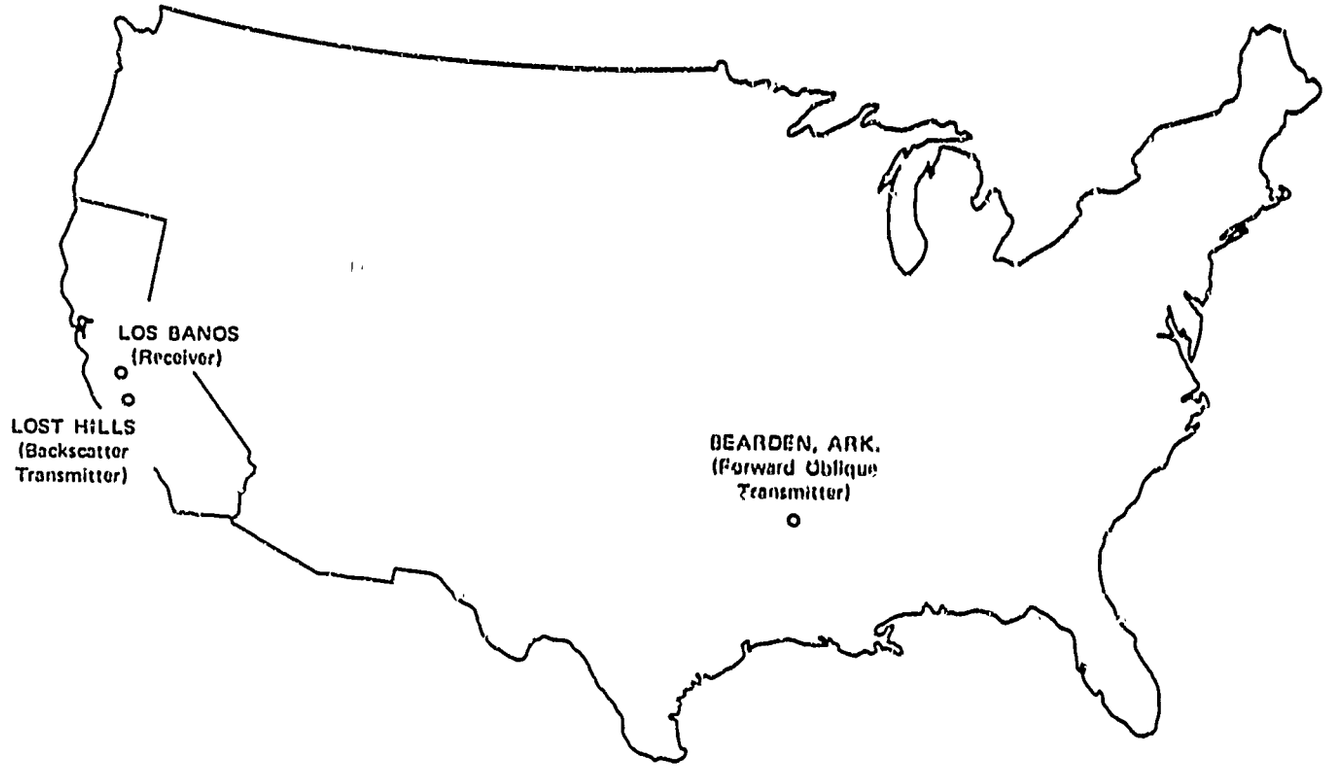

FIGURE 1 STATION GEOMETRY FOR HIGH-RESOLUTION BACKSCATTER SOUNDER

680274

beam. A ground screen stabilized ground impedance over the absolutely flat but chemically variable earth. This array was steerable by the use of delay cables in 1/4-degree increments ±16 degrees about its boresite direction of 90 degrees (true). Sweeney[13] presents in detail the design features and performance characteristics of this array, some of which are reproduced in Appendix A.

The waveform used here deserves special mention because it offers significant advantages for backscatter sounding of the ionosphere. The linear sweep-frequency, continuous-wave (SFCW) waveform familiar to radar specialists[14,15] has been shown to be useful for ionospheric sounding[17] and was recently used in a forward-oblique sounding experiment using the Los Banos array.[13] A transmitted frequency "ramp" (sweep) is received and mixed or deramped with a local frequency "ramp" which has appropriate, known offsets in its start time and start frequency. The received signal is then spectrum-analyzed to produce a display of signal amplitude vs. time delay. The processing technique is essentially that of a matched filter, and a short effective pulse is thereby generated by the pulse-compression processing. Pulse-compression ratios in excess of 10^5 are achievable with the SFCW generators used in this research.

Figure 2 is a block diagram of the sounder system. More processing details are presented in Appendix A. Advantages of SFCW modulation include (1) the capability of using a 100-percent transmitter duty cycle, (2) considerable suppression of fixed-frequency interference, (3) good time-delay resolution easily varied in reprocessing recorded data, and (4) amenability to reduction of the sidelobes in time delay, which produce self noise. One potential disadvantage is that a Doppler shift is interpreted as a change in time delay when "delay-only" processing of SFCW signals is used. This effect is neglected in this study since ionospheric Doppler is generally < 1 Hz, below the plausible upper limit

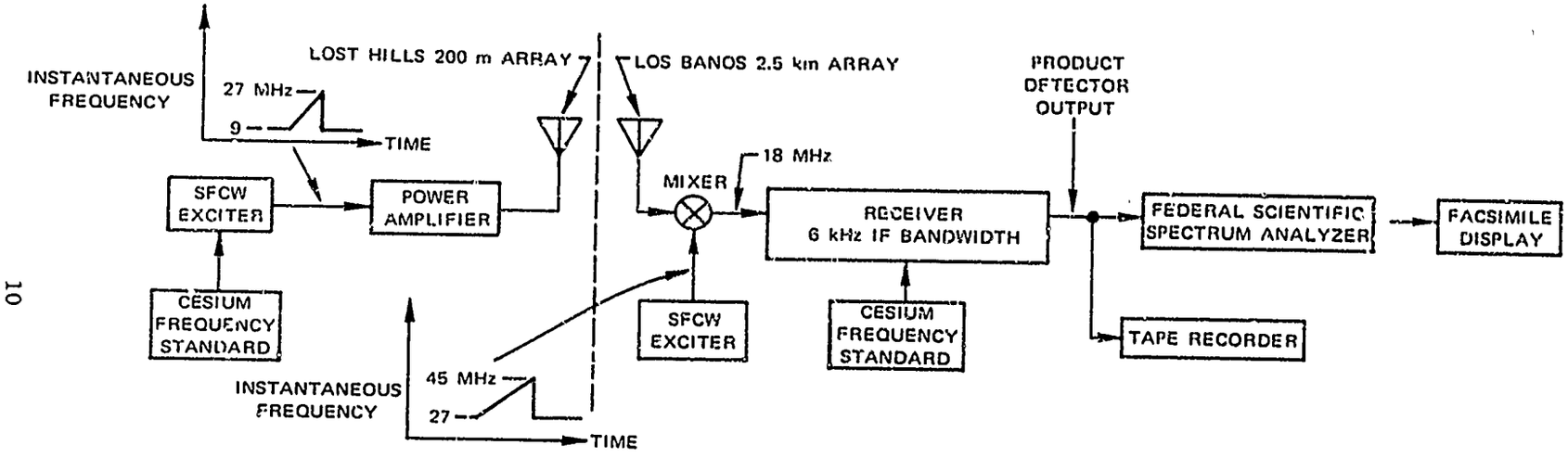

FIGURE 2 BLOCK DIAGRAM OF BACKSCATTER SOUNDER

668278

for a wavelength of 15 m (a 1-Hz Doppler implies a 72-km change in path length in one hour). Only during sizable disturbances and at dawn/sunset periods should this value be exceeded.[17,18] A Doppler spread however will deteriorate the quality of the effective pulse, not just shift the pulse in the time-delay domain.

A second potential disadvantage of using SFCW waveforms is that one must assume the medium to be stationary over the signal duration T (which varies from 0.1 to 1.0 s in this work). Changes on a time scale less than these values of T will not be observed. It is thought, however, that this feature does not influence the results presented here.

Two somewhat different experimental formats were developed for use in this experiment. The first was wide-sweep backscatter wherein the 9-to-27-MHz band was continuously swept, usually at a 250-kHz/s rate, repeating the 18-MHz sweep typically every 2 min. The frequency interval swept can be reduced, thereby reducing the repetition time to seconds. Repetition time is important in that it sets the scale of time changes that may be observed. Spectrum-analyzer output was commonly fed to a facsimile recorder to generate a plot of intensity-modulated difference frequency vs. time of day. Such a plot can be interpreted in the form of time delay vs. signal frequency (a backscatter ionogram). This display permitted visual observation of a 15-dB dynamic range in backscatter amplitude, and was used to observe ionospheric structure vs. frequency for a continuum of path lengths.

The second type of experimental format consisted of transmitting a narrower frequency ramp, typically of 500 kHz total bandwidth, at a 500-kHz/s rate once per second. This format provided highly resolved information on time delay vs. time of day. If the antenna arrays are steered synchronously with this repetitive sweep, a plot of time delay vs. azimuth (B-scan) can be generated. Azimuth information obtained in this manner

is incoherent, since only the energy in one delay cell is compared at adjacent antenna steer positions. Furthermore, the resolution of the equipment in slant range (time delay) is typically ten times as good as the resolution in cross range (azimuth).

Quantitative amplitude information was obtained by displaying backscatter amplitude vs. delay for each value of signal frequency for backscatter ionograms, or for various times of day or antenna azimuths in the case of repetitive, short frequency sweeps.

B. Observing Variation in σ_o in HF Backscatter from Terrain

This section will show under what conditions the variability of the ground-backscatter coefficient will appear in backscatter sounding data.

In sounding the ionosphere via HF ground backscatter, some experimenters[2,12] have been able to observe some variability in σ_o (backscatter cross section per unit area) from place to place on the earth's surface while others have not. (σ_o is a commonly used artifice determined by dividing the scattering cross section σ by the illuminated area A. It is particularly useful for dealing with extended scattering regions.) Several experimenters have observed the land-sea interface on backscatter data,[11,13,20] but until recently it was ambiguous as to whether the sea or the land scattered HF radio waves more efficiently. There is evidence that σ_o over land varies considerably and that upright objects on the ground (trees, buildings, power lines, etc.) may create locally strong echoes.[2,11] In a line-of-sight backscatter experiment[11] an echo from a power line was observed that was the same order of magnitude as that of a nearby mountain.

There are several contributory factors that may obscure observation of variations in σ_o. Some of these are (1) narrowband interference,

(2) lack of system sensitivity (i.e., power on target, receiver sensitivity, noise environment), (3) too large resolution-cell size and range-azimuth sidelobes (self-noise), (4) signal fluctuations that may obscure apparent differences in σ_o, and (5) a tendency for researchers not to be concerned with such variations. An example of this last factor arises when inferences about ionospheric structure are made only from the locus of the leading edge of backscatter returns.[21] However, the first three factors are believed to be the more important, and each of these will now be considered.

1. Interference Suppression in SFCW Sounding

Fixed-frequency interference typical of HF practice seriously degrades the quality of HF ionospheric sounding data. Pulse-compression techniques (specifically SFCW with very large time-bandwidth products) effectively discriminate against this interference, thereby allowing more detailed analysis of the desired signals. SFCW tends to suppress interference in this application by allowing the transmitter to use a unity duty cycle (which results in larger average signal energy at the receiver), by using a narrow receiver bandwidth while achieving high delay resolution, and by virtue of its large time-bandwidth product. Signal-processing techniques such as "clipping" and "self blanking" also perform well with the SFCW waveform.[22]

In Appendix B it is shown that for each interference signal encountered whose strength is much larger than that of the desired SFCW signal, the ratio of signal to interference is improved approximately in proportion to the time-bandwidth (TW) product. For this experiment, TW varies from 2.5×10^3 to 5×10^5. Thus the use of SFCW can provide a nominal 40-dB rejection of a single interference signal (which can be tens of millivolts at the receiver input) encountered over the bandwidth, W.

2. Effect of Narrow Beams and Short Pulses

Little information is available as to the specific nature of terrain scatter in the HF frequency band (3 to 30 MHz). As a first model of variable terrain reflectivity, consider a point echo (taken here to mean any echo not extended in time delay or azimuth) of total cross section σ immersed in an extended continuum of per-unit-area cross section σ_o. No Doppler component will be considered, as scatterers on the ground are assumed to be fixed, and the ionospheric component of Doppler is normally bounded below 1 Hz.[17,18] No polarization effects are considered in this section.

Here, short equivalent pulses and narrow antenna beams (azimuth only) are used to localize the region on the ground from which backscatter is received. To observe the discontinuity in reflectivity, it is desirable to increase the signal-to-clutter ratio where signal in this case is the return from the localized variation from the mean cross section and the rest of the scattered energy is clutter. A common approximation to this situation is to idealize the sounder's behavior by assuming a perfect rectangular pulse of length τ and a uniform beam of angular width θ. This cannot be achieved in practice because of infinite-bandwidth and infinite-aperture requirements, but it does provide a useful guideline. θ is often taken to be the 3-dB beamwidth, but the pattern factor may be evaluated more accurately;[23] and in fact this has been done in an application using the Los Banos antenna array.[20]

For a monostatic sounder (one in which the transmitter and receiver are collocated) the illuminated area on the ground is $(1/2\ c\tau \sec \psi) \cdot (R\theta)$ as indicated schematically in Figure 3. For clutter cross section σ_o, the total clutter signal returned is $\sigma_o c\tau \sec(\psi)\theta/2$, and some reasonable criterion such as desired signal equal to clutter signal is then adopted as a rule for detection of the

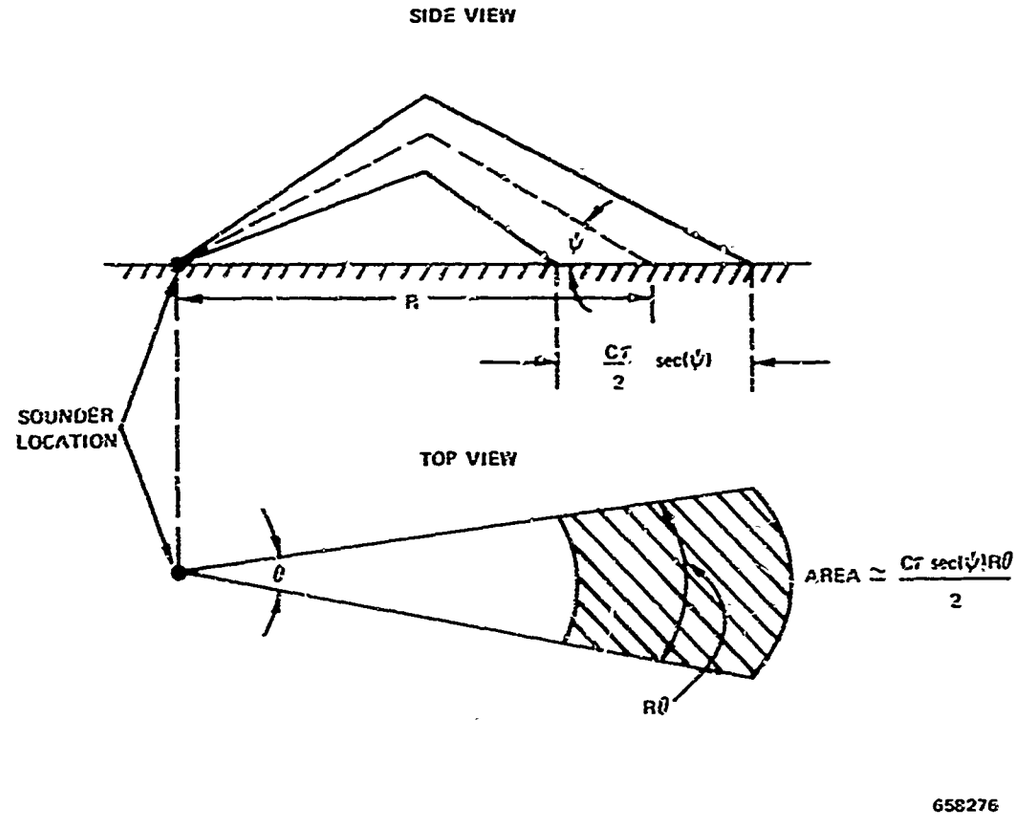

FIGURE 3 GROUND PROJECTION FOR MONOSTATIC SOUNDER WITH IDEAL PULSE AND IDEAL AZIMUTHAL BEAMWIDTH

signal of interest. This somewhat arbitrary criterion means that the cell adjacent to the cell of interest has 3 dB less power in it.

As a specific example, Barnum[10] measured HF backscatter cross sections for cement-block walls, extrapolating results to arrive at an estimate of 3.5×10^5 m^2 for the HF backscatter cross section of a city, at elevation angles in the neighborhood of 10 to 30 degrees. By way of illustration, take the average value of σ_o over land to be 10^{-4}. For observation of a prominence in the backscatter due to a spatially confined echo region at a range of 2000 km and an elevation angle of 15 degrees, a $\sigma \geq \sigma_o \frac{1}{2} c\tau \sec(\psi) R\theta$ demands that $\tau\theta \leq \sigma_o \times 1.85 \times 10^{-13} = 6.5 \times 10^{-4}$ seconds · degrees. Thus a pulse length of 100 μs and a beamwidth of 6.5 degrees should be adequate for providing localized city-echo return equal to the return from average rough land. This estimate is not exact due to the extended nature of cities (and forests).

To illustrate the changing requirements on τ and θ as σ_o changes, Figure 4 has been constructed. Range, elevation angle, and backscatter cross section are held fixed at 2000 km, 15 degrees, and 10^5 m^2, respectively. σ_o is varied from 10^{-1} to 10^{-7} in increments of 10. The required values of τ and θ for $\sigma_{\text{point echo}} = \sigma_{\text{clutter}}$ can then be read from the graph. Different values for $\sigma_{\text{point echo}}$ may be accommodated by proportionately varying the parametric values of σ_o--i.e., if $\sigma_{\text{point echo}} = 5 \times 10^5$ m^2, then the values for σ_o should also be multiplied by 5.

This graph indicates that only modest values of τ and θ are required to reveal variations in HF ground backscatter. A typical example is that a sounder with a 10-degree beam and an 18 μs pulse length should be able to discern point echoes of 10^5 m^2 cross section in the midst of rough surface scatter whose per-unit-area cross section is 10^{-1}. Even 20-degree beams and 100-μs pulse lengths would be likely to produce at least some indication of variable σ_o. Values of τ and θ achievable with the Los Banos sounder are plotted in Figure 4, as are those obtainable by conventional sounders. Although certain types of scattering should appear as point echoes (i.e., from towers, power lines, single buildings, specular reflections from mountain faces, etc.) other likely sources of deviation from the average will be spread in delay and azimuth (cities, mountain ranges, plains regions, lakes, etc.). Some such extended regions of interest should produce cross sections considerably lower than the average.

Interaction of the backscatter sounder's cell size and the "characteristic size" of variations in σ_o will determine to some extent whether such deviations are observable. In the limit of very small cell size the energy returned is so small that system noise will hinder detection of backscattered energy. For very large cell sizes the variations

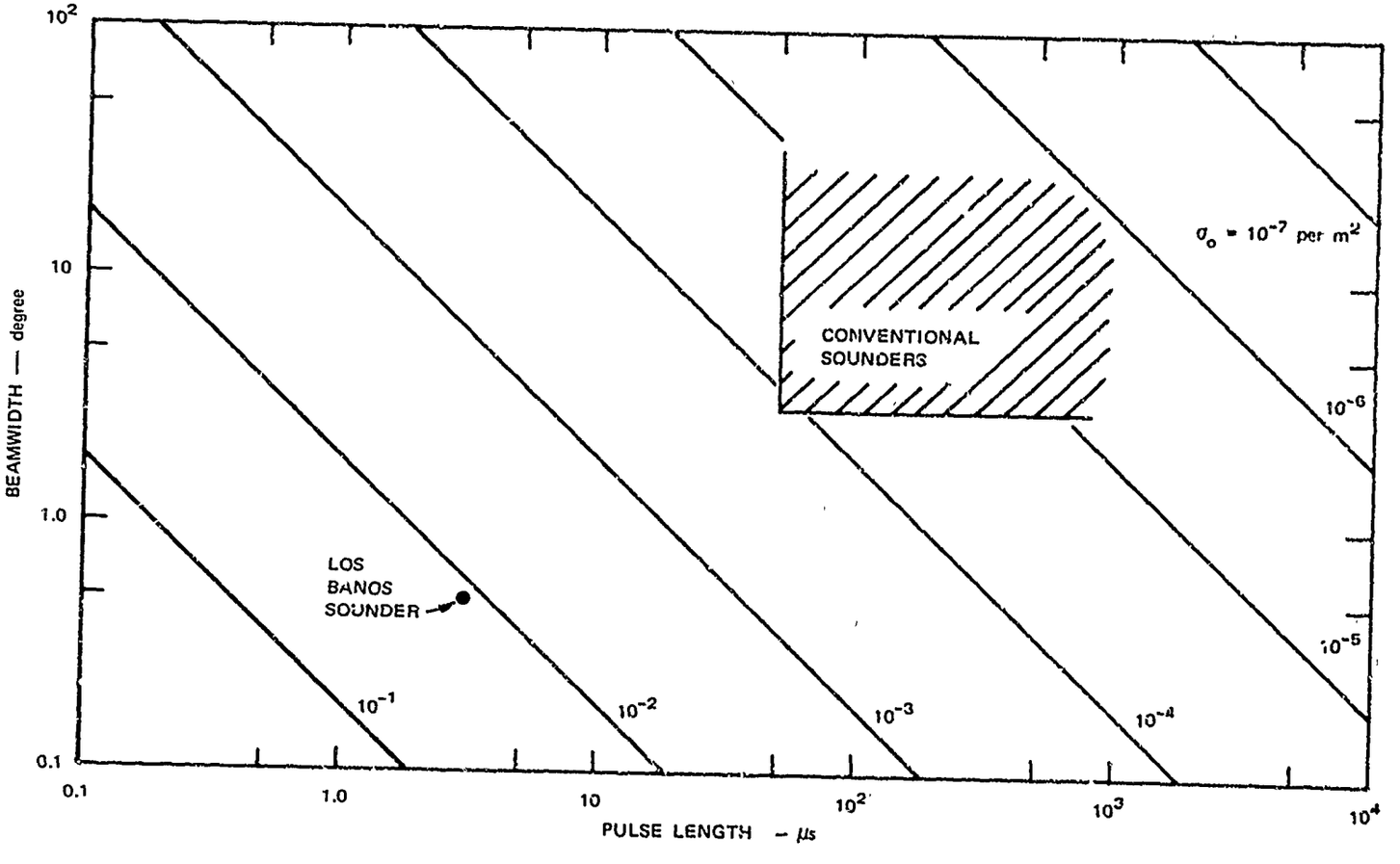

FIGURE 4 REQUIRED PULSE LENGTHS AND BEAMWIDTHS FOR σ (Point Echo) = σ (Extended Clutter). R = 2000 km, ψ = 15 degrees, σ (Point Echo) = 10^5 m^2.

in σ_o will be averaged out except in unique cases (land vs. ocean, perhaps). In between these extremes, where such variation should be readily apparent, the effects of range and azimuth sidelobes may contribute heavily; this effect will be examined in the following paragraphs.

3. Delay and Azimuth Sidelobe Energy

Short pulses and narrow antenna beams were used to localize the energy returned to the backscatter sounder. The earth/ionosphere combination is a significantly extended echoing region in the τ and θ domains. Even though large bandwidths and large apertures were employed to reduce the size of the resolution cell, there were inevitable delay and azimuth sidelobes through which energy could be returned. This self noise or self clutter can have serious consequences for the observation of variable scattering efficiency over the τ and θ backscatter domains.

For a uniformly scattering ground and a simplified ionospheric model, a portion of an average backscatter return is sketched in Figure 5.

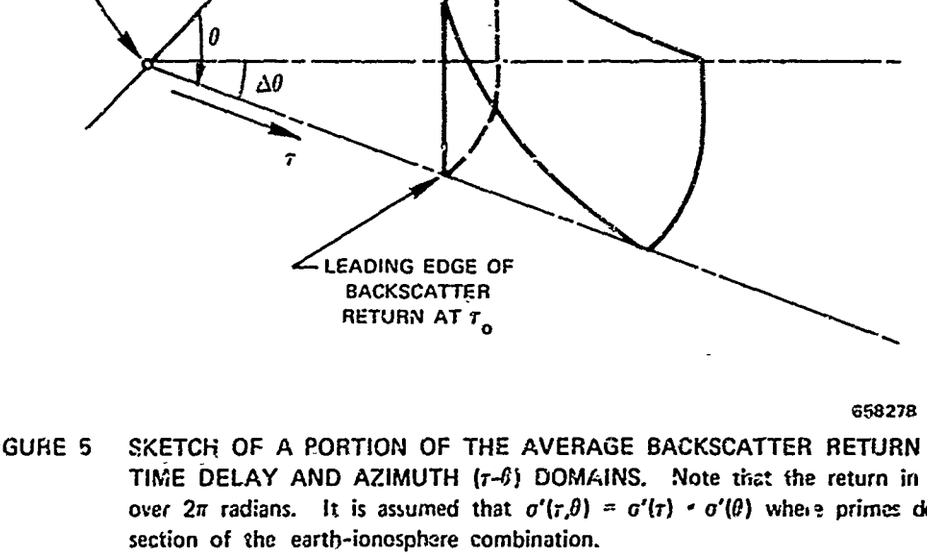

658278

FIGURE 5 SKETCH OF A PORTION OF THE AVERAGE BACKSCATTER RETURN IN THE TIME DELAY AND AZIMUTH (τ-θ) DOMAINS. Note that the return in θ is really over 2π radians. It is assumed that $\sigma'(\tau,\theta) = \sigma'(\tau) \cdot \sigma'(\theta)$ where primes denote the cross section of the earth-ionosphere combination.

Although the return is constant over θ it has a rapid decay with τ, beginning at the minimum time delay of backscattered energy. The decay in energy is principally due to "$1/R^4$" losses (really $1/R^3$, because the cell area increases linearly with range, R), absorption, and the probable decrease in average scattering coefficient with decreasing elevation angle (increasing delay). This energy fall-off is a prominent feature of backscatter ionograms and is roughly approximated by $\sigma'(\tau) \propto 10^{-\tau/4}$ for $\tau \leq 10$ ms, where τ is measured relative to the minimum time delay return. $\sigma'(\tau)$ is the effective cross section, which includes all the propagation factors above. It is the energy per unit delay returned via the earth/ionosphere combination.

Superimposed on this average return are numerous fluctuations. The ones of interest here are variations in the earth's backscatter coefficient.

It is assumed that the τ and θ domains are independent, both in terms of power returned to the sounder and in terms of the subsequent processing of the data. This approximation is not strictly valid, but is permissible for the purposes at hand. Thus, $\sigma'(\tau,\theta) = \sigma'(\tau)\sigma'(\theta)$, where the primes denote the cross section of the earth/ionosphere combination. As far as processing is concerned, τ and θ are independent for a monostatic sounder and for sufficiently narrowband systems where the signal bandwidth is less than 10 to 20 percent of the carrier frequency.

Earlier in this section it was described how a range-vs.-azimuth display was obtained by slowly scanning the antenna array (normally 1/4 degree per second) synchronously with repetitive SFCW sweeps. Azimuth information was obtained by comparing energy in a range gate for successive sweeps (which were made at adjacent antenna steer positions). To the extent that the echoes remained fixed over the period

of time it took to generate an azimuth scan, the azimuth "processing" is independent of the SFCW processing. Thus, the average power out of the sounder as a function of τ and θ may be described by a superposition of returns--namely

$$P_{\tau,\theta}(\tau,\theta) = \int \sigma'(\tau,\theta)\ h(\tau,\theta)\ d\tau\ d\theta$$

where $h(\tau,\theta)$ describes the processing in delay and azimuth performed by the backscatter sounder (antenna effects included). Both $\sigma'(\tau,\theta)$ and $h(\tau,\theta)$ are separable functions by assumption; so

$$P_{\tau,\theta}(\tau,\theta) = P_{\tau}(\tau)\ P_{\theta}(\theta) \quad .$$

Approximate evaluations of $P_{\tau}(\tau)$ and $P_{\theta}(\theta)$ are given in Appendix B. $P_{\tau}(\tau)$ is found to contain a convolution of $\sigma'(\tau)$ and the delay portion of the well known delay-Doppler ambiguity function.[14] This function has been studied extensively for SFCW waveforms.[14,15] $P_{\theta}(\theta)$ is approximately proportional to a convolution of the combined antenna patterns and $\sigma'(\theta)$. Figure 6 is a plot of $P_{\tau}(\tau)$ for a point

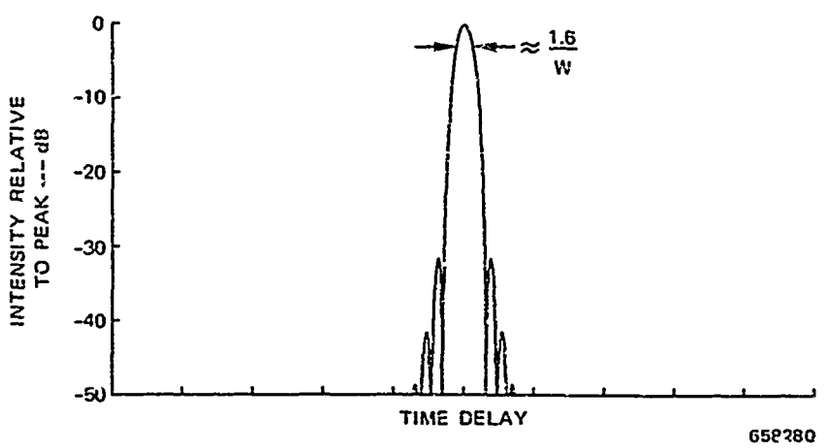

FIGURE 6 EFFECTIVE PULSE FROM SFCW PROCESSING. Signal duration is T s, total bandwidth is W Hz. Hanning window produces ideal largest sidelobe -32 dB from peak. Departure from ideal sweep can substantially increase sidelobe level, but does not broaden the mainlobe width.

echo in delay; its largest sidelobe is -32 dB relative to the peak and has a mainlobe width of 1.6/W (recall that W = bandwidth). Similarly, Figure 7 is the point-echo azimuth response for $-5° \leq \theta \leq 5°$ and $\lambda = 20$ m.

A generalized discussion in Appendix B of the effects of these sidelobes in time delay and in azimuth serves to emphasize the limitations they impose when one is probing the extended earth/ionosphere echoing region. Some general factors for determining the contribution of self noise from <u>all</u> sidelobes are described. Their effects will be pointed out in the data presented in the following section.

In brief summary, this section has determined "close-up" system response in time delay (Figure 6) and in azimuth (Figure 7). For backscatter sounding in particular, self noise can require a substantial correction factor for the idealized pulse and idealized beamwidth model for the illuminated region on the ground. Sidelobes have the effect of smoothing out variations in received energy such as would be produced by spatial variations in land-backscatter coefficient.

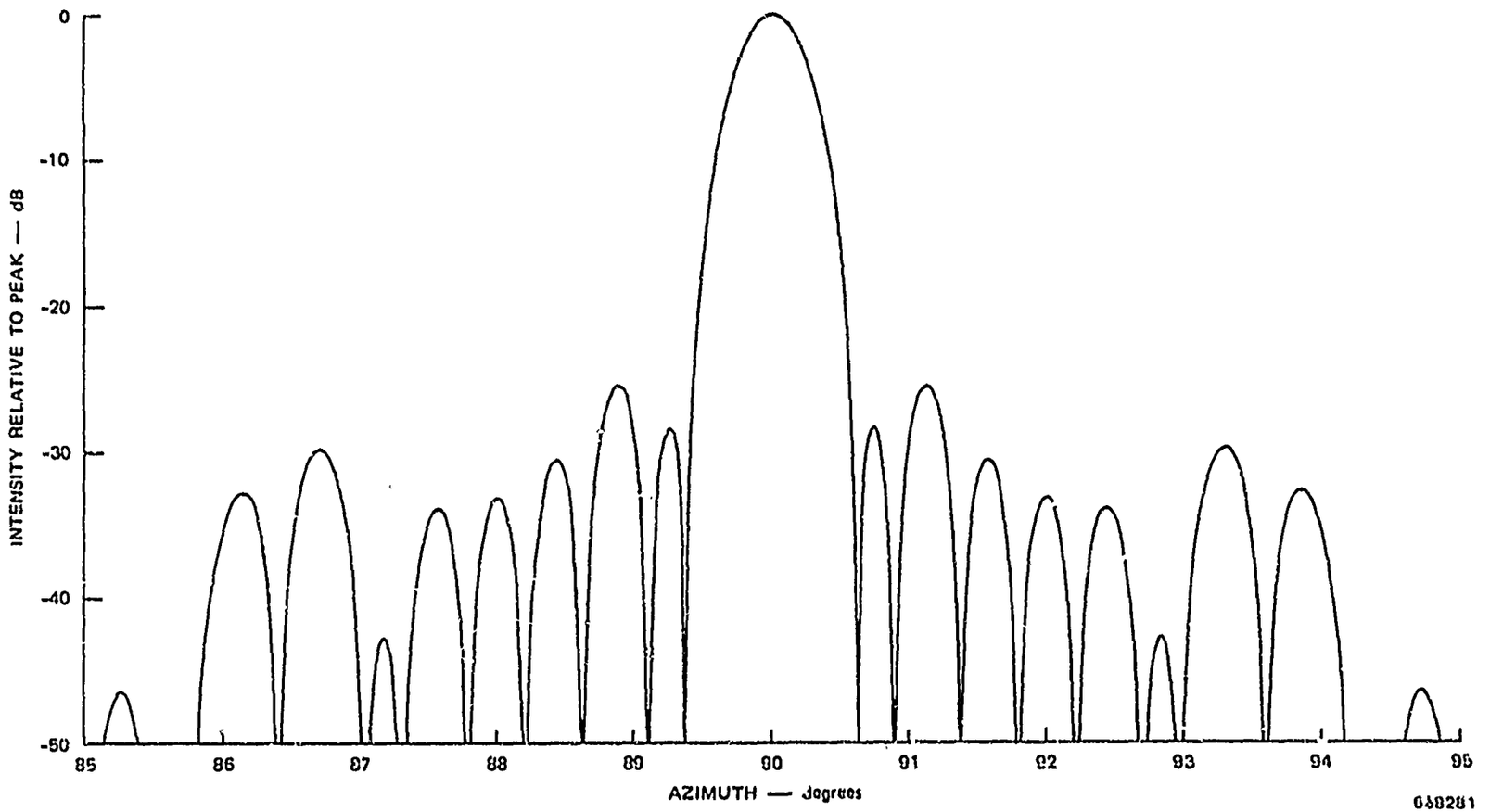

FIGURE 7 IDEALIZED AZIMUTHAL RESPONSE OF BACKSCATTER SOUNDER WITHIN 5 DEGREES OF BROADSIDE

III DISCRETE ECHOES IN SWEPT-FREQUENCY BACKSCATTER

Ultimately, we wish to understand how spatial variations in ground reflectivity will influence the study of the ionosphere via the backscatter-sounding technique. The procedure here will be to synthesize a very simple model for localized echoes in backscatter ionograms, the predictions of which we will then compare with observation.

To place this topic into perspective with previous efforts in backscatter research, consider Figure 8, which is a fairly typical backscatter ionogram made with the high-resolution sounder. Frequency was swept 9 to 27 MHz at 250 kHz per second, and a 4-Hz individual filter bandwidth in the spectrum analyzer yielded a theoretical time-delay resolution of 16 μs. Beginning at 9 MHz and 2.2 ms, the semivertical ionogram from Lost Hills to Los Banos is visible, providing a convenient check upon time-delay calibration. Backscatter appears to "grow out" of the two-hop ionogram as expected.[1] The leading edge of minimum-time-delay backscattered energy proceeds smoothly to higher frequency and longer delay, as is typical of a single-layer ionosphere under quiet conditions. The faintly visible splitting of this leading edge is due to separate time-delay-focusing lines for ordinary and for extraordinary modes; experimental support for this conclusion will be offered later.

One reason for the clarity of these data is the relative immunity to interference, which is attested to by a lack of vertical lines on the data. Only seven discrete interference lines are visible over 9 to 27 MHz. This is in marked contrast to high-quality, pulse-type backscatter soundings[24] which often showed 10 to 20 times as many interference lines over the same band.

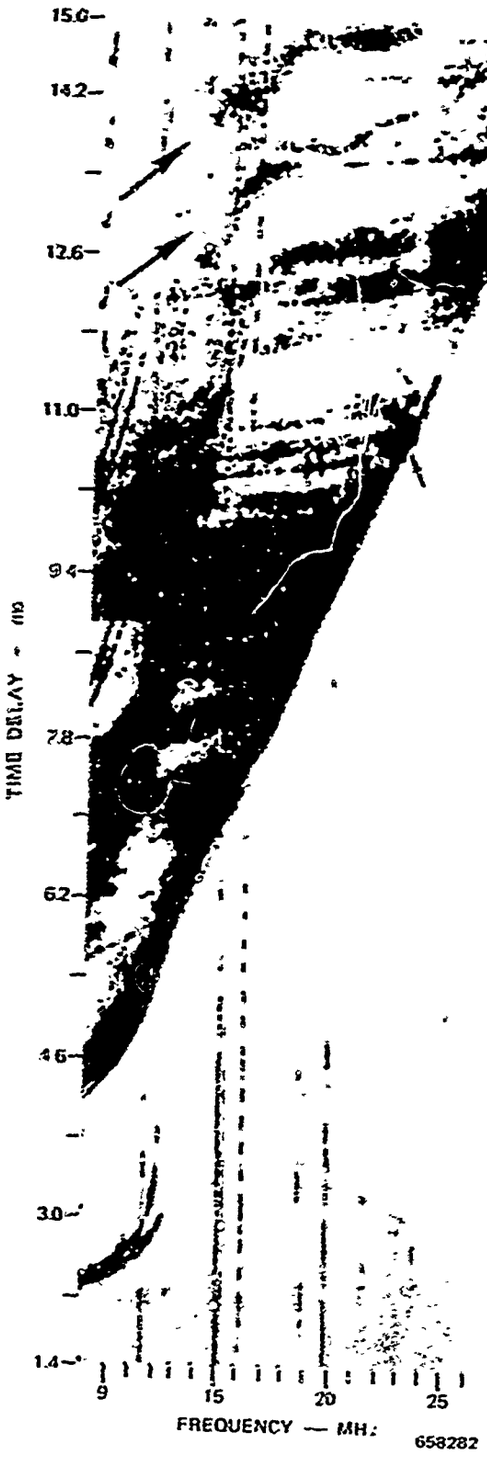

FIGURE 8 TYPICAL WIDE-SWEEP BACKSCATTER IONOGRAM SHOWING DISCRETE ECHOES (Small Arrows) AND DISTURBANCE-FOCUSING BANDS (Large Arrows)

This record displays unusual variations in signal strength. Several discrete echoes of nearly constant delay over several MHz are visible (a few are indicated by small arrows). In addition, there are large regions where the average backscatter energy is less than at shorter or longer delays. It will be shown that spatial variations in the ground-backscatter coefficient will account for these aspects of the backscatter ionogram.

Large arrows in Figure 8 indicate localized time-variable signal enhancements that are thought to result from an ionospheric disturbance.

Each of the discrete echoes on the backscatter ionogram show rapid, semi-regular amplitude variations as the signal frequency is swept: these will be shown to be related to Faraday rotation.

A. Interpretation of Single-Echo Structure on Backscatter Ionograms

In this section the backscatter-ionogram echo that would be produced by a point scatterer will be simulated. This simulation will be compared with observed echoes both from naturally occurring localized scattering regions and from the portable repeater described in Appendix A.

Consider an isotropic, point scatterer on the ground--say, 1500 km from a backscatter sounder. A single-layer ionosphere is assumed, one in which the QL approximation adequately describes the propagation characteristics. It should be noted that if the QL condition is occasionally violated, it will not affect the results here. This approximation is used mainly for convenience. Equal-strength ordinary (O) modes and extraordinary (X) modes are considered. Linearly polarized antennas are assumed, as is the case for the Los Banos backscatter sounder.

1. Case 1: Monostatic Sounder, No Polarization Sensitivity at Scatterer

Propagation from transmitter to scatterer may proceed by four different modes, corresponding to combinations of lower (L) and upper (U) rays, and ordinary (O) and extraordinary (X) modes. A sketch of a representative oblique ionogram is found in Figure 9(a). Upon scattering, ordinary rays (of circular polarization by virtue of the QL approximation) will return as ordinary waves; extraordinary rays will return as extraordinary. Incident rays, whether lower or upper, will each excite upper and lower rays upon scattering; any difference in characteristic polarization between upper and lower rays is neglected. Each returning mode will have circular polarization.

Figure 9(b) depicts the mode structure of such a two-way "composite" ionogram on a delay expanded scale. Modes are identified as (outgoing)/(incoming). Thus U/L means upper ray outgoing and lower ray incoming, and LO/UX would indicate lower-ray ordinary outgoing and upper-ray extraordinary incoming. Two U/L mixed modes appear; otherwise the composite ionogram has the shape of the one-way forward-oblique sounding. (Note that relative delay between modes is doubled in this two-way path.) Up to six modes will be present on this echo. As long as all modes are resolvable on a time-delay basis, each mode should have a relatively constant amplitude with frequency. When two modes are not delay-resolved (LO/LO and LX/LX, for example), then mode-interference effects can produce alternate peaks and nulls in the echo as frequency is changed. The mixed modes are each two modes having the same delay characteristics--LO/UO and UO/LO have the same total delay.

U/L mixed modes have been observed on two-hop forward-oblique soundings by Sweeney.[13]

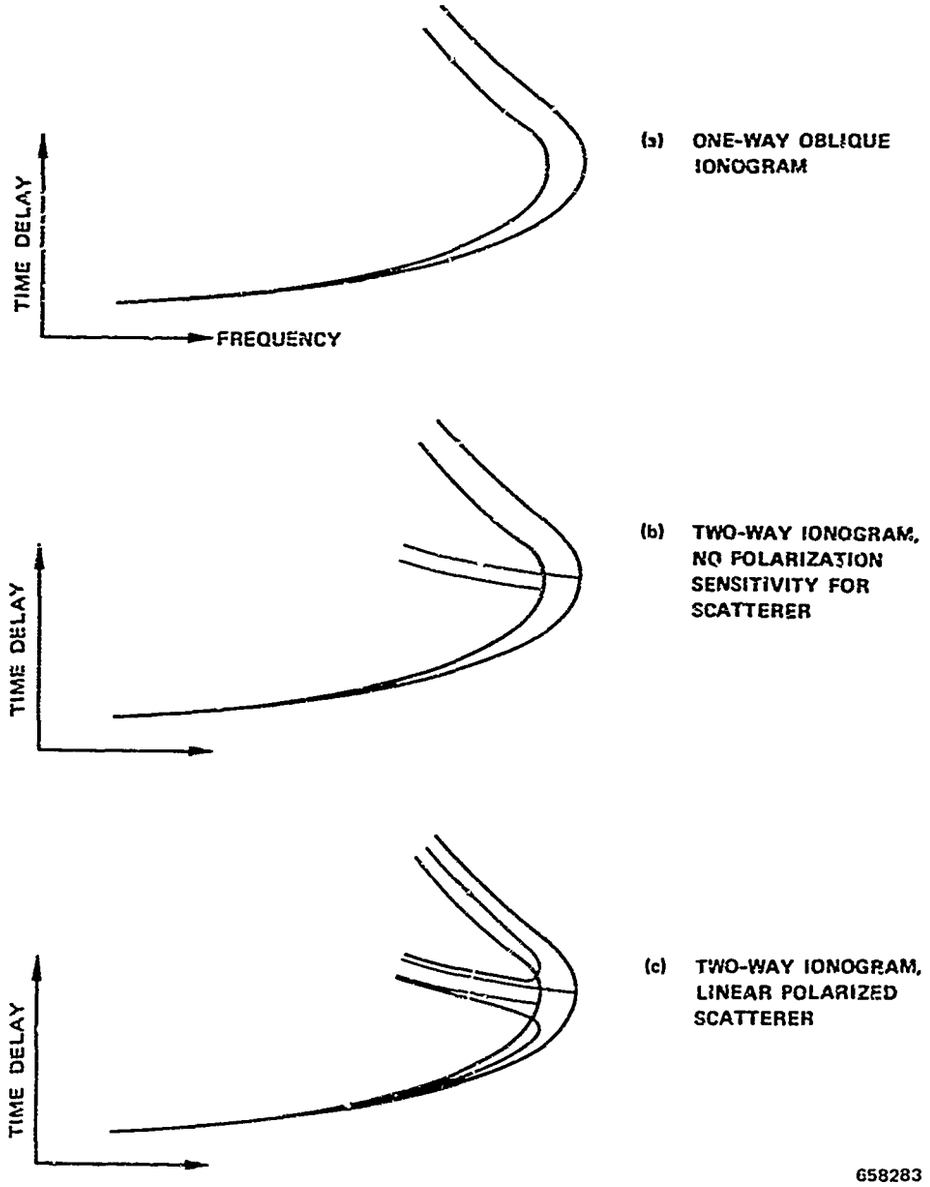

FIGURE 9 SKETCHES OF COMPOSITE IONOGRAMS IN SINGLE-LAYER IONOSPHERE FOR MONOSTATIC SOUNDER (Not to Scale)

2. Case 2: Monostatic Sounder, Linearly Polarized Scatterer

The principal difference from Case 1 is that here incident circularly polarized energy is scattered so that returning energy is initially linearly polarized. When this energy enters the ionosphere on the return path, the characteristic modes of right- and left-circular polarization appear.

Hence, incident energy of one magnetoionic mode excites both modes upon scattering. Four "crossed" modes are now added to those of Case 1; "crossed" modes are those where O rays couple with X rays (or vice versa) in these composite ionograms. Figure 9(c) is a sketch of the type of echo expected in this case; each of the additional modes is labeled. Each of these crossed modes is the superposition of two modes--i.e., LO/LX has the same delay as LX/LO. The total number of discrete modes here is ten.

3. Case 3: Bistatic Sounder, No Polarization Sensitivity at Scatterer

Analysis of high-resolution backscatter data is more complex for a bistatic configuration. Outgoing and incoming path segments may be essentially independent (midpaths for the Lost Hill-Los Banos sounder are approximately 90 km apart). For the purpose of synthesizing single-echo structures, the net result is that ordering of the path segments is important. Furthermore, for the ranges and azimuths this sounder used, the two path segments were always unequal in length. When propagating to the east the outgoing path was always shorter (nominally by 100 km), while the reverse was true for propagation to the west.

Consider that the path segments are sufficiently different in length to produce a visible difference in MUF's. [Figure 10(a) shows sketched ionograms for each of the two path segments.] No coupling

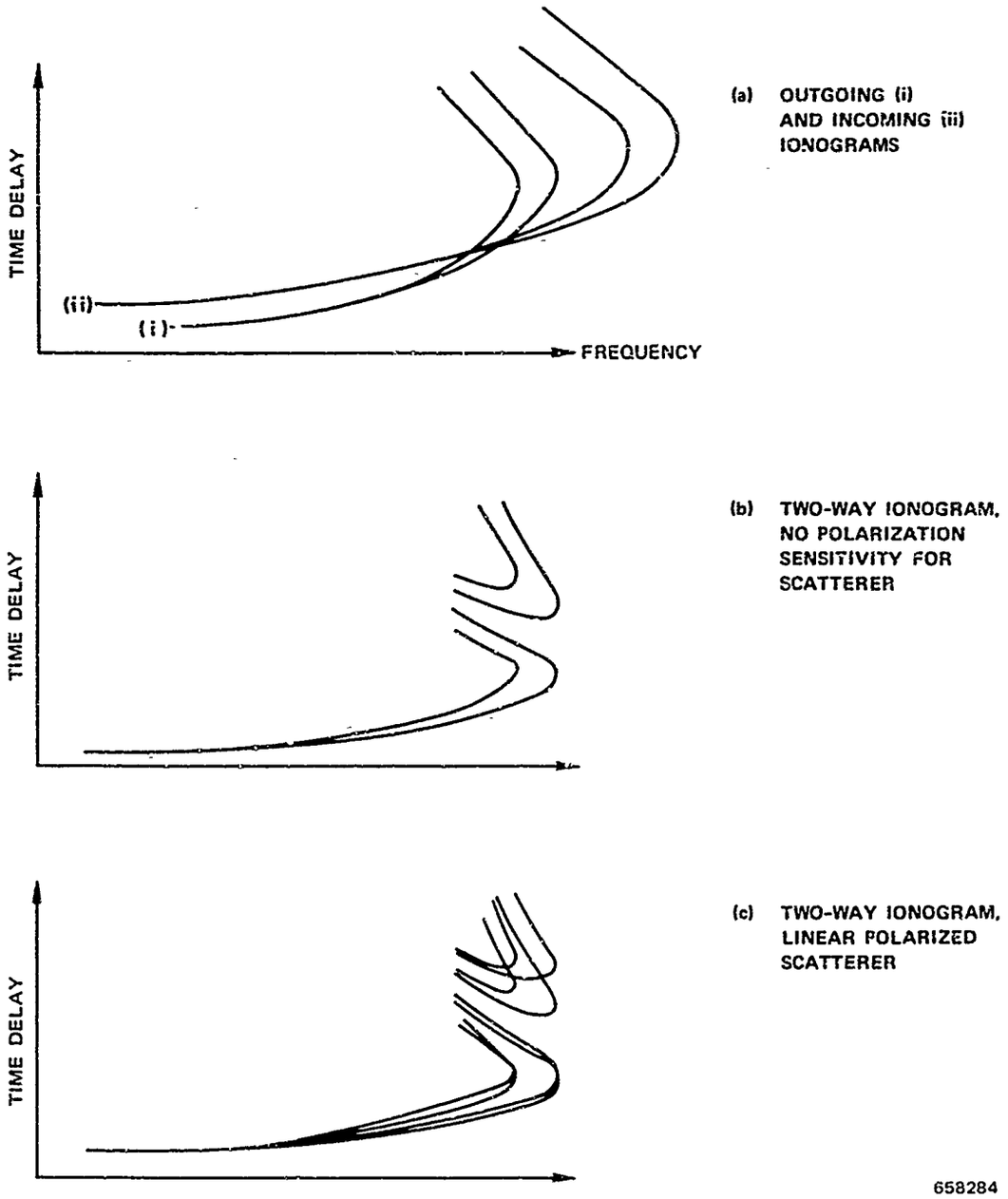

FIGURE 10 SKETCHES OF COMPOSITE IONOGRAMS IN SINGLE-LAYER IONOSPHERE FOR BISTATIC SOUNDER (Not to Scale)

between O and X occurs; but the two mixed modes of Figure 9(b) are now split into four delay-separated modes as indicated in Figure 10(b). A maximum of eight modes occur at some frequencies. Mode pairs such as LO/UO and UO/LO no longer have identical delay. Furthermore, since different MUF's exist for the two path segments, the one-way ionogram "nose" has two noses in the composite ionogram. This will take place anytime there is a difference between outgoing and incoming MUF.

The actual delay separation between modes is widely variable, depending on the extent of the difference in path segments, as will be seen later.

4. Case 4: Bistatic Sounder, Linearly Polarized Scatterer

As well as having to account for the ordering of modes, one must allow for coupling between O and X. Up to sixteen discrete modes can now occur, producing a rather complex composite ionogram [see the sketch in Figure 10(c)]. Some of these modes will generally be separated by only a few microseconds and thus be difficult to resolve. Amplitude fading as a result of the interference between two modes will take place, but it is more complicated for bistatic paths than for monostatic ones. Barnum[20] accounts for this in simulating families of polarization lines in backscatter from the ocean. Here it is required that ground range to the point echo be fixed, while Barnum required that slant range (time-delay) remain fixed, and then looked at the effects of polarization rotation/mode interference at a fixed time delay.

Because Case 4 represents a fairly general situation for the Lost Hills-Los Banos backscatter sounder, it is desirable to obtain a good simulation of the discrete echo that results. Rather than using an expensive backscatter-simulation routine, a point echo may be synthesized by raytracing from transmitter to scattering location and back to

receiver. For this purpose the Jones raytrace routine* [25] has been employed to trace rays in a three-dimensional ionosphere that includes the magnetic field but does not include collisions.

A sufficient number of rays are traced over an outgoing path of interest to define an ionogram with O and X modes and upper and lower rays. A similar set of rays is then traced over the incoming path from scattering location back to the receiving site. A supplemental routine combines the rayset information for both path segments to obtain $T_{ij}(f)$. This is the total delay for outgoing mode i (say lower-ray ordinary) and incoming mode j (say upper-ray extraordinary) as a function of frequency f. $T_{ij}(f)$ is simply the sum of $T_{1i}(f)$ and $T_{2j}(f)$, which are the delays for outgoing and incoming modes respectively. In this way a composite ionogram in a backscatter record may be constructed.

A point-source echo for Case 4 synthesized with this procedure may be found in Figure 11. The ionospheric profile is an α-Chapman layer where $N_{max} = 10^6$ electrons/cm^3. Outgoing and incoming ionograms of roughly 1200- and 1300-km path lengths, respectively, are included in the inset of this figure (note that the MUF's differ by about 1 MHz). The composite ionogram for the backscatter case is plotted τ_{excess} vs. frequency where τ_{excess} is the excess time delay over the minimum (ground range) delay. Indeed, 16 discrete modes are found near the MUF, which are identified in the figure caption, ordered by increasing delay at 15 MHz. The ordering of these modes is found to be sensitive to the particular time-delay-vs.-frequency characteristic of each path segment, and some of them may change their position in the overall composite echo with a small change in the ionospheric profile.

---

*Mr. David Bubenik modified the Jones raytrace routine to work on the Stanford University IBM 360/67.

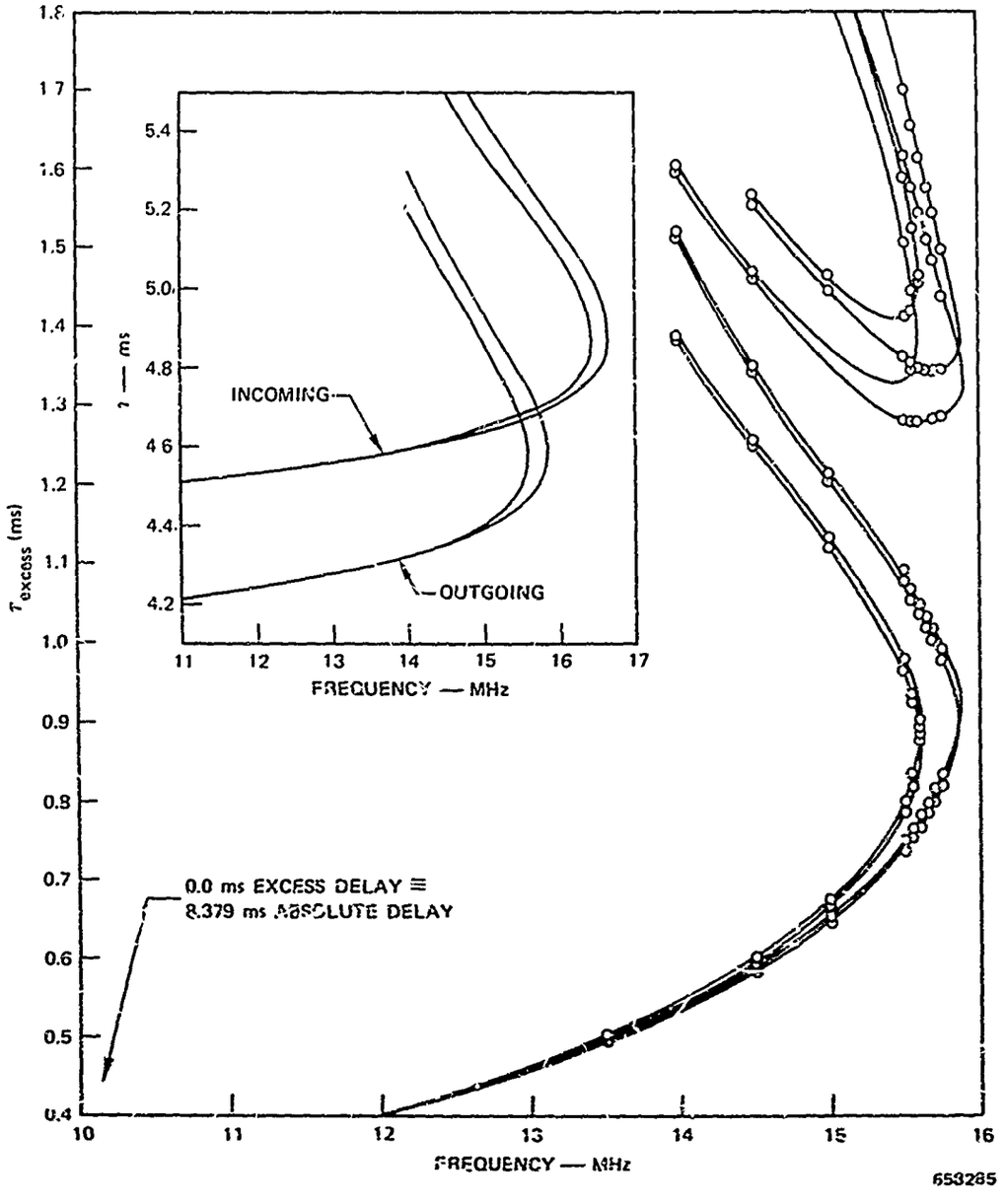

FIGURE 11 RAYTRACING SIMULATION OF COMPOSITE IONOGRAM FROM POINT ECHO (Linear Polarized) FOR BISTATIC SOUNDER. α-Chapman layer, N_{max} = 10^6 el/cm^3. Ionograms for both path segments shown in insert. Modes in order of increasing delay at 15 MHz are (1) LX/LX, (2) LX/LO, (3) LO/LX, (4) LO/LO, (5) UO/LX, (6) UO/LO, (7) UX/LX, (8) UX/LO, (9) LX/UO, (10) LO/UO, (11) LX/UX, (12) LO/UX, (13) UO/UO, (14) UO/UX, (15) UX/UO, (16) UX/UX.

An example of a high-resolution backscatter ionogram exhibiting a particularly prominent discrete echo may be found in Figure 12. This single echo is also visible in Figure 8 beginning at 10.2 ms delay, but little detail of the echo structure is visible there. Theoretical time-delay resolution is 4 μs, although only increments of 10 μs may be discerned from this figure. Spectrum-analyzer integration time was one second, during which time the sounder swept 250 kHz. This feature of the data-reduction procedure, together with dispersion in the ionosphere, combine to produce slight blurring along the frequency axis.

Generally speaking, the observed echo structure compares well with the simulation; in fact, the parameters of the simulation were chosen to agree with the actual conditions under which the data were obtained. The fact that observed and simulated MUF's are quite different is easily remedied by scaling up the peak electron density in the simulation. The (lower ray)/(lower ray) modes are so strong that they saturate the facsimile display; however, eight distinct (lower ray)/(upper ray) modes may be observed (at 21 MHz) in agreement with the prediction. Four (upper ray)/(upper ray) modes are present, although much weaker than the other modes. This is expected, since antenna gains decrease with increasing elevation angle. Furthermore, upper-ray energy is considerably defocused relative to lower-ray energy, which may be verified by appealing to the reflectrix construction.[4] By graphical means, one may show that the energy per unit elevation angle is much less for upper-ray energy than for lower-ray energy. For the path in question, where scattering took place in New Mexico and for F-layer propagation, lower-ray elevations ranged over 10 to 24 degrees, while upper-ray elevations were 24 to 40 degrees.

The nose of the discrete echo coincides with the leading edge of the backscatter. The ordinary MUF lies on one focusing line while

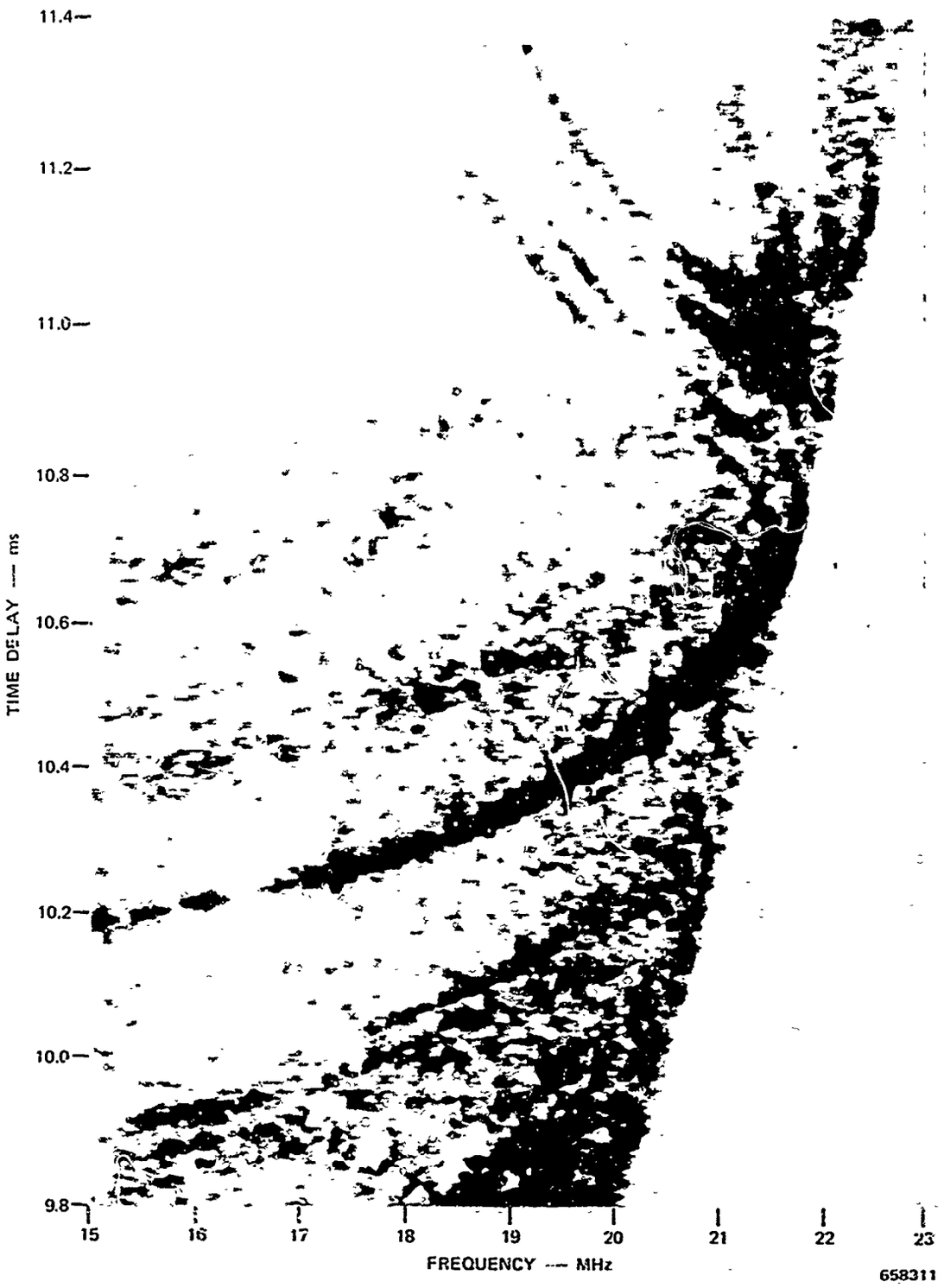

FIGURE 12 PORTION OF BACKSCATTER IONOGRAM SHOWING DISCRETE ECHO WITH MULTIPLE MODES

the extraordinary MUF lies on the other focusing line. These focusing lines are separate ordinary and extraordinary minimum-time-delay focus lines. If enough composite ionograms of various path lengths are plotted together on a delay-frequency graph, one can see how a backscatter sounding is generated from such two-way ionograms over a continuum of ranges. The time-delay focusing lines are lines drawn tangent to the MUF region of the ionograms. This was done for the simulation of Figure 11, and a more or less constant separation of 80 μs resulted, comparable to that of the experimental example in Figure 12.

The exact characteristics of leading-edge focus lines are dependent on path geometry as well as on the ionospheric profile. For a bistatic path the longer-delay nose of a composite ionogram could produce a focusing line of its own, admittedly weaker because the modes involved are (upper ray)/(lower ray) modes or vice-versa. Because bistatic effects vary with range, the delay separation between focus lines would be range-dependent. A single example of this unusual situation has been observed (see Section III-C).

One obvious extension of the simple viewpoint put forth here is to consider more complex ionospheric layers. When two or more layers are present, the maximum possible number of modes will increase considerably. The most general case of a two-layer ionosphere may produce up to 64 modes. Details of discrete echoes in a multilayer ionosphere are quite sensitive to many factors, and a lengthy catalog listing of such echoes would be necessary to include all echo shapes. However, two examples of single echoes observed in a multilayer ionogram are included here to indicate the types of echoes observed. For these two examples, the portable repeater was used to simulate an intense point-echo source.

The first example shown (Figure 13) was obtained by modulating the transmitted signal of the repeater at an audio frequency

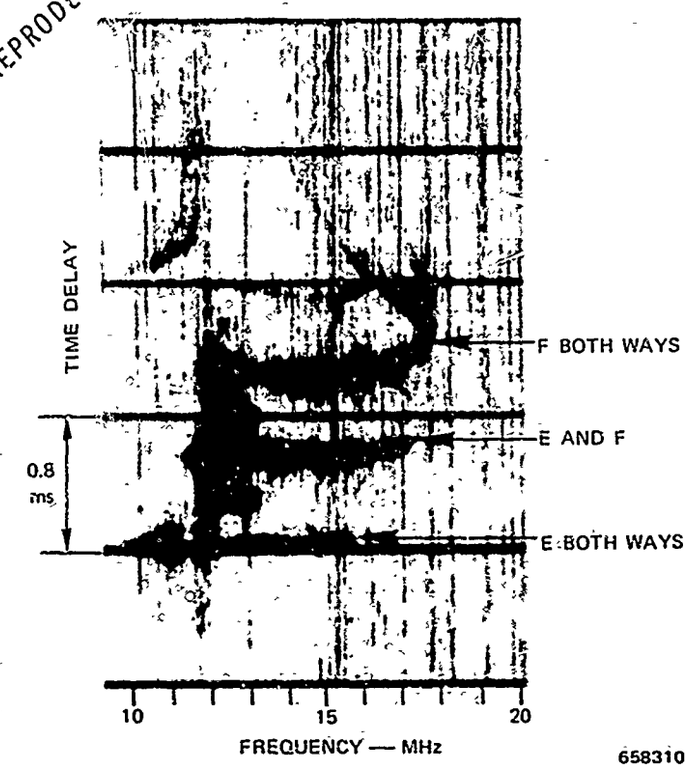

FIGURE 13 REPEATER ECHO SHIFTED AWAY FROM GROUND BACKSCATTER SHOWING E, F_1, AND F_2 LAYER RETURNS

(approximately 5 kHz). With the SFCW waveform, this modulation has the net effect of delay-shifting the repeated energy away from the ground-backscattered energy. Apparent delay shift is given by (modulating frequency) times 1/(sweep rate). A sweep rate of 250 kHz/s would thus give a 20-ms delay offset. By shifting the range gate of the receiver one can display the repeater return unobscured by normal backscatter. The discrete echo displayed in this way has three separate portions; forward-oblique ionograms show that at this time there were E and F_1 layers as well as the F_2 layer. The shorter delay portion used E propagation both ways up to 16.5 MHz. The middle-delay portion used F_1 and F_2 propagation one way and E-layer the other way (f_0F_1 of 13 MHz and f_0F_2 of 17.5 MHz). Finally, the longer-delay portion was comprised of

F_1 and F_2 propagation both ways. Between 15 and 18 MHz on this segment of the echo there are several mixed modes, while on the middle-delay portion (E/F modes) no such combinations occur. Mixed modes may be propagating near the F_1 MUF for the longer-delay portion, but the data are unclear at those frequencies.

Figure 14 is another example of a repeater echo in backscatter, except that the repeater was unmodulated and so its echo lies within the

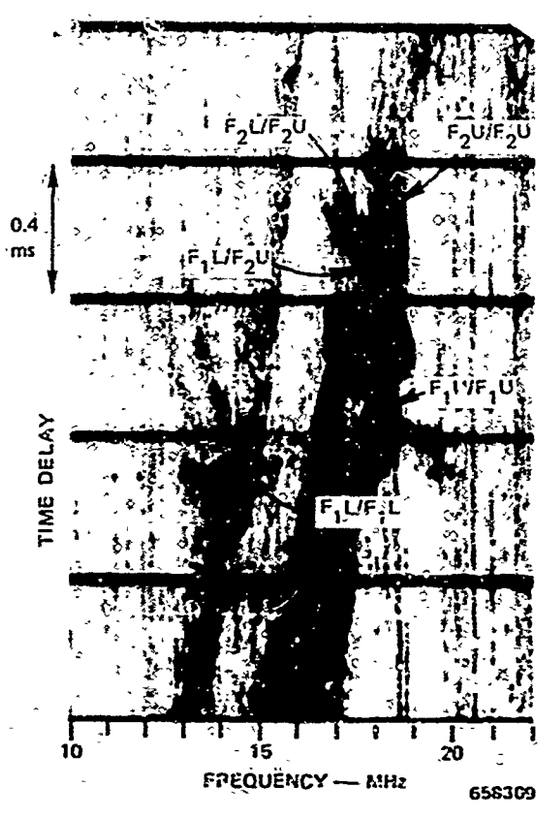

FIGURE 14 REPEATER ECHO IN GROUND RETURN IN PRESENCE OF STRONG F_1 LAYER

normal backscatter. The F_1 MUF exceeded the F_2 MUF, a condition not uncommon during summer. The interpretation given to the modes observed on the repeater echo is indicated in the figure. Unfortunately, these data were not available for reprocessing and thus cannot be studied

further. A broadened leading edge of the normal backscatter is seen to coincide with the F_2 focusing regions. A second focusing region at lower frequency for given delay is probably due to normal E layer or a multiple-hop mode; however, backscatter from the Pacific Ocean to the west cannot be ruled out.

For Figure 14 in particular, there is only a slight indication of a double nose structure on the discrete echo. When these data were obtained, the repeater was located at the Bearden, Arkansas field site. The segments of the backscatter path for this geometry are only 2 percent different in length, thus accounting for a small difference in MUF.

It is concluded that linearly polarized point-echo sources in a bistatic geometry do simulate the discrete echoes observed here. However, the many mixed modes depicted in Figure 12 are not always observed. By referring to the simulation of Figure 11 it can be seen that the eight longer delay modes all return by upper ray. Now upper-ray modes are more susceptible to azimuthal tilts than are lower-ray modes.[13] Because of the very narrow azimuthal beamwidth, these longer-delay modes are often shifted out of the receive beam. Even without the effects of azimuthal tilts, these (upper)/(upper) modes may be 30 to 40 dB weaker than the strongest lower-ray modes. The net result when these tilts occur is that the (upper) (upper) modes are not seen (even on the very strongest discrete echoes) for half to two-thirds of the time.

The principal conclusion to be drawn from this discussion is that numerous bright echoes in backscatter ionograms obtained with the Los Banos sounder behave much like a point-echo source on the ground--that is, much like a point repeater. As will be demonstrated further, backscatter from the ground can be characterized as a collection of these "point echoes."

B. Discrete-Echo Occurrence

As a key to understanding the appearance of discrete echoes in backscatter data, one would like to determine their distribution over the ground and their rates of occurrence. Although it will not be attempted here, such data could then be correlated with ground features to determine the source(s) of such intense echoes. Furthermore, if one can show that a "sufficient" number of such echoes are observable reliably, then they might find use in ionospheric study.

Two types of data are investigated for discrete echo occurrence--backscatter ionograms (τ vs. f) made at a fixed antenna steer, and slant-range-vs.-azimuth (τ vs. θ) records obtained with a relatively narrow, repetitive frequency sweep.

1. Backscatter Ionograms

Since this form of data is used so often it is of special interest to determine rates of occurrence of discrete echoes with it. Two hundred ten frames of backscatter ionograms made in two periods spanning six hours on a winter day (F-layer propagation) were examined. The frequency was swept from 15 to 26 MHz every minute at an antenna steer of 90 degrees true. A 4-ms range gate (10 to 14 ms) was chosen in which the rates of occurrence of discrete echoes were to be determined. Figure 15 summarizes the conditions employed and includes a typical data frame out of this sequence.

The 10 to 14-ms range gate illuminated a region on the ground extending from northeastern New Mexico through the northern part of the Texas Panhandle into western Oklahoma.

The criteria employed for deciding that a discrete echo due to enhanced ground scatter is present are somewhat conservative. Probably many discrete echoes exist that were not counted. Since the ionospheric

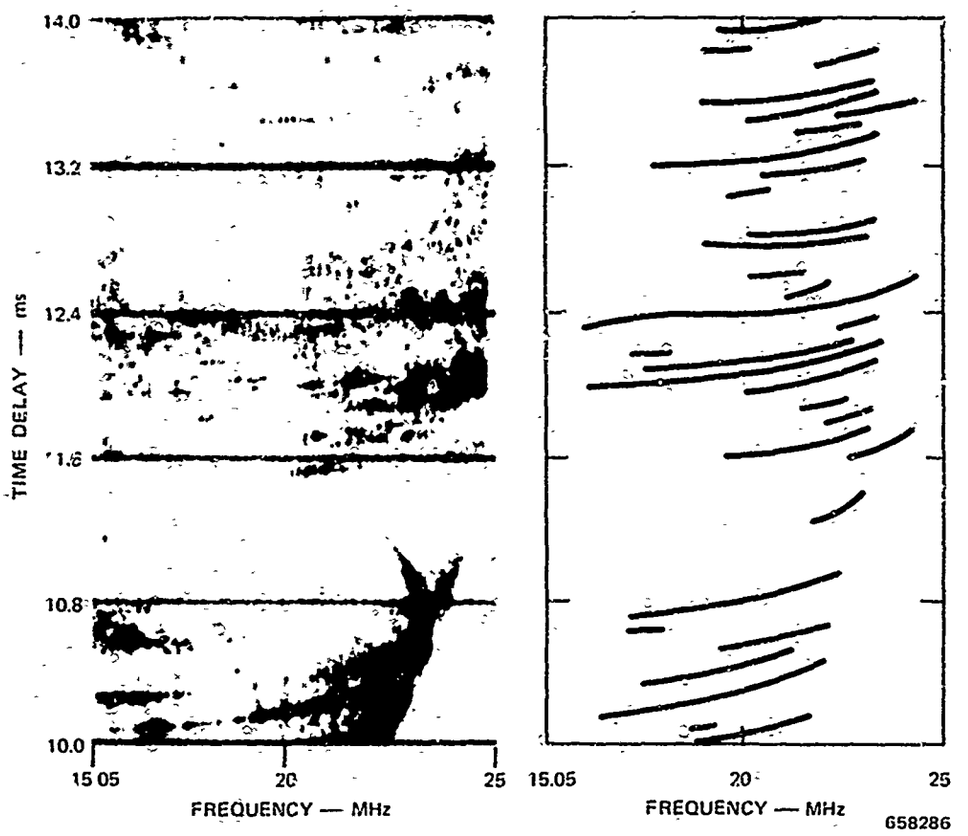

FIGURE 15(a) TYPICAL BACK-SCATTER IONOGRAM FROM 210-FRAME SEQUENCE

FIGURE 15(b) OVERLAY FOR 10-TO-14 ms GATE

layer structure is known from an oblique sounding, an echo must have an oblique ionogram "shape" on the backscatter ionogram; and it must be visible over a frequency extent of at least 1 MHz. Such an echo is required to have a delay width less than 100 μs. The data indicate that the discrete echoes are often resolved into several components, but these are not counted as separate echoes. Finally, each echo must have suitable time duration to establish that it is indeed fixed in delay and not a moving ionospheric focusing enhancement.[4] If a suspected fixed echo disappears, it must reappear elsewhere in the 210-frame sequence in order to be counted.

A transparent overlay may be constructed with all suspect discrete echoes sketched upon it. Then, as the viewer proceeds through the frames one by one, visible discrete echoes may be noted and recorded. There is very little chance of counting an echo's mixed modes as separate echoes (particularly with the single-layer ionosphere). Under other ionospheric conditions this could indeed become a problem. It is difficult to judge the delay width of these echoes on intensity-modulated data, and so a conservative attitude is adopted toward this criterion. 100 μs was taken as an upper bound on the delay width of the echoes recorded, although other data indicate that 50-μs is a better upper bound.

Figure 15(b) is a sketch of the overlay constructed for this data sequence (only the shortest delay mode is used). Due to normal diurnal changes and also to the presence of large-scale TID's during the latter portion of this sequence, the echo traces on this overlay change with time. However, by sliding the overlay both in frequency and delay for a "best fit" to the stronger echoes, confusion as to echo identity is minimized. It should be noted that amplitude changes with frequency occur on all echoes from one data frame to another, and the traces in Figure 15(b) are not always representative of the echo trace.

A total of 31 discrete echoes were observed throughout the 210-frame sequence; four of these were questionable under the above criteria for selection. In addition, two echoes may possibly be one echo doubly counted. Figure 16 is a histogram of the rate of occurrence of these echoes, 8 of them observed more than 50 percent of the time and 2 of them observed 100 percent of the time. The number of echoes per frame varies from 4 to 16 with a mean of 9.7.

It is also of interest to determine how long an observing time is required in order to observe a large fraction of these echoes. Seven independent twenty-minute sequences were scaled to determine this rate

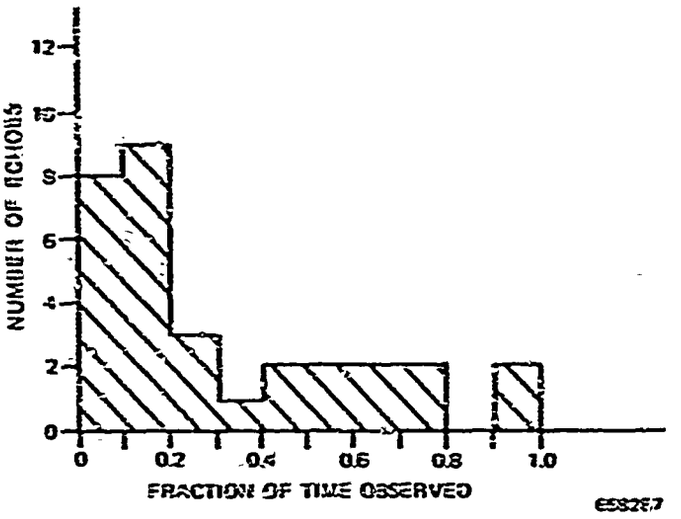

FIGURE 16 DISCRETE-ECHO OCCURRENCE ON BACKSCATTER IONOGRAMS— 4-5 MARCH, 1969. Total of 31 echoes, mean number of echoes/frame = 9.7.

of buildup of observed echoes, and the result is plotted in Figure 17. Initial buildup is rapid; then the slope decreases as 80 percent of the total number of echoes have become visible in the first 18 minutes.

Backscatter ionograms made at other antenna headings produced roughly the same total number of discrete echoes under similar ionospheric conditions. The 6 to 10-ms range gate showed about the same number of echoes, although they did not stand out as much, relative to the background backscatter level. If the range gate was chosen much further out (say, beginning at 16 ms or so) generally one observed fewer discrete echoes. One factor in this decrease in number of echoes as range increased is that system sensitivity was decreasing and signal-to-noise ratio decreased too. Little effort has been made thus far to look specifically for discrete echoes at long delays. At the longer delays in the geographic area studied, relatively flat land is illumirated, in comparison to that illuminated in the 10 to 14-ms range gate. Subsequent experiments will look at the long-delay region more closely.

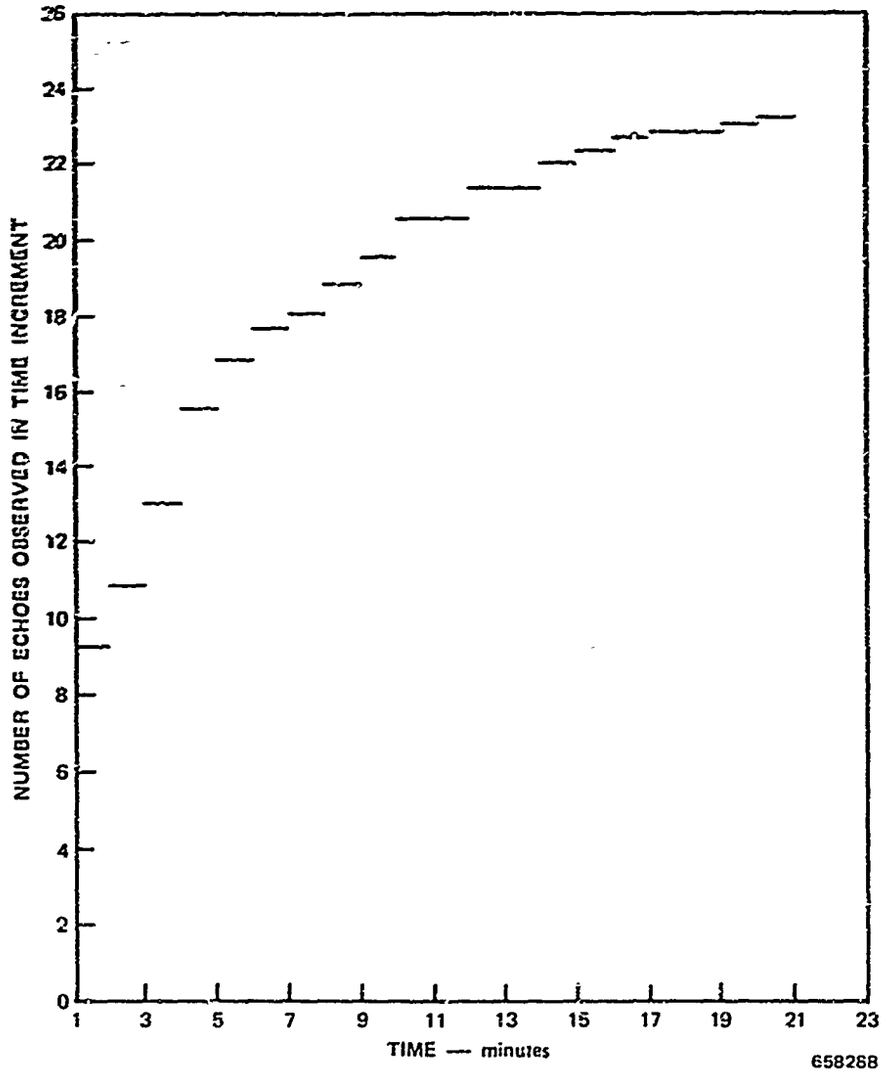

FIGURE 17 AVERAGE TOTAL NUMBER OF DISCRETE ECHOES OBSERVED VERSUS OBSERVING PERIOD FOR BACKSCATTER IONOGRAMS OF 4-5 MARCH, 1969

It should be noted that the echoes at one time or another were visible at all frequencies that illuminated the region on the ground from which they arose. Through disturbance-focusing, the effective sensitivity of the backscatter sounder is alternately increased and decreased. Weaker echoes then will occasionally become visible for brief periods (a few minutes). The majority of discrete echoes have this broadband characteristic, which may be a useful clue in discerning the sources of the enhanced scattering.

Although no large data samples were obtained on subsequent days of observation, about two-thirds of the echoes in Figure 15(b) were identifiable in a thirty-minute sequence of backscatter ionograms made under similar operating conditions (time of day, antenna steer, range gate). When the ionospheric profile changed considerably, so did the single-echo visibility. Under multiple-layer conditions such as those indicated in Figure 14, fewer single echoes were seen, and when one was, it was not possible always to determine which echo modes were being observed. Particularly during summer months, discrete echoes were visible only near the highly focused leading edge, and here dispersion and multiple modes made echo identification difficult.

2. Range-vs.-Azimuth Backscatter Displays

Sweep-frequency backscatter ionograms are subject to the effects of apparent antenna beam swinging because of azimuthal tilts. A one-degree azimuthal shift (which is not altogether uncommon) produces more than a 20-dB change in signal from a point scatterer. A range-azimuth display removes this source of uncertainty, and so in this section the occurrence of discrete echoes on this type of backscatter display will be investigated.

Under the same winter daytime ionosphere as described in the previous section, a sequence of 30 range-azimuth displays were obtained two minutes apart around midday (single F-layer propagation). A sample display is found in Figure 18(a), in which the operational parameters are also indicated. As in the previous case, discrete echoes were counted in a 4-ms range gate (8.8 to 12.8 ms) over a 30-degree azimuthal sector (75 to 105 degrees).

The transmitting antenna was steered as indicated in Figure 18 to maintain good beam convergence in this range gate. Unfortunately the antenna-steering format sometimes did not accomplish this very well, but it was consistent from frame to frame and so may be taken into consideration. The receiver was operated at fixed gain.

On the range-azimuth display the criteria for discrete, fixed echo occurrence are: (1) that the 3-dB delay width must be less than 100 μs (it usually is less than 50 μs), (2) that the echo has azimuthal extent commensurate with the azimuthal response plotted in Figure 7, (3) that echoes have suitable time duration (10 percent of the data frames), and (4) if they disappear they must reappear at the same location at some later time. With this short data sequence, which cannot be statistically valid, these criteria are used conservatively in order to set lower bounds on the number and occurrence of the discrete echoes.

As before, a transparent overlay was constructed to record single echoes; this is reproduced in Figure 18(b). A total of 71 distinct echoes were accounted for in this 30-frame sequence. Five of these are slightly questionable, and three may be the same echo source propagating via different ionospheric modes. A frequency-of-occurrence histogram of the echoes is found in Figure 19. For the 600-by-700-km region (range and cross-range respectively) on the ground there are some 21 discrete echoes observed more than 50 percent of the time and 5 observed greater

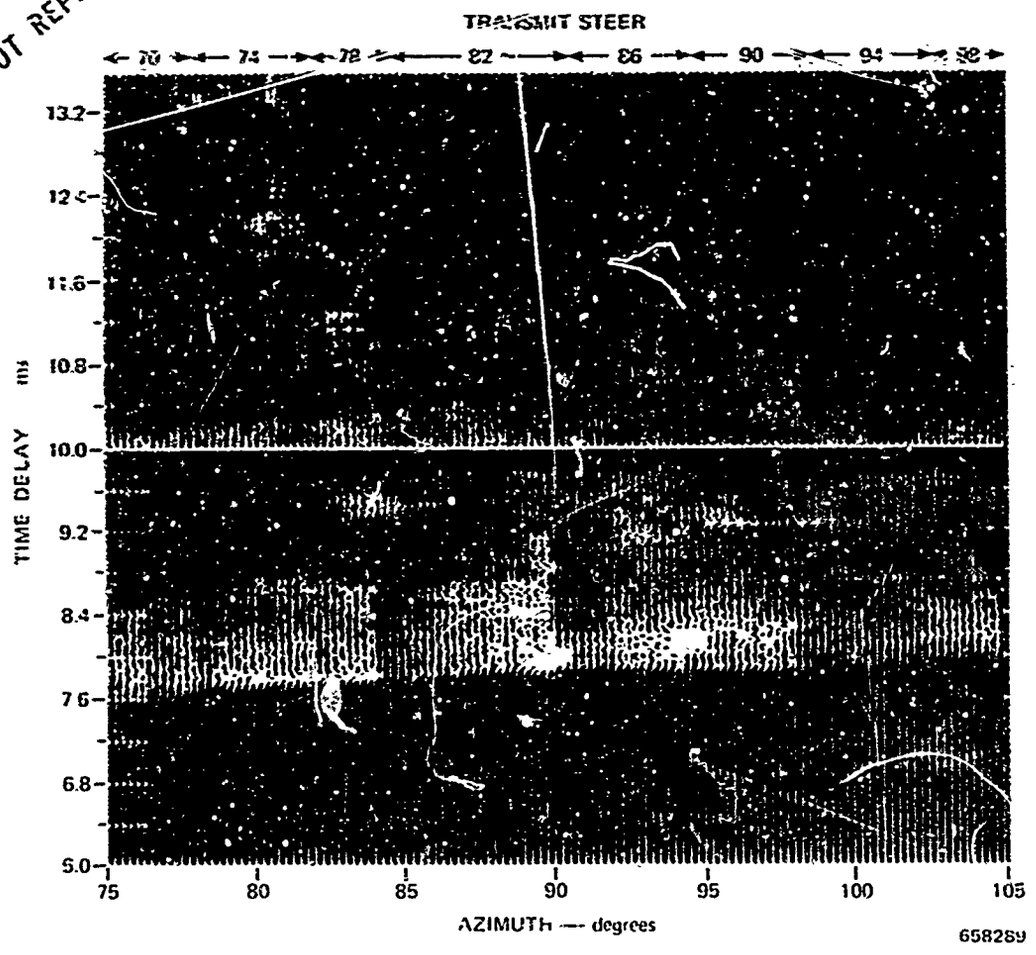

FIGURE 18 TIME-DELAY-VERSUS-AZIMUTH BACKSCATTER DATA— 5 MARCH, 1969, 2102-2202 GMT

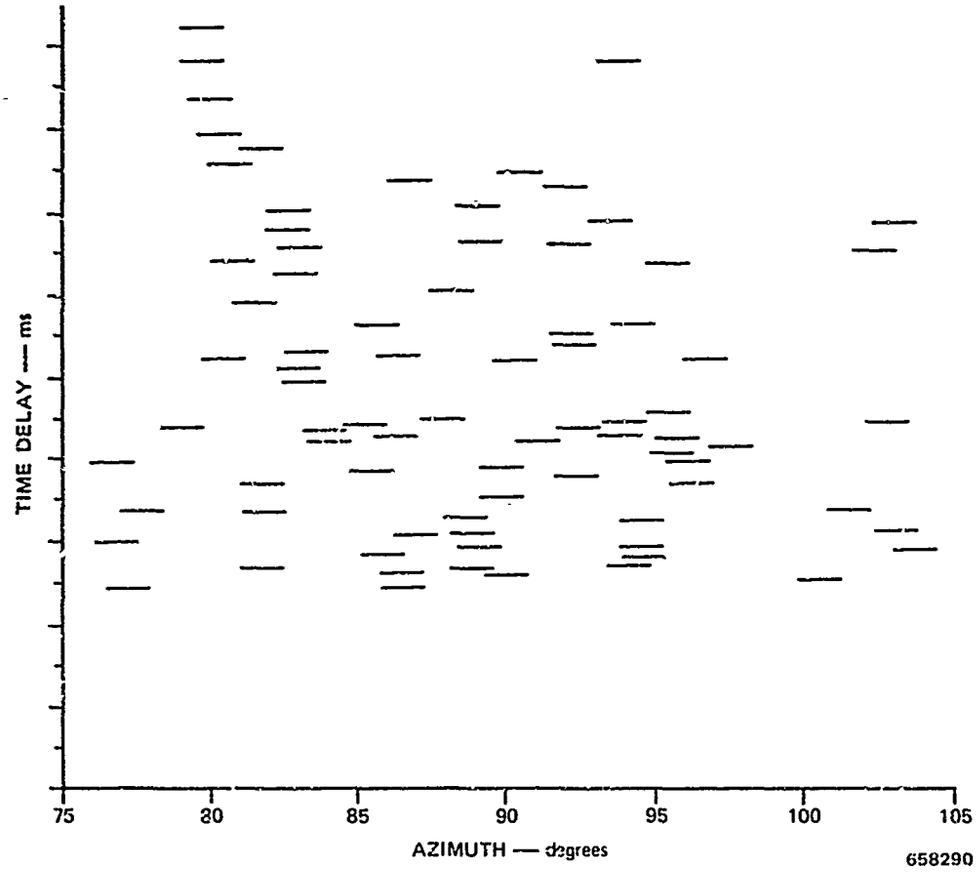

FIGURE 18 TIME-DELAY-VERSUS-AZIMUTH BACKSCATTER DATA— 5 MARCH, 1969, 2102-2202 GMT (Concluded)

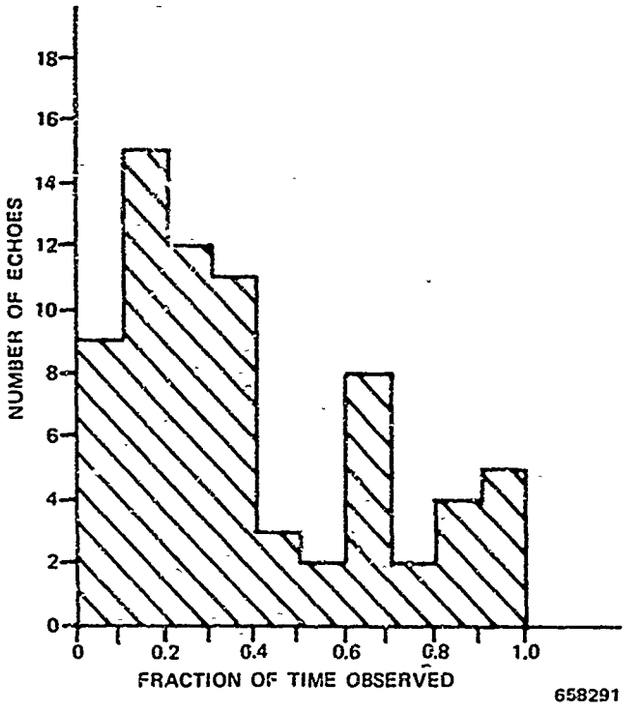

FIGURE 19 RATE OF OCCURRENCE OF DISCRETE ECHOES ON TIME-DELAY-VERSUS-AZIMUTH BACKSCATTER DATA—5 MARCH, 1969. Total number of echoes is 71. Average number of echoes/frame = 25.8.

than 90 percent of the time. The number of echoes per frame varies from 19 to 36, with a mean value of 25.8.

Data obtained on different days showed that one could quickly identify the strongest of discrete echoes (those visible more than 50 percent of the time) on the range-azimuth display. There have not been any other sufficiently long time sequences of data to verify the recurrence of the weaker echoes.

The density of discrete echoes in Figure 18 decreases with increasing delay. If the average backscatter coefficient varies with elevation angle as shown in Figure 5 in Section II, then the variations about this average value would produce an amplitude-vs.-delay plot of

backscatter at a fixed frequency as sketched in Figure 20. At longer delay relative to the minimum delay, a localized brightness must be proportionately larger than the mean level of σ_o at that delay in order to be seen. This may be remedied by (1) filtering out the close-in

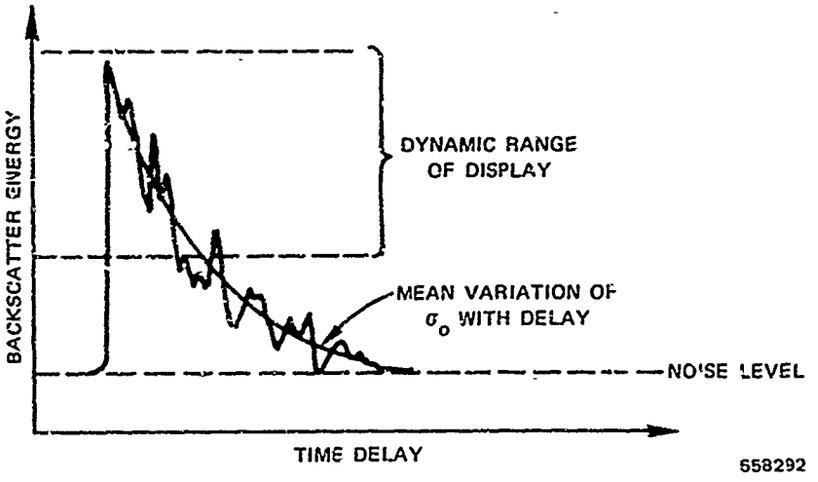

FIGURE 20 SKETCH SHOWING HOW DYNAMIC RANGE OF DISPLAY INTERACTS WITH AVERAGE ENERGY FALL-OFF WITH DELAY. In Section II this variation was approximated by $10^{-(\tau-\tau_o)/4}$ with τ in ms and τ_o = delay at leading edge of backscatter.

strong echoes, (2) allowing the display (but not the spectrum analysis) to saturate on strong echoes, or (3) adjusting system response vs. range (really audio frequency vs. range with the SFCW technique) to offset this decrease in signal with increasing delay.

It is difficult to compare discrete echo occurrence on the two types of backscatter display discussed here. Backscatter ionograms used automatic gain control to handle the large variation in signal strength as frequency was varied, while the range-azimuth display used a fixed-gain receiver. A good example is found in the fact that the strong echo at 10.2 ms and 90 degrees in Figure 18 is the same echo as the one at 10.2 ms in Figure 15. In the latter it is visible 100 percent of the time, while in the former it is seen 67 percent of the time. The

facsimile display saturates on this echo in Figure 15, so that its amplitude variations with time are not being observed. On the range-azimuth data the display gain was set so that its amplitude variations cause it to disappear one-third of the observing time.

3. Spatial Extent of Discrete Echoes

Earlier in Section III it was stated that the discrete echoes appear nearly as "point echoes." Now it is appropriate to determine if the short-pulse, narrow-beamwidth capabilities at hand are sufficient to resolve the localized bright scattering regions. Usually an echo is considered extended if its spatial extent is appreciably greater than the resolution cell size. Those that are much smaller than the cell size are point echoes, and those that are comparable to the cell size are indeterminate.

For this system the minimum cell size was 3 μs in delay and 1/4 degree in azimuth. The useful cell size achieved was roughly 3 to 10 μs by 1/4 to 1/2 degree; at a 1500-km range this produced a cell 0.45 to 1.5 km by 6 to 12 km. Several recent studies[13,38,27] have each investigated ionospheric limitations on the minimum beamwidth obtainable in the HF band. Although statistics are not yet available, it is apparent that this 2.5-km aperture is useful 90 percent of the daytime on one-hop lower-ray F-layer propagation; and furthermore, an aperture ten times as large should be useful a fair fraction of the time.[26]

Delay resolution is controlled by the bandwidths supportable in ionospheric propagation. Dispersion, Faraday rotation (more generally magnetoionic splitting), and inhomogeneities are the principal limitations on bandwidth. One hundred to five hundred kHz has been found to be the range of useful bandwidths for observation of discrete echoes. However, by choosing operating parameters carefully, one should be able to employ

1-MHz bandwidths[28] without resorting to some form of dispersion compensation. (The transmitter limited usable bandwidths in range-azimuth backscatter data to 500 kHz in this experiment.)

An important feature of the Lost Hills-Los Banos backscatter sounder was that the ratio of cross-range resolution to range resolution was large (nominally 10:1). Generally, one should be better able to resolve echoes in delay than in azimuth. The self clutter imposed by range and azimuth sidelobes (Section II) can only serve to increase the apparent extent of echoes when in fact they may in reality not be extended.

The 30-frame sequence of range-azimuth displays that produced 71 discrete echoes (Figure 18) has been analyzed for individual echo range and azimuth extent. These data obscure the measurement of spatial extent since (1) the data sample is not large in a statistical sense; (2) signal fluctuations have not been compensated for (to be discussed in Section IV); and (3) steering the transmitting antenna produces discontinuous gain changes. However, by choosing particular echoes that fortuitously avoided the last source of ambiguity, one may study representative examples of these localized echoes.

These examples were chosen using the following criteria: The frequency of occurrence must be greater than 0.5 in order to determine that the apparent extent in delay and azimuth persisted over the one-hour observation time. These echoes must not be located at azimuths where the transmit array is steered. Echoes are selected away from the leading edge to reduce delay spread from dispersion and to reduce the possibilities of multiple moding. Whether an echo is resolved or not is partly a subjective judgment and depends on the criteria used. It is worthwhile to note that the 10-dB beamwidth for this frequency is 0.78 degrees. The 10-dB delay width due to equipmental considerations is roughly 25 μs.

About a fourth of the echoes tabulated in Figure 18 are marginally spread in azimuth. More than a half of them are clearly resolved in delay.

Figure 21 shows two intense localized echoes, labeled H1 and I1, that are delay-resolved by 100 μs. Because of the delay separation

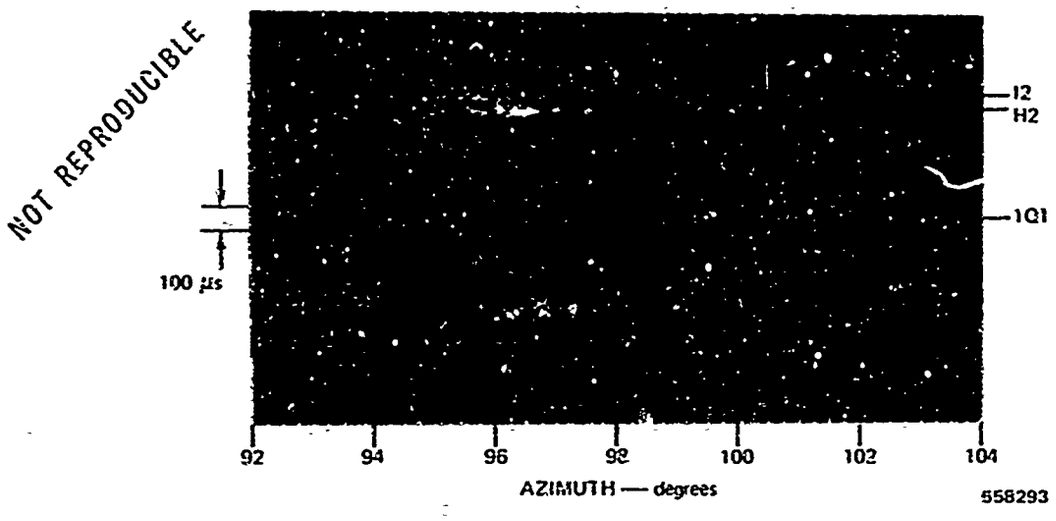

FIGURE 21 DEMONSTRATION OF AZIMUTHAL SEPARATION OF DELAY-SEPARATED ECHOES (H1 AND I1)

one can also discern a one-degree azimuth separation in the peaks of these echoes. Echo H1 has azimuthal "sidelobes" 5 to 6 degrees away from the main peak and only 11 dB down, which are considerably larger than predicted by the azimuthal response of Figure 7. However, in the absence of a measured azimuthal response it is uncertain whether H1 is azimuthally extended.

Echo 1Q1 in Figure 21 appears not to be resolved in delay or azimuth, although separate azimuth sidelobes are visible. The fact that these sidelobes are almost as large as the main lobe is partially attributable to the fact that this echo is only slightly above the background level at adjacent locations on the $\tau - \theta$ display.

In addition to the well localized discrete echoes, typical examples of which are given in Figure 21, there are whole regions on $\tau - \delta$ backscatter displays where the average backscatter level is considerably different from adjacent regions. These regions are easily resolvable in delay (up to a few ms delay width) and in azimuth (3 to 5 degrees extent). However, within these regions one sometimes observes a discrete echo that in itself is not resolved.

As in backscatter ionograms, there are abruptly varying discrete echoes that are of special interest in this study, and there is also a more smoothly changing component in the ground reflectivity from place to place.

A good example of both types of backscatter echoes is found in Figure 22. The portable repeater was operated near the observed region in central New Mexico. Echoes H1 and I1 are indicated by arrows and have the same features as in Figure 21. This is rather remarkable because Figure 21 is F-layer data obtained in March, while Figure 22 is

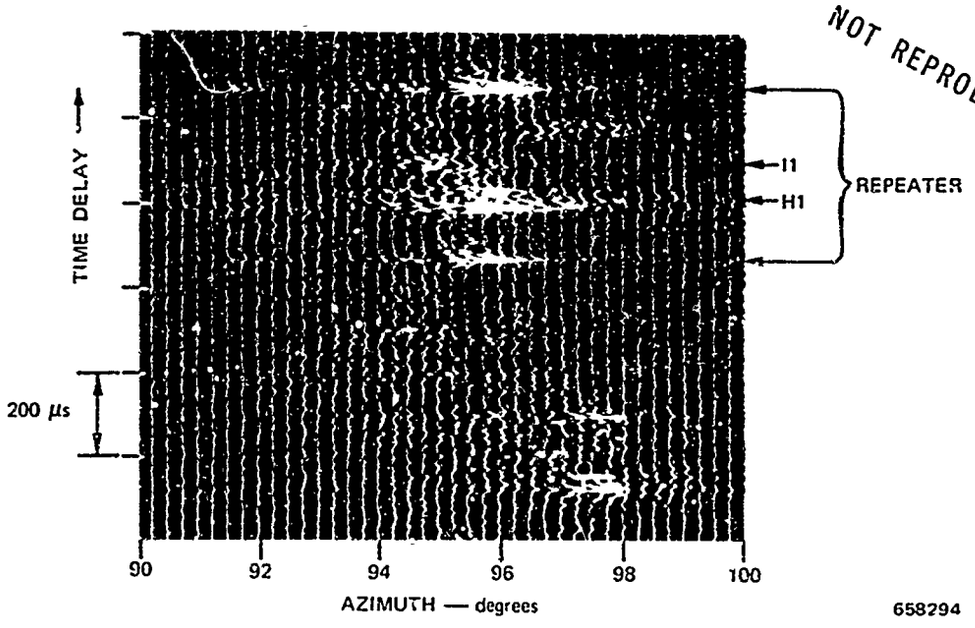

FIGURE 22 HIGH-RESOLUTION TIME-DELAY-VERSUS-AZIMUTH BACKSCATTER

E-layer data obtained four months later in July. Particularly on the July data (where the transmit antenna was not steered), extended regions of heightened reflectivity occur and are persistent. In Figure 22 one such region some 400 μs by 5 degrees in extent is visible at short delay and mid azimuth.

As a further example of the marginal azimuthal resolution of discrete echoes, amplitude-vs.-azimuth plots were made for discrete echo H1 in Figure 22. In addition, the echo amplitudes for the repeater sidebands are also included. Figure 23 shows these plots for the repeater and two-delay-resolved components of echo H1.

The azimuthal distribution of the repeater is plotted from the average amplitude of the repeater's two sidebands at each azimuth. These sidebands appear some 400 μs apart on the $\tau - \theta$ display. The repeater response peaks between 95-3/4 degrees and 96 degrees steer. (The true azimuth to the repeater was calculated to be 95.81 degrees.)

Echoes H1a and H1b are components separated by 40 μs. H1a peaks at 96 degrees while H1b appears slightly skewed toward 96-1/4 degrees azimuth. This slight separation is not necessarily real; one would have to average over many such $\tau - \theta$ displays to discern real azimuthal separations less than 1/4 degree. Although the azimuth sidelobes of the repeater return are large, the width of the main peak is comparable with the theoretical azimuth response of the sounder.

In summary, then, it can be said that discrete echoing regions are plentiful (at least in the Colorado-New Mexico area), that they produce multimoded echoes much as a point repeater would, and that they are in some instances delay-extended (up to 50 μs or so); but it is indeterminate whether they are azimuth extended. In the next section the way in which these characteristics interact with various aspects of ionospheric propagation will be considered.

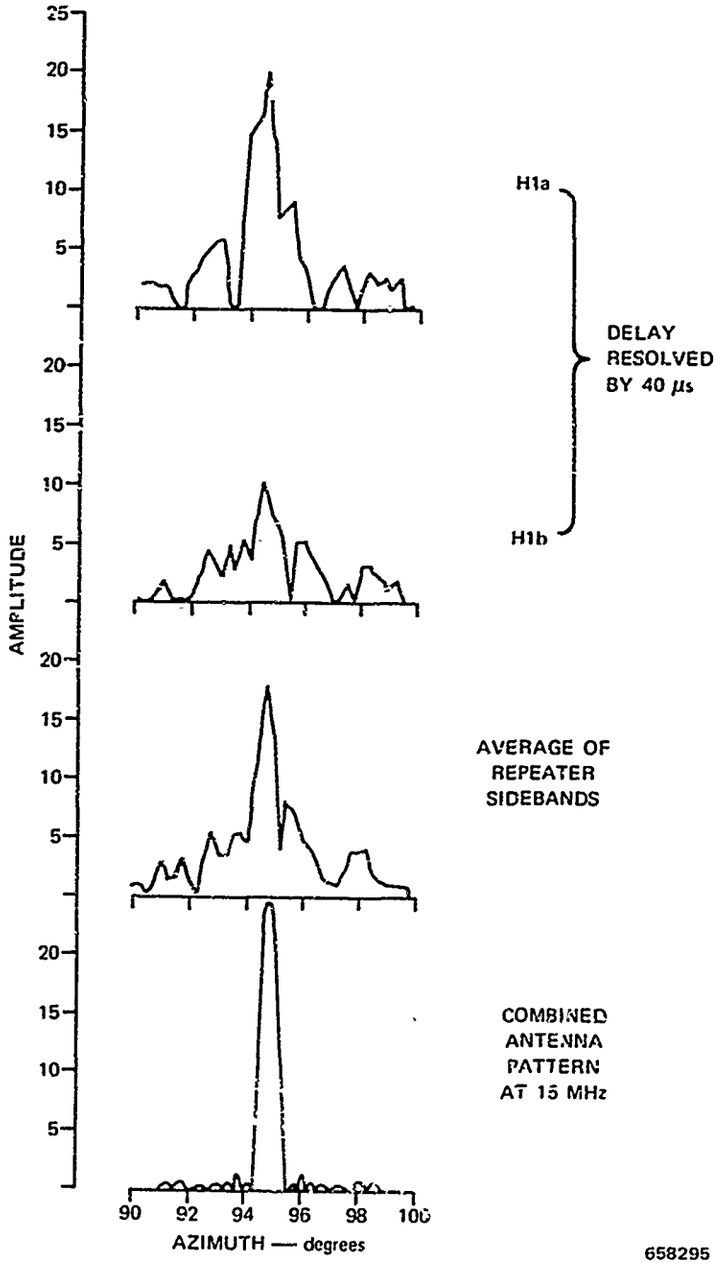

FIGURE 23 AZIMUTHAL ECHO DISTRIBUTION FOR ECHO H1, 1 JULY, 1969, 1743 GMT. E-layer propagation, center frequency 16.25 MHz, Range 1300 km.

C. Interaction of Discrete Echoes and Ionospheric Phenomena in Backscatter

1. Relation to Undisturbed Focusing

Focusing of backscattered energy occurring due to increased ray density may be a result of time-delay focusing[1] where energy from different locations on the earth arrives at the same time delay. Or else it may be of the geometrical focusing variety (such as skip-distance focusing) where one-way transmitted energy is focused by ionospheric refraction. Both have been studied in depth,[3,6,29] and these phenomena have been accounted for in backscatter-simulation procedures. With the Los Banos sounder, focusing indications show a certain amount of fine structure, principally because the sounder antenna does not average over a large azimuthal segment.

One prominent feature of these focus lines is the presence of separate focus lines for ordinary and extraordinary propagation. Data from the Lost Hills-Los Banos sounder shows O - X splitting in minimum-time-delay focusing from propagation via $1F_1$ (one-hop F_1 layer), $1F_2$, and $2F_2$. Occasionally this splitting is seen in maximum time-delay focusing (interlayer focusing, Ref. 29). The presence of discrete echoes was used to verify that this interpretation of separate focus lines is correct. Figure 24 is a sample backscatter ionogram in which O - X splitting of the $1F_2$ skip-distance focusing line is visible. A discrete echo is also visible showing O and X "noses" tangent to each focus line. The discrete echo simulation predicts as many as four resolvable focus lines under bistatic geometry where a two-nosed composite ionogram may occur. However, propagation via upper-ray one way is less intense since the maximum amount of focusing is occurring over only one portion of the backscatter path. To date only one example of more than two focus lines has been recorded, occurring during a modest ionospheric disturbance. It showed a three-fold splitting in the minimum-time-delay focus line over a delay increment of 2 ms.

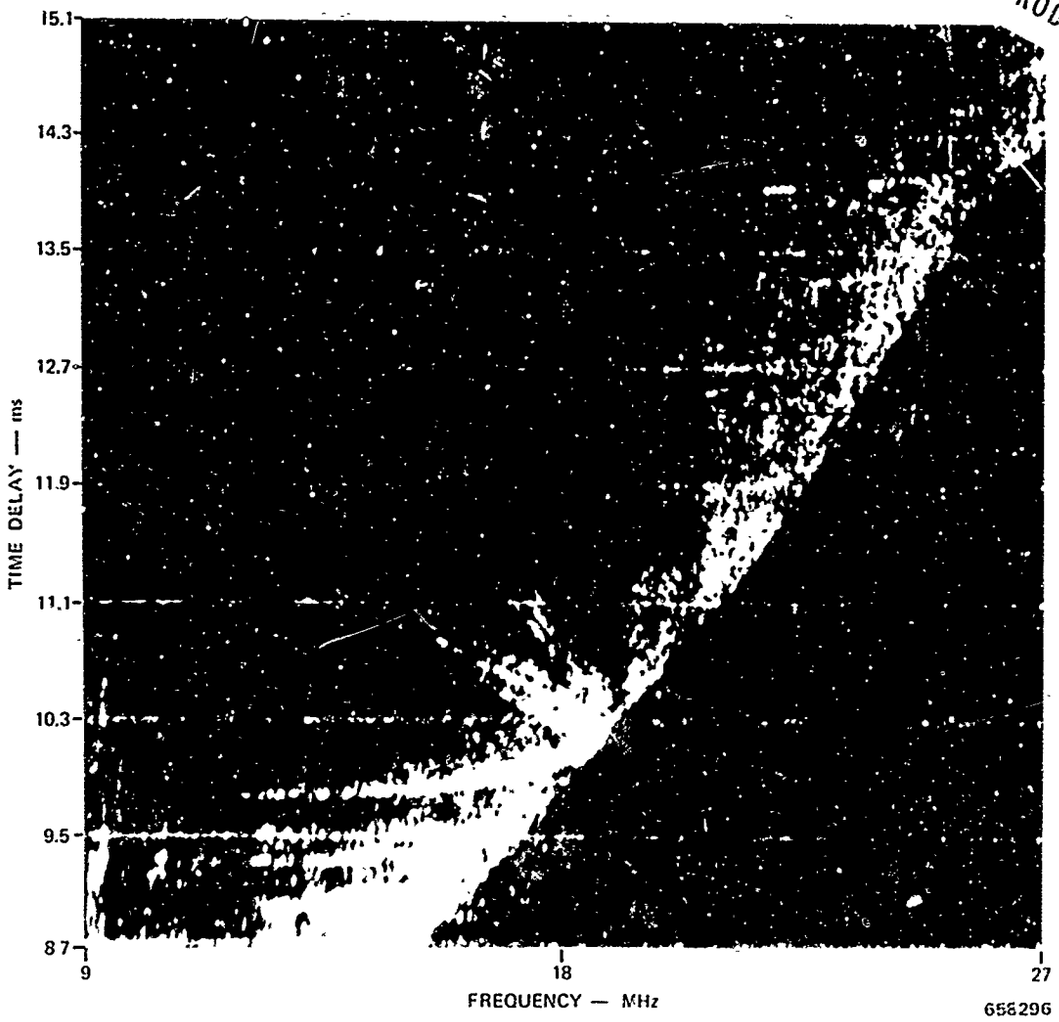

FIGURE 24 BACKSCATTER IONOGRAM SHOWING O-X SPLITTING IN MINIMUM-TIME-DELAY FOCUSING LINE

Under single F-layer propagation conditions this focus-line splitting is observable 75 percent of the daytime. It is most consistently observed on an intensity-modulated display where visual integration assists in making the identification. Furthermore, receiver and display gains must be carefully adjusted in order to not exceed the dynamic-range limitations. Magnetoionic splitting typically separates focus lines by 50 to 150 μs, with an average 3-dB delay width of 50 to 75 μs for each focus line.

This focus-line separation is generally most clearly discernable at lower frequencies; although occasionally it may be faintly visible up to the maximum frequencies propagated--i.e., the frequencies corresponding to the maximum skip distance for one-hop propagation.

Whether or not O - X splitting is discernible in any focusing enhancement depends not only on system sensitivity and the resolution in time delay and azimuth; it also depends on the characteristics of the focusing enhancement itself. The reflectrix construction [29] graphically determines how much energy may be concentrated in a focusing enhancement; it is not uncommon to have only an abrupt termination at a focusing line but with no energy enhancement.

2. Faraday Rotation on Discrete Echoes

Early in Section III it was shown that magnetoionic splitting was identifiable on composite ionograms from some discrete echoing regions. Ordinary-extraordinary splitting in ionospheric focusing lines is a second manifestation of magnetic-field effects in backscatter data. Now the existence of Faraday rotation as a function of frequency on a single echo at a time will be demonstrated and verified.

Mode interference producing a variation in Faraday rotation as the signal frequency changes is a well-known phonomenon in one-way

ionospheric propagation.[30,31] Recently[20] it was demonstrated that the resulting polarization rotation affects the amplitude of high-resolution backscatter from the sea surface. When linearly polarized antennas are used, families of polarization lines appear in backscatter data that correspond to alternate alignment and crossalignment of the antenna to the net incoming polarization. As much as 10 dB variation in backscatter amplitude, due to this effect, has been observed by Barnum.[20]

This effect was not observable over land because the abrupt variations in σ_o from location to location obscured it. In more than 1400 backscatter ionograms obtained with the high-resolution sounder under winter daytime ionospheric conditions, no clear example of families of polarization lines could be found.

Discrete echoes observed over land with the Los Banos-Lost Hills sounder do exhibit regular amplitude variations with frequency, some of which can be verified to be due to mode interference/polarization rotation.

The portable repeater was operated in central New Mexico for the purpose of comparing the behavior of artificial and natural echoing sources. Figure 25 is a portion of a backscatter ionogram that resulted under winter conditions. The repeated signal was modulated at an audio frequency of 500 Hz, displacing its echo ±500 Hz (±2 ms for a sweep rate of 250 kHz/s) on the delay-frequency backscatter display. Only one repeater sideband is visible here. It has been shifted completely out of the ground backscatter return.

Nearly periodic amplitude variations of 125 ±25 kHz spacing are visible over 18 to 20 MHz on the repeater echo; at higher frequencies dispersion resolves the echo into two modes, neither of which exhibits this regular amplitude variation with frequency. Reprocessing this data

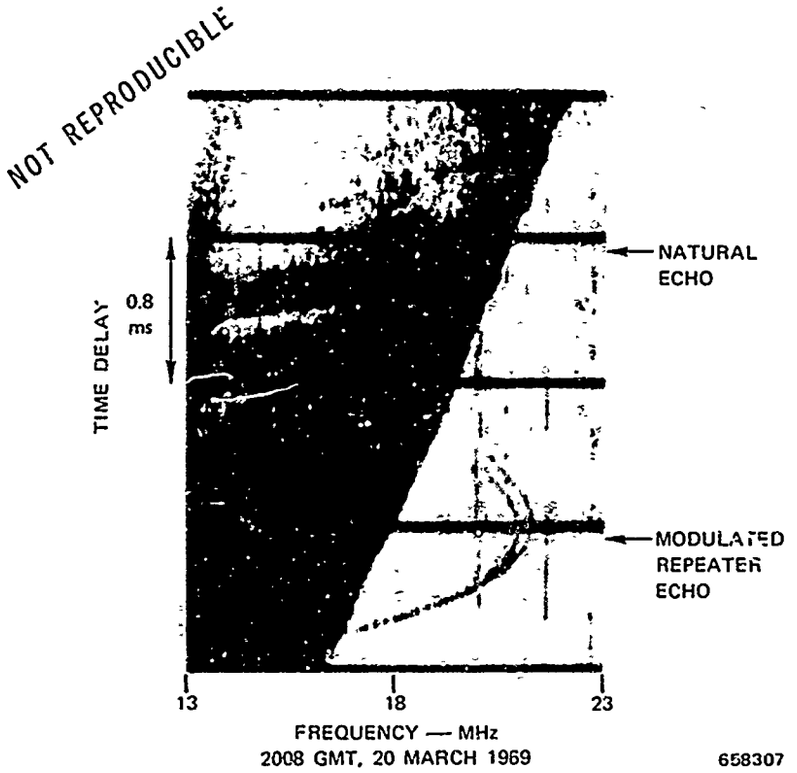

FIGURE 25 PORTION OF BACKSCATTER IONOGRAM WITH REPEATER LOCATED NEAR NATURAL ECHOING REGION IN NEW MEXICO

frame with different delay resolutions shows that at the frequency where these two modes become delay resolved, the beating effect is reduced.

According to the point-echo model of Section III-A, there should be up to 16 discrete modes present. The eight longer-delay modes are significantly weaker and thus not seen in this figure. Of the remaining eight modes, only four distinct modes are apparent; however, some indication that they exist may be found in Figure 26. Here, displaced A-scans of the spectrum analyzer output are plotted so that amplitudes may be measured. The gain settings were used in order to observe the amplitude structure of the natural discrete echo as well as that of the repeater echo.

The point of interest here is that the natural echoes has a pattern of amplitude fluctuations similar to that of the repeater--

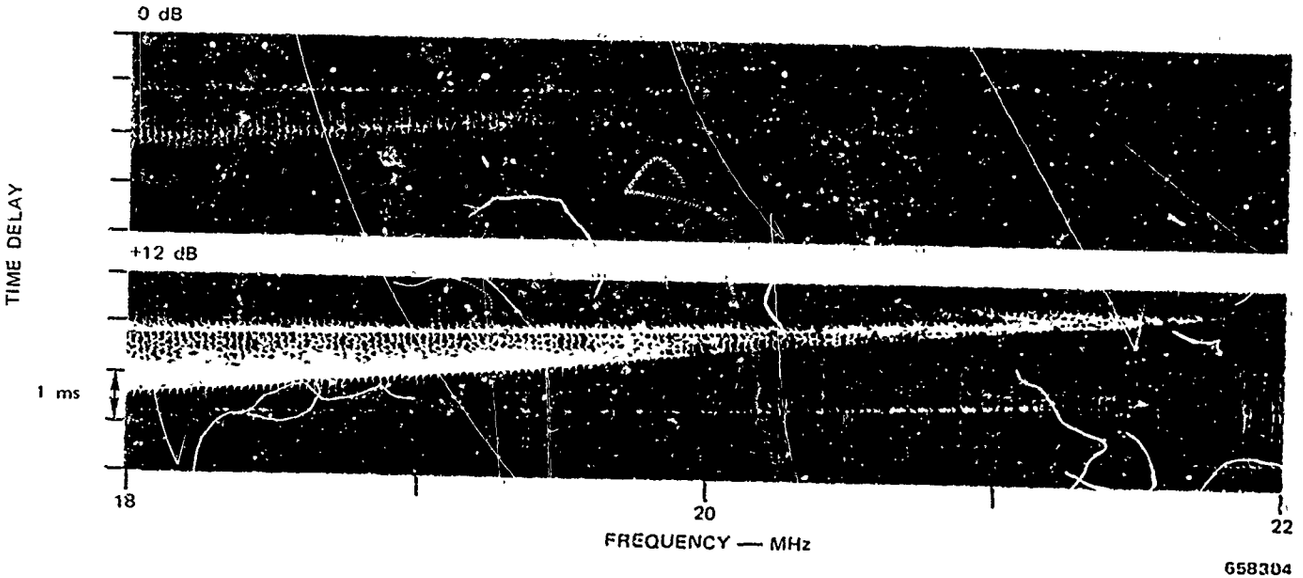

FIGURE 26 EXPANDED PORTION OF FIGURE 25 PROCESSED AT TWO GAIN SETTINGS TO SHOW FLUCTUATION WITH FREQUENCY FOR REPEATER AND FOR NATURAL ECHOING SOURCE

further evidence that the natural echoing region is of small spatial extent. If it were larger than roughly 100 μs (15 km) in delay depth, the polarization of energy received from different portions of the scattering region would be sufficiently variable to cancel out regular amplitude variations with frequency due to this mechanism.

Regular amplitude fluctuations produced by mode interference/polarization rotation are a common attribute of discrete echoes observed with the high-resolution backscatter sounder. The 210-frame sequence of backscatter ionograms described in Section III-B produced some 31 discrete echoes in a 4-ms range gate. All of these echoes exhibit these quasi-periodic amplitude variations, which result in a "blobby" echo structure. Blob spacing varies from 100 kHz (the smallest spacing observable for the data display used) to 1.5 MHz at frequencies of 0.6 to 0.9 MUF.

It has been found that several distinct types of amplitude fluctuation are occurring. Most echoes exhibit closely spaced blobs (100 to 200 kHz) at one time or another over a frequency extent up to several MHz. In addition, there is a more slowly varying component (in frequency) that often occurs simultaneously with the rapid fluctuation. Finally, there are numerous changes in amplitude associated with modest ionospheric disturbances; such amplitude changes are focusing enhancements that alternately increase and decrease the energy from a region in the delay-frequency domain. Examples of each of these three types of amplitude fluctuations are reproduced in Figure 27.

Rapid amplitude fluctuations with signal frequency [Figure 27 (a)] are reasonably associated with the mode-interference mechanism just discussed. Ionospheric disturbance fluctuations are easily picked out of a rapid time sequence of ionograms; groups of discrete echoes along some locus in the delay-frequency domain vary in signal strength almost in unison [Figure 27(c)].

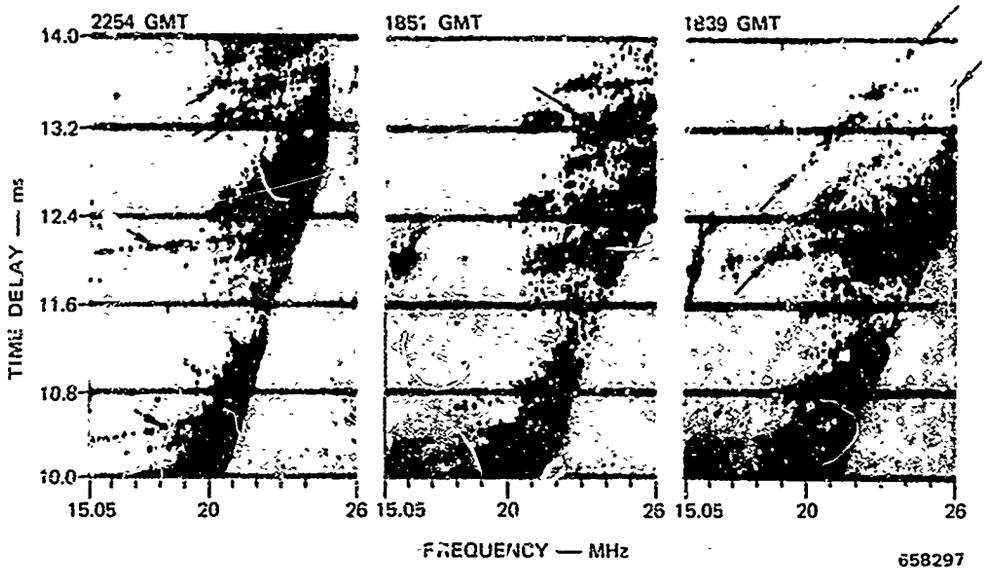

FIGURE 27 TYPES OF AMPLITUDE FLUCTUATIONS WITH FREQUENCY SEEN ON DISCRETE ECHOES—4 MARCH, 1969

The amplitude variations in Figure 27(b) are somewhat ambiguous as to their origin. In only a few instances may they reasonably be thought to arise from disturbance focusing. One would have to observe related variations in nearby echoes with the passage of time, and this is not discernible. Certainly mode interference/polarization rotation could produce some of the slower fading component. However, the fact that closely spaced discrete echoes may exhibit widely different amplitude variations with frequency leads one to suspect that the ground-scattering processes may contribute to these fluctuations.

To investigate the specific scattering characteristics of discrete echoes is beyond the range of this study. The types of behavior one might look for that could produce fairly complex signal-strength variations with frequency would be (1) polarization sensitivity, (2) extended targets, whose net cross section could vary rapidly with frequency, (3) sources of backscatter enhancement such as resonant structures that would produce strong echoes and would be frequency sensitive.

One further manifestation of mode interference/polarization rotation has been observed on intense discrete echoes that show mixed modes. Somewhat rarely all mixed modes are visible and of the proper strength, so that alternate peaks and nulls may be observed. Figure 28(a) shows the mixed modes in such a data frame. Comparing this echo to the simulation of Figure 11 one identifies "mode" (i) as unresolved UX/LX and UX/LO modes and "mode" (ii) as unresolved LX/UO and LO/UO modes. Over 19 to 20 MHz both of these mode pairs show nearly periodic signal-strength fluctuations with frequency. At 21 MHz these mode pairs become delay-resolved by dispersion, and the regular fluctuation with frequency is no longer apparent.

The rotation of the received net polarization angle ψ with frequency is proportional to the difference in phase path between the O and the X modes when they are not delay-resolved.[33] Relating phase path to group path (T) one has the simple relation $\delta\psi/\delta f = \pi(T_o - T_x)$. This means that a blob spacing of 1 MHz (π radians in the phase angle ψ over a change in frequency of 1 MHz) corresponds to $\Delta T = T_o - T_x = 1$ μs.

For the mode pairs (i) and (ii) considered here, the modes are different over one portion of the path only. Thus (i) contains O - X mode interference on incoming only, while (ii) has it on outgoing only. The above relation is usable as in one-way propagation. In Figure 28(b) the delay separation vs. frequency for these mode pairs is plotted in part from measuring blob spacing and converting to delay separation, and in part from direct measurement of mode separation. Apart from a signal dropout over 20.1 to 20.8 MHz, these curves indicate that mode interference is taking place. As delay separation increases, the modes eventually are resolved and the beating effect ceases. Since the outgoing path was shorter than the incoming path, O - X separation at frequencies near the MUF is expected to be larger on mode pair (ii) than on mode pair (i). This is borne out by Figure 28.

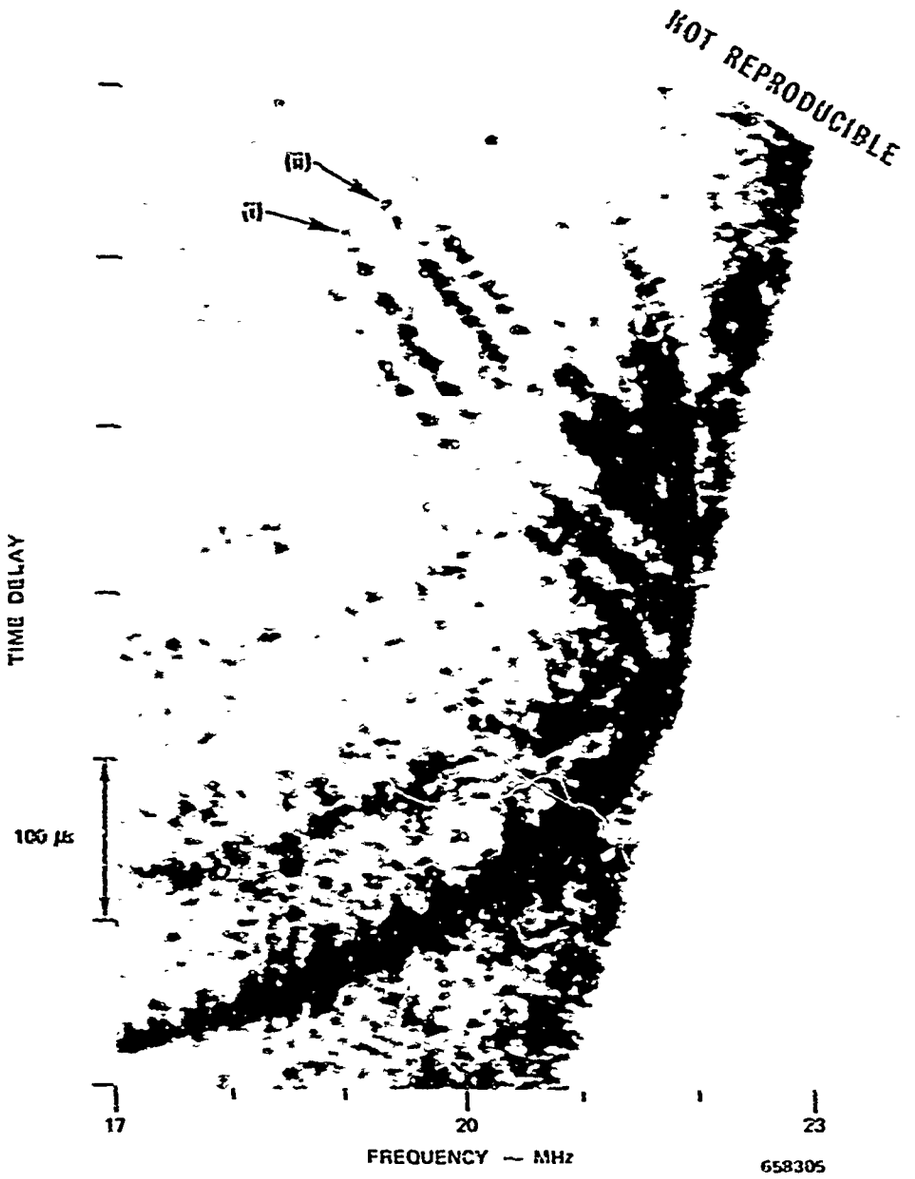

FIGURE 28(a) PAIRS OF MIXED MODES (i and ii) ON DISCRETE ECHO FOR WHICH DELAY SEPARATION IS INFERRED BY BLOB SPACING AND ALSO DIRECTLY MEASURED—4 MARCH, 1969, 2234 GMT

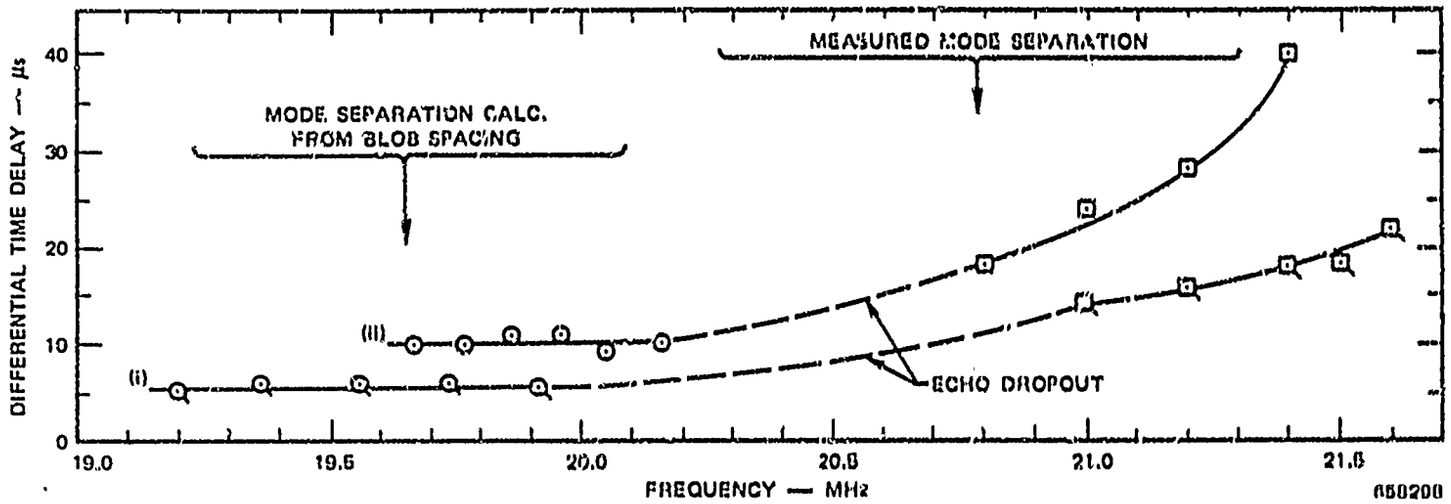

FIGURE 28(b) EVIDENCE OF FADING CAUSED BY MODE INTERFERENCE BETWEEN (I) UX/LX AND UX/LO, AND (II) LX/UO AND LO/UO

It should be mentioned that a modest disturbance was present at the time of this data run, and it produced focusing, which made the echo unusually strong. This does not affect the argument at hand.

In addition to providing further verification of the presence of polarization rotation effects on discrete echoes, this example brings one to a significant conclusion: This mode interference would not have happened unless the scatterer were of predominantly linear polarization.

3. Ionospheric Disturbances

It is not the intention of this report to investigate ionospheric-disturbance phenomena as viewed with the high-resolution sounder. However, some rather remarkable disturbance echoes (particularly on backscatter ionograms) have been observed by the author while using this system. For the purposes at hand it will be sufficient to describe how disturbance phenomena interact with discrete echoes.

One type of disturbance commonly observed affects the leading edge of the backscatter ionogram. It has a well known counterpart in forward-oblique soundings,[32] as Figure 29 can attest. A Bearden-Los Banos forward-oblique sounding in part a of this figure exhibits a wave-like structure that proceeded to lower frequencies as time progressed. A backscatter ionogram obtained four minutes later exhibited the back-scatter signature for this particular disturbance. Note the existence of backscatter energy from the west; it is not disturbed.

One should recall again that under undisturbed conditions the leading edge is principally determined by the outgoing portion of the backscatter path. Under severe conditions it may alternate between the outgoing and incoming portions of the path. This type of disturbance echo is of no further interest here except to note that under daytime winter conditions, it has been observed to occur at rates of 0 to 15 times a day.

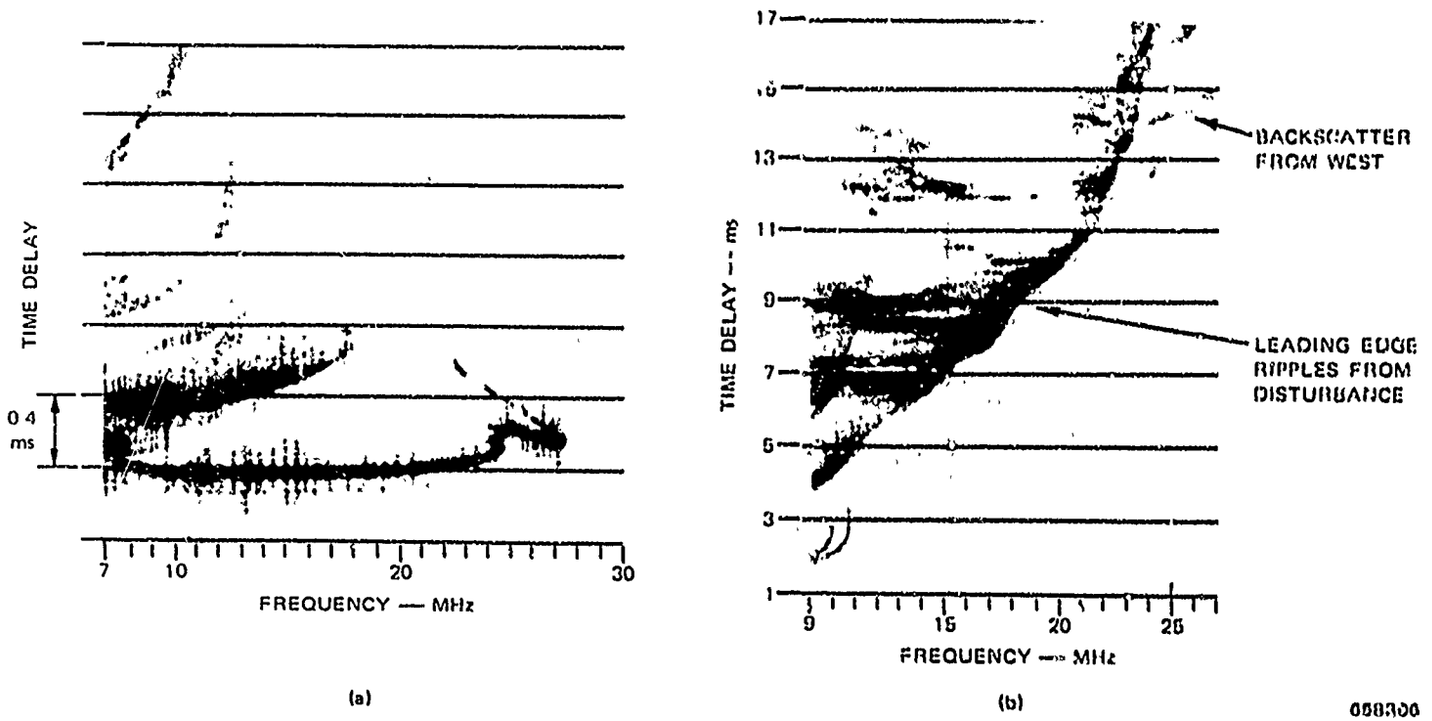

FIGURE 29 RELATION BETWEEN DISTURBANCE EFFECT ON OBLIQUE IONOGRAM AND DISTURBANCE EFFECT ON BACKSCATTER IONOGRAMS

A second type of disturbance echo, much more commonly observed than the first, is characterized by focusing (and defocusing) bands within the backscatter return. Frequently these disturbances do not alter the leading edge of the backscatter return. Examples of two such focusing bands are shown in Figure 30: arrows are attached to each fo-

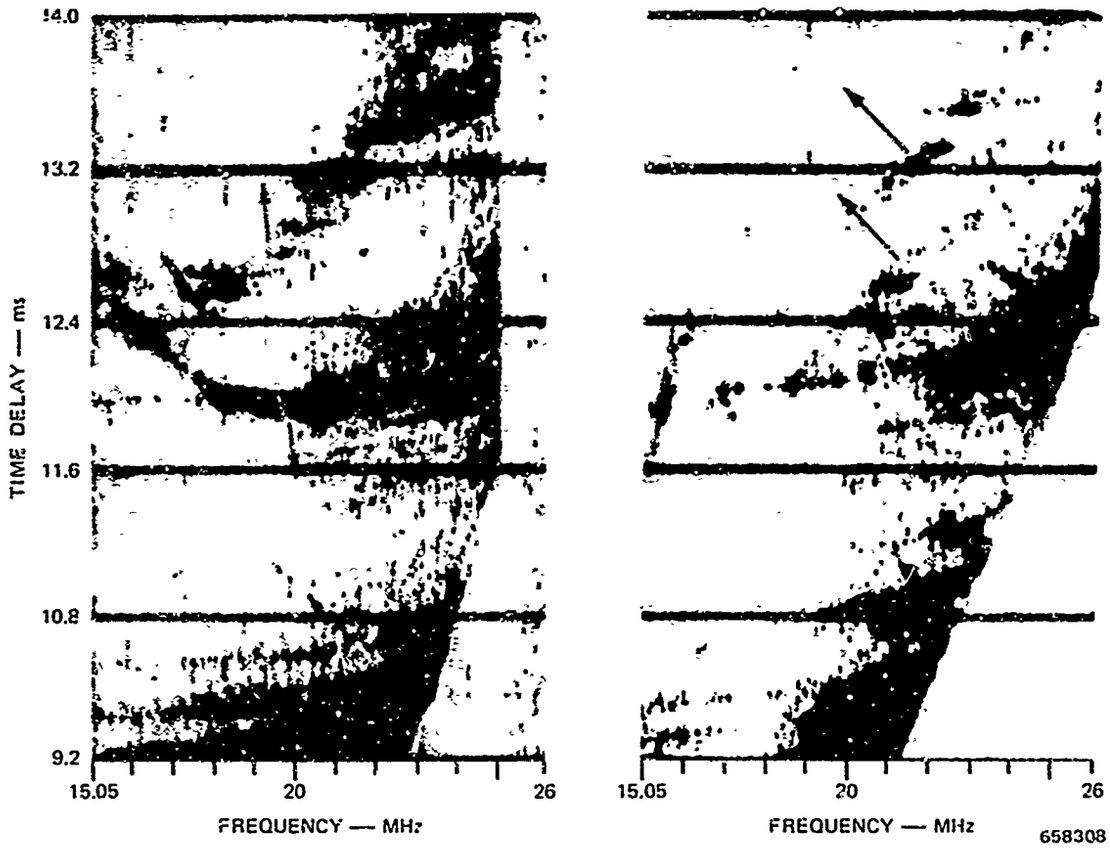

FIGURE 30 TWO TYPES OF DISTURBANCE EFFECTS FROM MODERATE DISTURBANCES

cusing enhancement indicating its general direction of movement with time. Backscatter ionograms must be made at least once per minute to follow the movement of these disturbance echoes.

These bands produce a focus-defocus effect on the signal strengths of discrete echoes, usually resulting in a 3-to-10-dB peak enhancement over the undisturbed condition. Rarely, the enhancement may be as large as 20 dB.

The dynamic range of this type of display frequently does not allow observation of a discrete echo throughout the entire passage of a disturbance. However, when it is visible, a discrete echo at frequencies less than 0.9 MUF exhibits only small delay movement. Occasionally no delay variations are discernible, but a large fraction of the time the delay shift is less than 100 to 200 μs. It is felt that the portion of a disturbance where maximum delay shift would be seen corresponds to the defocus region. Thus, large delay shifts are usually not recorded.

Disturbance signatures on backscatter ionograms produce simultaneous amplitude fluctuations on groups of discrete echoes that are sufficiently densely located. The focus of the focusing band may shift to different frequencies as it affects different discrete echoes (e.g., a slanted band on a backscatter ionogram). Nevertheless, one may still characterize disturbance focusing as a phenomenon that affects "clusters" of discrete echoes.

While comparing backscatter simulation with available backscatter data, Georges and Stephenson[5] expressed concern that focusing enhancements from ionospheric disturbances may be confused with localized echoes due to the variation in ground reflectivity. With the high-resolution sounder used in the present studies, it has been found that this ambiguity is not present even if only a single backscatter record is available. While the average delay spread of a discrete echo is 50 μs or less, a focusing enhancement is characterized by several times this delay extent. Secondly, discrete echoes are ionogram-shaped, while only rarely will a focusing enhancement exhibit an ionogram-like structure on

a backscatter ionogram. Finally, the rapid quasi-periodic amplitude variations with frequency found on discrete echoes are not observed on disturbance enhancements. A rapid time sequence of soundings (preferably one per minute) is useful in separating persistent discrete echoes from the continually varying disturbance enhancements, but it is not necessary.

Straightforward separation of discrete echoes from disturbance signatures was found to be more difficult when using a subarray (1/8 the total aperture) for receiving at Los Banos. Fewer discrete echoes were discernible with the broadened beam, and these were more spread in delay. The full 2.5-km aperture is needed to make this very clear distinction between fixed, discrete echoes and disturbance enhancements.

IV STRENGTH OF DISCRETE ECHOES

A. Visibility Measurements

The numerous discrete echoes described in Section III are a manifestation of localized increases in the ground reflectivity. In this section measurements concerning the brightness or strength of these echoes will be presented. Visibility measurements demonstrate that the echoes are a prominent feature of backscatter data obtained with the high-resolution sounder. Visibility here is taken to mean the intensity of a discrete echo relative to the intensity of backscatter at adjacent values of delay and azimuth. While this measurement does not give values of absolute cross section of the discrete echoing areas, it is a good indicator of the cross section relative to the background. Values of discrete echo visibility are sensitive to the characteristics of the sounding system used (as described in Section II).

In Section III a 30-frame sequence of time-delay-vs.-azimuth backscatter displays was analyzed to find some 71 discrete echoes. For these data the integration time T was 0.5 s, the minimum effective pulsewidth was 8 μs, and the 3 dB azimuthal beamwidth was 0.38 degrees. Propagation was via the F layer (a center frequency of 19.122 MHz), and the elevation angles ranged from 10 to 20 degrees.

Of the discrete echoes identified, half of them were considered scalable in terms of a visibility ratio. Of the remainder, several were ambiguous due to transmit antenna steering. Others were too close to the leading edge, where ionospheric focusing varies rapidly with small changes in delay and azimuth, and also where mixed modes on discrete echoes are most likely to cause confusion. There were discrete echoes

at the longer delays in the 10-to-14-ms range gate that were strong enough to be recorded, but the surrounding background backscatter return was too weak to allow a measurement of visibility.

The visibility of a discrete echo is measured when its amplitude is at a peak, thereby minimizing the uncertainty imposed by polarization rotation with time. On the other hand, the factors in the radar equation change slowly with small changes in time delay (<200 μs) and azimuth (<1 deg), so that visibility is a good measure of cross section relative to the background. In order to minimize the influences of delay and azimuth sidelobes on the measured background energy, the background is measured at a different delay and a different azimuth from those of the discrete echo of interest.

With these limitations in mind the "reliable" echoes showed visibilities ranging from 6 to 29 dB, with a mean around 14 dB. The lower value of 6 dB is set because it was one of the criteria for selection of a localized backscatter echo as a discrete echo.

One cannot directly compare discrete echo visibilities on time-delay-vs.-azimuth displays with those found on time-delay-vs.-frequency backscatter ionograms. The backscatter ionogram display is usually an intensity-modulated facsimile readout with maximum dynamic range of 15 dB. It can be said, however, that the visibilities of 10 to 20 percent of the discrete echoes found in backscatter ionograms (under F-layer conditions at mid-ranges of 8 to 15 ms) exceed the dynamic range of the display. For the particularly intense discrete echo found on the backscatter ionogram with A-scan display in Figure 26 the maximum visibility was 25 dB.

B. Effect of Incoherent Integration

The visibility measurement is approximate in that it does not consider sources of fluctuation such as noise and interference plus the incoherent fluctuating nature of scatter from extending surfaces. Any measurement of cross section per unit area σ_o is meaningful only as an ensemble average (frequently approximated by a time average). It should be noted, however, that the effect of Faraday rotation is not removed by incoherent integration of the data. Average echo strengths are most reliable when measured during a peak in this amplitude variation.

Repetitive, once-per-second frequency sweeps over 500 kHz were made at a fixed antenna steer for a ten-minute period in July of 1969 and in October of 1969. Propagation was via sporadic E (some normal E is present, too) for the July experiment, while the October experiment used F-layer propagation. The receiver was operated at fixed gain, and a 1-ms range gate near 9 ms was chosen to place several strong discrete echoes within the analysis range. For the July experiment the portable repeater was operated in the vicinity of these discrete echoes (central New Mexico); it was not available for the October experiment.

At a later time the analog-recorded product-detector output was A/D converted with sufficient prefiltering to remove the dc component and any aliasing above 500 Hz. The sample frequency was 2020 Hz and the record length was 1968 samples (filled out with zeroes for a total of 2048). Sampling was synchronized by a timing signal from the cesium clock that had been recorded on the analog tape. The time samples were weighted with a Hanning window in order to reduce sidelobes (Figure 6), and then digital spectrum analysis (using FFT procedures) was performed to obtain 1-Hz resolution. By averaging the squared modulus (energy) of the computed spectrum for various periods of time,[33] the averaged spectrum becomes a measure of average backscatter power vs. delay.

The parameters of this experiment are summarized in Table 1. Experimental conditions were nearly identical for the July and October

Table 1

EXPERIMENTAL PARAMETERS FOR THE RUNS OF JULY 28, 1969 AND OCTOBER 23, 1969

Date	7/28/69	10/23/69
Time	2125-2135 GMT	2214-2221 GMT
Antenna Steers	Transmit 86° Receive 90°	Same
Frequency	16.501-16.0 MHz	16.0-16.499 MHz (0.85 MUF)
Elevation Angle	6° nominal	15-20°
Repeater	Used	Not Used
Ionospheric Conditions	Sporadic E, some normal E-layer	F-layer, undisturbed
Comments	All equipment same, especially receivers in fixed-gain mode. Data processing same for both days.	
Digital Parameters	Sample frequency, 2020 Hz; sample size, 1968 plus zeroes equals 2048; $(\text{cosine})^2$ time weighting.	

runs, the principal difference being E_s propagation for the July run and F-layer propagation for the October run. Although signal frequencies were nearly the same, elevation angles were 6 degrees for the E_s-layer data and nominally 15 degrees for the F-layer data.

The effect of incoherently integrating successive frequency sweeps of one-second duration is demonstrated for the July data in Figure 31, where backscatter power vs. time delay is plotted for 1-, 5-, 20-, and 40-second averages. The repeater was modulated at 100 Hz to produce

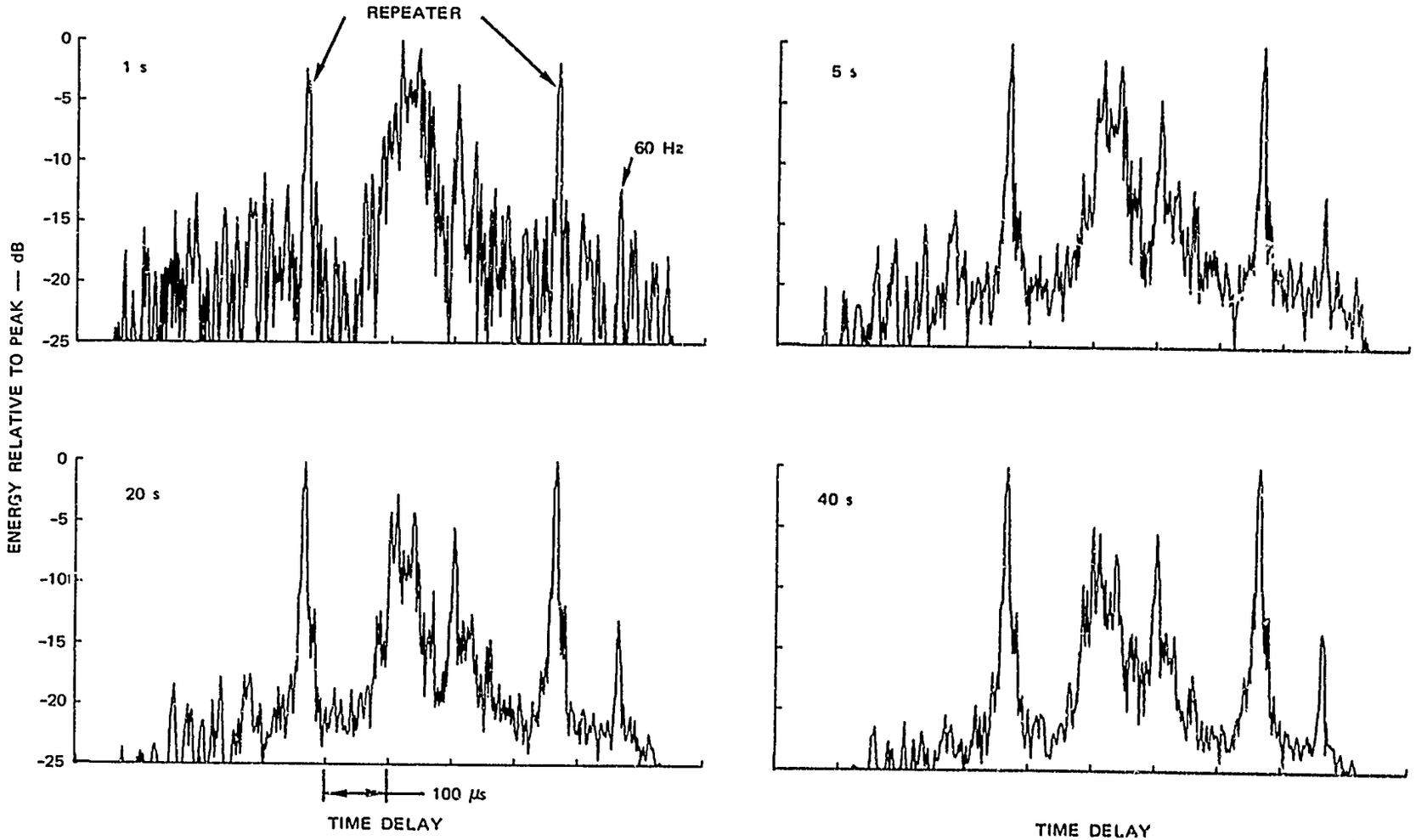

FIGURE 31 BACKSCATTER ENERGY VERSUS TIME DELAY FOR VARIOUS INCOHERENT-INTEGRATION PERIODS— 28 JULY, 1969, 2125 GMT

sidebands 200 Hz (400 μs) apart as indicated in the figure. Each plot is normalized to the peak echo, which is the repeater return in this case. A 60-Hz-power-line component is present in much of these data (frequency of the spectrum analysis increases in the direction opposite to increasing time delay).

Numerous sources of second-to-second fluctuations on this data run are minimized by the averaging procedure. Noise and interference contribute to such fluctuation, but it was also discovered that second-to-second incoherence of the SFCW generators may produce a sizable fluctuation. This last source of fluctuation is removed with about 5 seconds of integration. Propagation via the sporadic-E mode may also be responsible for signal-strength variations with time. Finally, it is reasonable to expect a fluctuation component due to the nature of signals scattered from the extended surface of the ground.[23] For the purposes at hand it is sufficient to note that these short-period fluctuations are effectively removed by integrating for 10 to 20 seconds.

A one-to-two-minute fluctuation is also present on these data, whereby discrete echo amplitudes may vary. Discrete echo components do not fade synchronously, but rather this fluctuation progresses across the delay gate with time. The fluctuation also affects the repeater return. It is conjectured that this fluctuation is caused by Faraday rotation variation with time.

Figure 31 represents a 40-second period in which the repeater echo and the strong discrete echoing region between the repeater sidebands were reasonably steady. Note that the delay width of the repeater return after averaging for 40 seconds is only 7 μs; the minimum achievable with the processing parameters used is 3 μs. This fact allows one to rule out ionospheric factors such as dispersion and magnetoionic splitting as sources of the delay spread in the natural echo.

The bright natural echo in Figure 31 (the same echo identified as echo H1 in Figure 22) has several impulse-like components within the total echo width of 80 μs. A separate discrete echo is also seen about 100 μs from the main echo.

Some three months later this experiment was repeated under F-layer conditions but without the benefit of the portable repeater. Figure 32 shows a typical set of 1-, 5-, 20-, and 40-second integration periods for these data. Although the range gate is slightly shifted, the delay profile of echo H1 is remarkably similar to that of the summer run. That is, as delay increases, a localized decrease in the reflectivity is followed by a 20-dB increase about 80 μs wide, which in turn is followed by separate point-like components. At short delays in Figure 32 the 300-μs-wide region of apparent increased reflectivity is real.

The slow fluctuation with time is slower on the F-layer data roughly by a factor of 2.

Attempts at using longer integration periods have several effects, pointed out in Figure 33 where 120-s averages are compared for the two runs. First, the slow fluctuation on echo H1 is apparent for the July data, as it is now some 5 to 10 dB weaker relative to the repeater return. The localized decrease in reflectivity just ahead of this echo is slightly less apparent for both the July and October runs. Thus, while 40-second averaging periods made when the slow fluctuation is at a peak generally produce similar delay profiles for echo H1, the longer 120-second averaging period usually shows the effects of this fluctuation.

The conclusion reached here is that judiciously choosing short integration periods reduces the effect of rapid fluctuations and increases the visibility of discrete-echo components. Longer periods do not further increase the visibility, and the slow fluctuation often causes discrete-echo components to vary in strength. Polarization control of the sounder

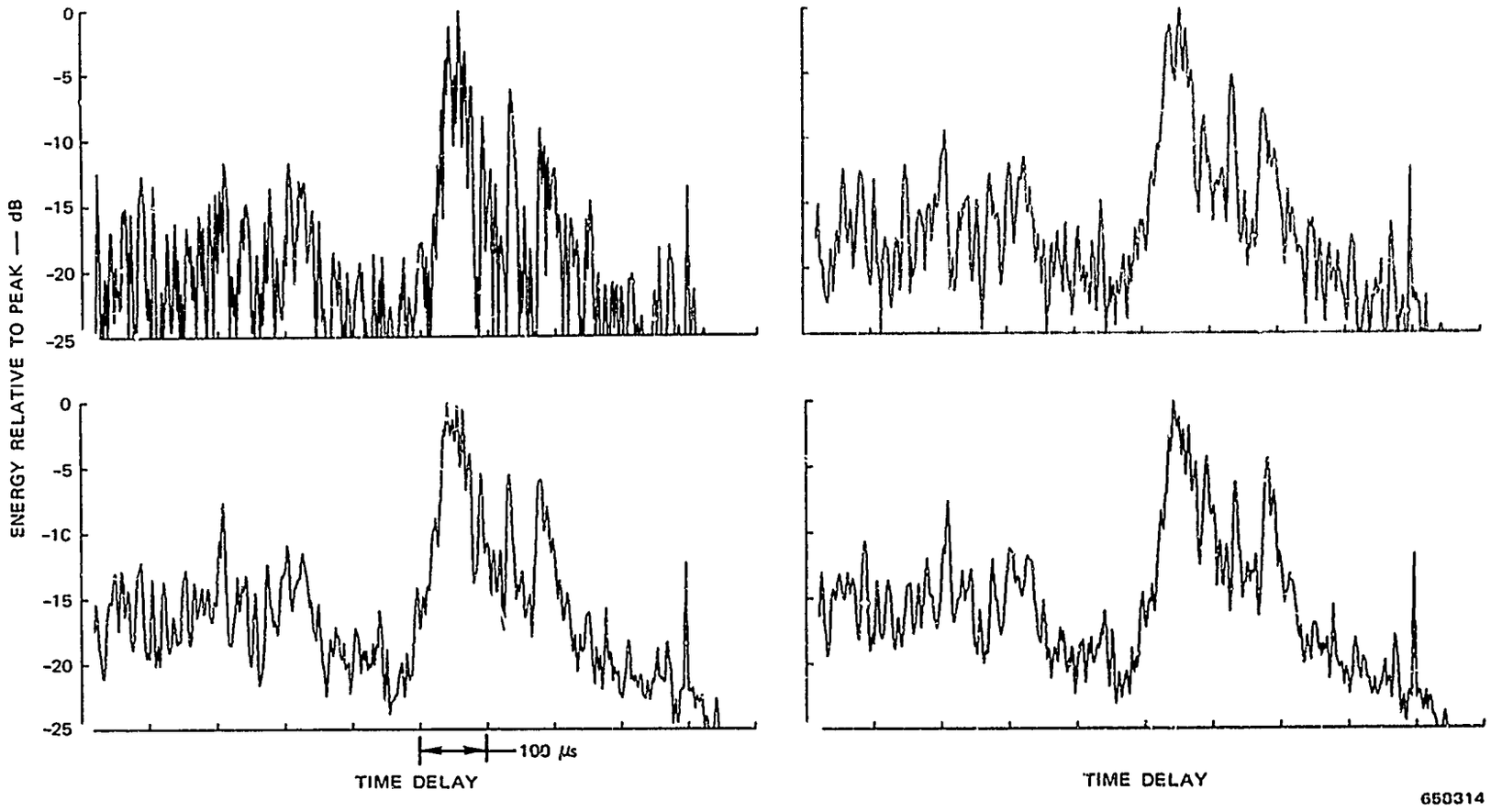

FIGURE 32 BACKSCATTER ENERGY VERSUS TIME DELAY FOR VARIOUS INCOHERENT-INTEGRATION PERIODS— 23 OCTOBER, 1969, 2214 GMT

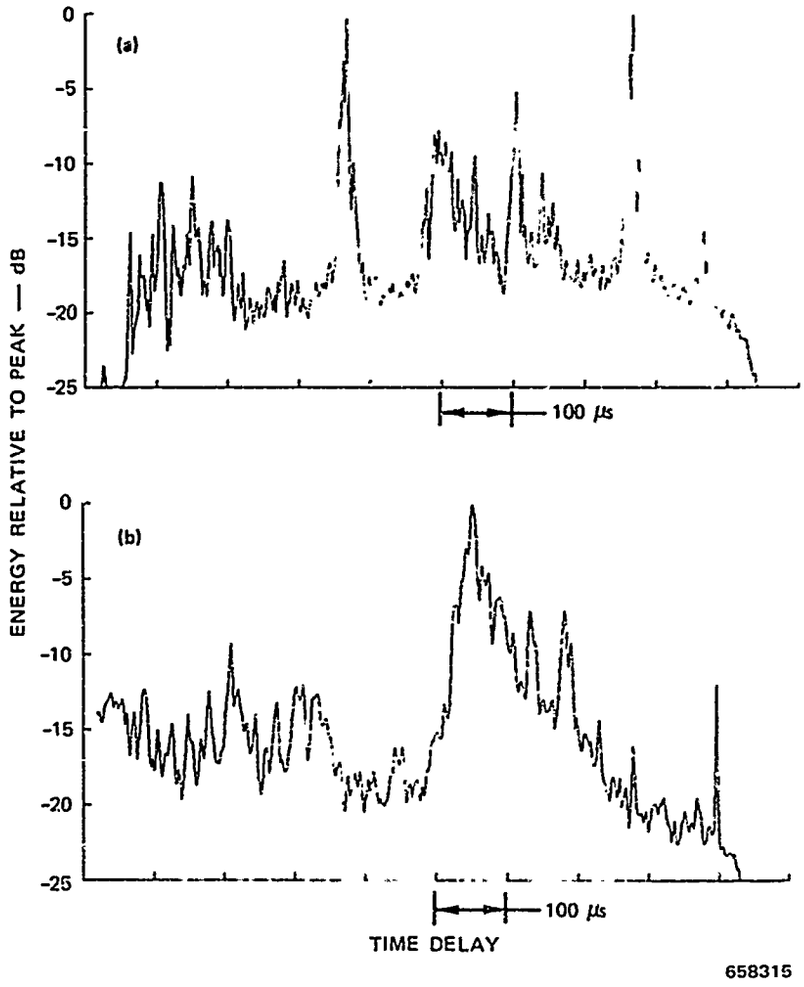

FIGURE 33 COMPARISON OF 120-SECOND INCOHERENT-INTEGRATION FOR THE JULY AND OCTOBER RUNS (a and b respectively)

antennas would help to reduce a slow fluctuation caused by Faraday rotation with time.

C. A Measurement of Cross Section Per Unit Area

During the summer experiment it was possible to use the repeater to measure the absolute cross section of echo H1. When the repeater is located sufficiently close to a discrete echo of interest, ionospheric effects and the various factors of the radar equation are essentially

the same for the repeater echo and the natural discrete echo. Comparison of the repeater echo with the natural echo gives a measure of cross section since the repeater cross section (σ_R) is known (see Section II). The major uncertainty in σ_R arises because the repeater antenna gain is not measured in the field; thus the antenna gain uncertainty is placed at 3 dB.

Figure 34 is a 10-second average of backscatter power vs. delay when both repeater and echo H1 were at a peak in the Faraday-rotation-with-time variation. The actual repeater delay is indicated by an arrow. At this time the repeater parameters were adjusted for a cross section of 2×10^6 m^2.

The approximate ground area for locally strong echoes where the self noise problem is minimal is approximated as 0.6 km in range and 13.6 km in cross range. These values correspond to the delay and azimuthal widths 6 dB down from the peak. Thus in Figure 34 the level of the repeater return corresponds to a σ_o (cross section per unit area) of 2.5×10^{-1}. The vertical scale is labeled in values of σ_o relative to this peak value.

Within 100 μs of the actual repeater location, where this measurement is most accurate, the discrete echo has values of σ_o exceeding 10^{-1}. This discrete echo is one of the two or three brightest observed in this study; however it is estimated that several other discrete echoes are within an order of magnitude of the strength of echo H1.

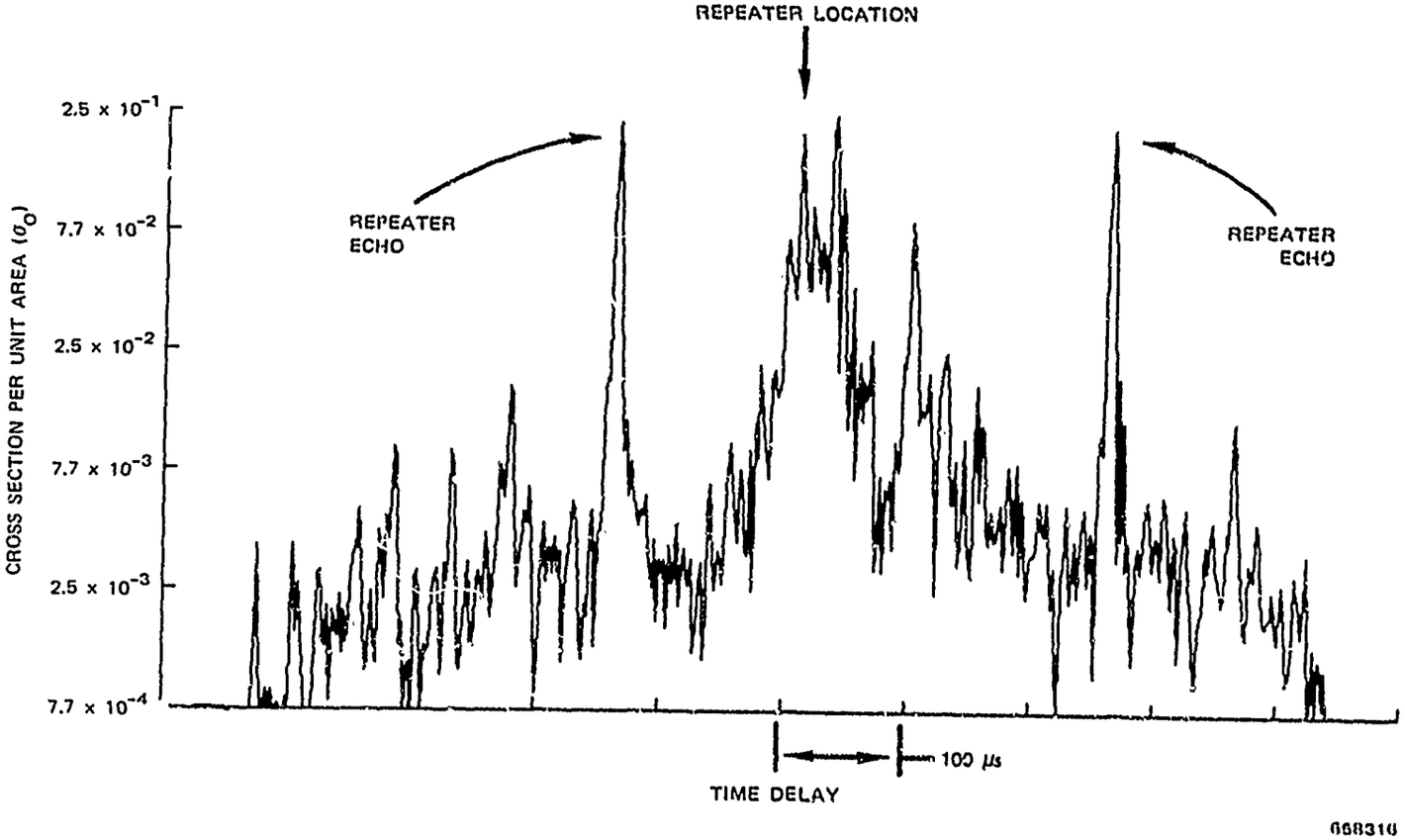

FIGURE 34 BACKSCATTER POWER VERSUS TIME DELAY, 10 SECOND AVERAGE

V SUMMARY OF RESULTS, AND CONCLUSIONS

A. Discrete Echoes in Backscatter Soundings

At this point it is appropriate to draw together the various new observations made possible by using a high degree of time-delay and azimuth resolution in backscatter sounding of the ionosphere. It is worth repeating that these measurements and the inferences therefrom have sought to explore the use of discrete echoing sources on the ground for separating out the effects of ground scatter.

Numerous fixed, prominent echoes in backscatter soundings are observed to appear when one employs an antenna with a beam six times narrower than any previously used, and a waveform that can realize very short equivalent pulse lengths while effectively discriminating against the interference typically met in HF practice. These fixed echoes are a manifestation of very localized, abrupt increases in the ground-backscatter coefficient.

These bright spots are superimposed on the more smoothly varying background return. With the increased resolution used in the previous study, it is now possible to discern directly from backscatter data that over large areas nominally a few hundred km on a side the background reflectivity may differ from that of adjacent areas of comparable size by amounts up to 15 dB. However, the point-like echoes are the most prominent feature of varying ground scatter as viewed with this type of sounder, and this study has concentrated on exploring the use of their characteristics.

Over a 600-by-700-km region, principally in Colorado and New Mexico, it is possible to identify 70 such point-like echoes. Ten percent of

these echoes are visible more than 80 percent of the observing time (daylight hours).

It is found that such discrete echoes appear in wide-sweep backscatter ionograms as "composite ionograms"--the two-way counterparts of one-way, forward-oblique ionograms. For the first time it is possible to discern detail in composite ionograms from which detailed inferences about ionospheric propagation can be made.

The strongest of these discrete echoes show numerous mixed modes that are shown to be a consequence of time-delay-separated combinations of (upper)/(lower) rays. In addition, it is now possible to delineate (ordinary)/(extraordinary) mode splitting on these echoes. A raytracing simulation including the magnetic field shows that on backscatter ionograms the observed discrete echo shape with its multiple modes can be explained by assuming that the scatterer is a linearly polarized point scatterer. For a single-layer ionosphere at frequencies near the MUF, sixteen separate modes are predicted, and a maximum of fourteen of these modes have been observed on a single backscatter record.

Discrete echo strength varies widely from one mode of illumination to another. Upper-ray modes in particular may be as much as 30 to 40 dB weaker than the strongest lower-ray mode. They are weaker because these modes are inherently defocused relative to lower-ray modes, and because their increased dispersion spreads the energy in time delay. Furthermore, these modes are more susceptible to ionospheric tilts, which have the effect of changing the azimuth angle of arrival and therefore causing energy from a given scatterer to arrive at angles outside the receiving antenna main lobe.

Virtually all discrete echoes show a quasi-periodic fluctuation with signal frequency. This effect is explained as a Faraday-rotation variation with frequency. A 100-to-200-kHz frequency spacing between successive

signal peaks is common for winter, daytime, F-layer propagation. Operating the sounder in a repetitive, narrow frequency sweep at a fixed antenna steer position, it is now possible to observe the variation of Faraday rotation with time on a single echo at a time. One- to four-minute periods are typical.

Backscatter from land was inspected for evidence of the families of polarization lines observed by Barnum[20] in backscatter from the sea. From the scattering viewpoint, if land were as spatially uniform as the sea surface, and if backscatter from land were mainly linearly polarized, then one might expect to see the families of lines that indicate constant received polarization. In more than 1400 such ionograms obtained for winter daytime conditions for which this effect is clearly observable over the sea, no clear example of polarization lines from land backscatter could be identified. It is conjectured that the ground-scatter coefficient changes sufficiently over small increments of time delay and azimuth to preclude the appearance of polarization lines. Furthermore, over regions of land where the scattering is uniform from place to place (plains areas for example), it is likely that the scatter coefficient is weak relative to that of the bright spots. Thus, inefficient scattering on the ground precludes observation of polarization lines, a property of ionospheric propagation.

In principle, the loci of polarization lines could be determined by connecting corresponding Faraday-rotation signal peaks from discrete echo to discrete echo. However, the discrete echoes observed in this study were too widely separated to permit constructing loci in this way.

Discrete-echo signal strength is shown to be also affected by ionospheric disturbances; the principal effect of small disturbances is focusing and defocusing of the backscattered energy. Larger disturbances cause similar focusing effects, but they also produce delay shifts as

large as a millisecond in the leading edge of backscatter. Away from the leading edge--say, at frequencies less than 0.9 MUF for the time delay of interest, large delay shifts on the discrete echoes themselves are seldom seen. It is reasoned likely that the causative disturbance tends to defocus the echo at the same time that the largest shifts occur. It is shown that by carefully inspecting a sequence of backscatter ionograms taken at least once per minute, this source of echo fluctuation may be recognized.

There is yet another component of echo fluctuation on discrete echoes in backscatter ionograms that has been observed. This fluctuation is discernible in the remarkable detail conferred only by the use of high resolution. Several discrete echoes, individually resolved but comparatively close together in slant range and azimuth, occasionally display different patterns of signal strength variation with frequency. For example, two discrete echoes might have rapid echo fluctuations of the same spacings in frequency, while a third echo situated between the first two might have a much larger frequency spacing between peaks and nulls and not be as nearly periodic in this fluctuation. No explanation for this fluctuation in terms of ionospheric factors has been found.

Subsequent work should consider how the characteristic of the scattering source(s) on the ground might contribute to these fluctuations. It is possible that some scatterers are electrically resonant. Alternatively, complex scatterers consisting of the superposition of individual component scatterers may give rise to resultant echoes sensitive to small changes in frequency, elevation and aspect angles, and polarization.

An attempt is made to use the unique capabilities of the sounding system to resolve the "point-like," discrete echoes in slant range and azimuth. Processing up to 500 kHz bandwidths shows that discrete-echo delay widths (the delay interval between points 10 dB down from the peak

return) vary from the minimum discernable 10 μs up to 80 μs. The clearly delay-resolved echoes display point-like components within their delay structure. For one particularly bright echo of 80 μs total delay width, a means is developed to eliminate ionospheric effects (such as multimodes and dispersion) as sources of delay spread by using a portable repeater within the area under study.

In the azimuth domain even the use of the 2.5-km receiving aperture is found not adequate fully to resolve these discrete echoes. The measured minimum values of effective resolution on the ground are 450 meters in range and 6 km in cross range.

Some discrete echoes have visibilities (strength relative to the background return) exceeding 20 dB.

It is noteworthy that the visibility of a given echo seems to a first approximation to be independent of the angle of elevation of the incident energy. Discrete echoes are observed at elevation angles ranging from six to more than forty degrees. The brightest 10 percent of the discrete echoes that can be observed with high reliability have strengths relative to the surrounding continuum that are roughly constant over this whole range of elevation angles. If in the case of discrete echoes, the echo strength decreases as one approaches grazing incidence, then it follows that discrete echoes and the surrounding continuum must decrease together.

Incoherent integration of the FMCW spectrum analysis output was applied to repetitive, narrow-frequency sweeps made at a fixed antenna steer to reduce the effect of signal fluctuations. It is found that several types of short-period fluctuations can be effectively averaged out in 5 to 10 seconds, increasing discrete echo visibility and giving a clearer picture of the variation of ground reflectivity with time delay.

Faraday rotation with time affects the strength of discrete echoes. Since at any instant the Faraday rotation also varies with the length of the path, the echoes do not all fluctuate in amplitude synchronously. By choosing the time interval to be integrated so as to avoid a Faraday null at the time delay of interest, the effect of this fluctuation can be considerably reduced. Averaging periods as long as 120 seconds were used without seriously degrading the structure of the backscatter-power-vs.-delay profile over a delay interval of a hundred microseconds.

A procedure was developed to use a portable repeater to obtain a reasonably reliable measurement of the backscatter coefficient of a particularly bright discrete echo. By placing the repeater in close proximity to the discrete echo of interest and comparing the repeater echo strength (of known cross section) with that of the natural echo, it is possible to show that the peaks in the spatially varying cross section per unit area exceeded 10^{-1}.

As one result of this study it is demonstrated for backscatter coming from the Colorado-New Mexico area that sufficient numbers of discrete echoes are visible for large enough fractions of the time to make detailed inferences possible about propagation to and from localities at many ranges and many azimuths. The resulting composite ionograms greatly assist in identification of specific details of ionospheric propagation discernible clearly for the first time by the use of a high-resolution sounder. The following comments illustrate this:

(1) It is known that there are two major types of ionospheric focusing--time-delay focusing and geometrical focusing.

(2) Presence of such focusing in backscatter ionograms is characterized by curving lines in the time-delay-vs.-signal-frequency domain, whose loci are determined by the ionospheric profile.

(3) The delay and azimuth discrimination afforded by this type of backscatter sounder shows clearly for the first time separate ordinary and extraordinary components of these focus lines.

(4) One- and two-hop minimum-time-delay focusing in the F_1 and F_2 layers exhibit discernible splitting half the time during the day, while trailing-edge focusing exhibits this splitting only rarely.

(5) The O and X MUF's (where focusing is known to occur) on composite ionograms lie exactly on these focus lines--strong evidence for the above interpretation.

The research that has been described here shows that improved time-delay and azimuth resolution can extend the usefulness of ionospheric study with the backscatter technique. The somewhat fortuitous presence of bright, point-like echoing regions on the ground together with the unprecedented clarity with which they are observed here, serve to allow a partial separation of ground-scatter effects from those of ionospheric propagation. A rough model of these echoing regions has been constructed in this study; they behave nearly as point, isotropic, broadband, linearly polarized scatterers. Some of the measurements call for refinements on this simple characterization (e.g., delay extent up to 80 μs), but for the purposes of ionospheric sounding such refinements are judged usually unnecessary.

Part of the purpose of this work is to determine whether the separation described above can be effected without resorting to specific location/identification of the scattering sources and direct measurements thereupon. As far as discrete echoing regions are concerned, the latter procedure would serve only academic interests. The degree of resolution achieved is adequate to resolve individual scattering sources; one

implication of this result is that it is not necessary to know what they are.

B. Further Work Recommended

By reducing some of its inherent uncertainty, this research paves the way for backscatter sounding to reach its full potential. The obvious next step is to apply this knowledge to ionospheric study. As one example, it is of interest to determine whether useful information is gained by measuring differential delays and azimuths among two or more discrete echoes. With a procedure similar to that leading to the discrete echo overlays of Figures 15(b) and 18(b), one might be able to study ionospheric distortions without knowing the absolute echo locations.

The author (and probably the reader) is left with a desire to know what are the sources of discrete echoes in backscatter, whether or not this knowledge is of practical importance. By knowing the physical and electrical characteristics of these scatterers one may predict the signals they produce in backscatter soundings. Such knowledge should help to explain the component of echo fluctuation, which is not understood at this time.

The portable repeater will be an invaluable tool in the location and identification of discrete echo sources. Furthermore, the repeater can be used for a precise measurement of the levels of sidelobes in time delay and azimuth. This measurement may be accomplished by modulating the repeater completely out of the ground-backscatter return. Measured values of sidelobe levels will better enable one to assess the output at one particular time delay and azimuth, due to echoes located at all other time delays and azimuths.

It is also thought worthwhile to observe other regions of the U.S. with this type of backscatter sounder. This will mean looking at

longer ranges where elevation angles are generally lower and where the fixed azimuthal beamwidth represents a large ground area illuminated. A few discrete echoes have been recorded that come from locales in the flat midwest, and it is desirable to measure their rates of occurrence and visibilities.

The research that has been described in this report draws on measured characteristics of the localized peaks in the ground-backscatter coefficient. A question arises as to the size and strength of the valleys in the scatter profile. It is inherent in measurements that the valleys or dips tend to be filled in; in this case it is done by noise, interference, and especially self noise. If an experimenter wanted to use the energy backscattered from a specific area, and the backscatter cross section was (say) 60 dB below the average, then the energy received, if any, would most probably arrive from other areas on the ground through the system sidelobes. Thus, the valleys may have importance as well as the peaks, and only through knowledge of system noise factors and sidelobe properties can one assess this importance.

Appendix A

EQUIPMENT AND DATA PROCESSING

Appendix A

EQUIPMENT AND DATA PROCESSING

At the Lost Hills transmitter site up to 30 kilowatts of transmitter power was available through the use of three Collins 208 U-10 transmitters. These were automatically tuned via servomechanisms and could be made to follow swept-frequency sounding signals at rates up to 500 kHz/s from 2 MHz to 30 MHz. Energy from these transmitters was fed to an 18-element array of vertically polarized, broad-banded monopoles. These elements were spaced 12 m apart over a total aperture of 204 m. The frequency range was 9 to 27 MHz. Azimuthal sidelobes were reduced with the aid of a power taper in the aperture-illumination function. With this taper the array at 15 MHz provided a 3-dB beamwidth of 6 degrees, a beamwidth between first nulls of 14 degrees, and a largest sidelobe 17 dB down from the peak. A 70-ft backscreen behind the array reduced backlobes to the west by 20 dB. The array was delay-cable steerable in increments of four degrees from 62 degrees to 122 degrees true, the boresite direction being 90 degrees true.

A representative azimuth pattern for the transmitting array near 15 MHz as computed from model measurements is shown in Figure A-1. Nominal array gain is specified to be 18 dB. The presence of fairly sizable side- and backlobes influence the data as indicated in the text. Vertical gain falls off smoothly with increasing elevation to a 15 dB null at 35 degrees; however, at higher frequencies this null is found at lower elevations.

The receiving facility in Los Banos employed an azimuthal aperture of 2.52 km boresited 90 degrees true. Two hundred fifty-six 18-ft vertical

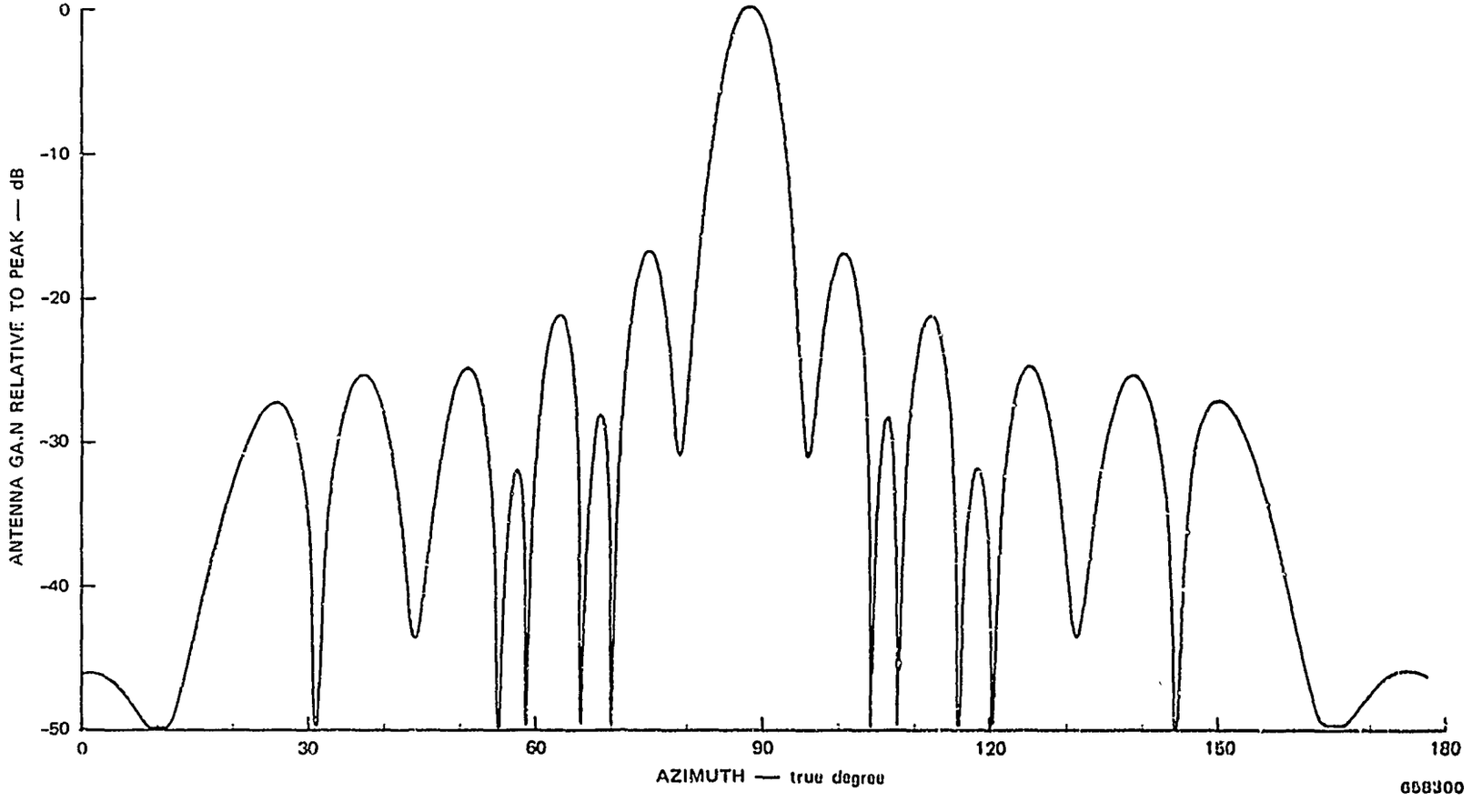

FIGURE A-1 TYPICAL AZIMUTHAL ANTENNA PATTERN FOR BACKSCATTER TRANSMITTER AT LOST HILLS, CALIFORNIA

monopoles were equally spaced over this aperture. A 72-by-8500-ft ground screen of 2-ft square mesh had been installed to stabilize ground impedance over the absolutely flat but chemically variable earth. Signals from unmatched elements were summed together in binary fashion into eight 32-element subarrays. Amplitude taper and sufficient gain to overcome cable loss was then inserted before the eight subarray lines were fed back to the equipment trailer where they were combined into a single array output. Voltage gain for a linear array increases with the square root of the number of elements, giving a directive gain of 24 dB for the 256 elements. Delay-cable array steering had been installed to allow steering in increments of 1/4 degree to ±16 degrees from boresite. Sweeney[13] presents the design features and performance characteristics of this array in detail and applies it to a study of forward-oblique HF skywaves.

The antenna pattern of the receiving array at 15 MHz is found in Figure A-2; its calculation is described in Appendix B. Suffice it to note here that the pattern has a 0.48-degree, 3-dB beamwidth and a peak sidelobe level of -25 dB at 15 MHz. Since there was no front-to-back discrimination in this array, energy could arrive from the west. Although the transmit array was rated for a 20-dB front-to-back ratio, backscatter from the Pacific Ocean to the west can create ambiguities in the data of Sections III and IV. Extraneous focusing lines are one source of such ambiguity, but these are usually easy to identify using forward-oblique ionograms or ionospheric predictions. A second source of ambiguity could arise in measurement of the absolute level of backscattered energy from a specific region over land. The cross section per unit area σ_o over the ocean can be an order of magnitude stronger than the <u>average</u> σ_o over land (Ref. 20 and references therein).

The waveform used here for backscatter sounding is the linear swept-frequency, continuous-wave (SFCW) waveform familiar to radar specialists,[14,15]

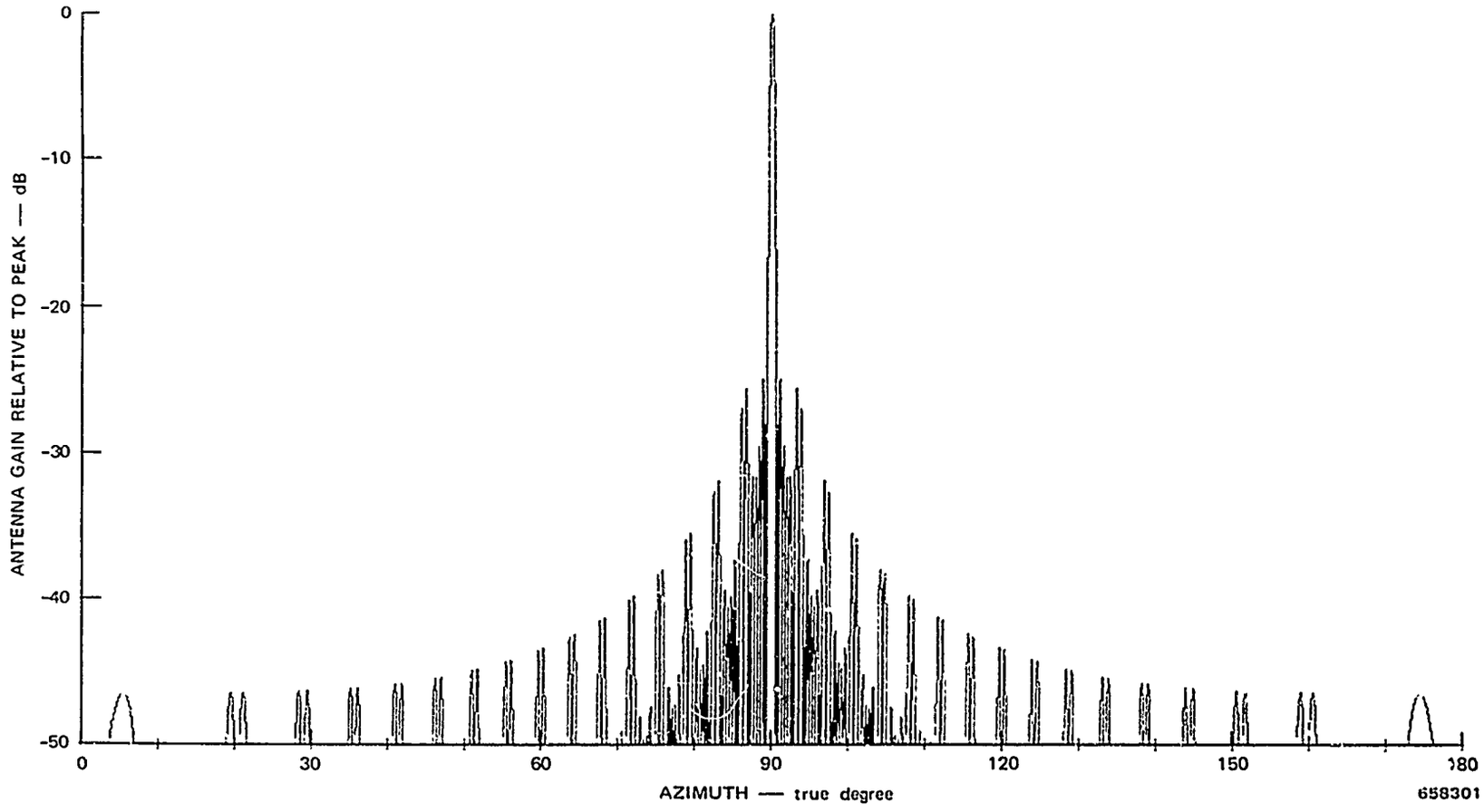

FIGURE A-2 ANTENNA PATTERN FOR LOS BANOS 2.5 km ARRAY WITH MODIFIED DOLPH-CHEBYSCHEFF TAPER

which has been shown to have features attractive for ionospheric sounding.[13] Recently these properties have been described[13] for a forward-oblique sounding application.

The SFCW waveform has a complex amplitude

$$A(t) = \begin{cases} \sqrt{\frac{1}{T}}\, e^{jbt^2} & |t| < T/2 \\ 0 & |t| > T/2 \end{cases}$$

where T is the signal duration and b = 2π × (rate of frequency sweep in Hz/s). The sweep rate is also given by W/T where W is the total bandwidth swept. A transmitted frequency "ramp" is received and mixed with an identical local frequency "ramp" which has appropriate, known offsets in its start time and start frequency. The difference frequency Δf (at an IF of 18 MHz) out of this mixer is proportional to $F_c \Delta t$, where F_c is the rate of frequency sweep and Δt is the transmission time. After sufficient amplification and frequency conversion this energy is spectrum analyzed to provide amplitude vs. delay. This processing is essentially that of a matched filter[15] except for the mismatch produced by weighting the signal to reduce delay sidelobes. A block diagram of the sounder system is found in Figure 2 in Section II.

The above modulation scheme has a number of advantages for ionospheric sounding. Because peak power equals average power, weaker requirements were placed on the transmitter and its antenna in order to achieve a given level of sensitivity. Secondly, this waveform resulted in good fixed-frequency interference suppression, since a narrow-band receiver could be used even when very short effective pulse lengths were realized. The receiver bandwidth need only be as large as the delay increment of interest times the sweep rate; for example, a delay window of 1 ms and a

sweep rate of 250 kHz s requires a 250-Hz receiver bandwidth. In wide-sweep backscatter sounding (9 to 27 MHz for this experiment) the total delay window may be 20 ms or more, requiring a 5-kHz bandwidth. A typical interfering station remains in the receiver pass band 5/250 = 20 ms. Phillips[22] showed that by allowing the receiver to limit on interference peaks, interference energy is spectrally spread and signal-to-interference ratios are nearly maximized.

SFCW allows very high time-delay resolution that is easily variable. If 1 T is the filter bandwidth of the spectrum analyzer (T being the filter integration time) and F_c is the sweep rate, then effective pulse length is (1 T) × (1 F_c). Typical parameter values of T = 1 second and F_c = 250 kHz s give a 4-μs effective pulsewidth, which, as mentioned above, is achievable without large peak power and with a small receiver bandwidth. It is worth noting, as an example of the inherent flexibility of SFCW, that recorded data may be reprocessed with variable filter bandwidths in order to achieve variable delay resolution, a useful feature in analysis of backscatter data where dispersion and inhomogeneities often limit the available resolution. Self noise is a question of importance for pulse-compression techniques;[14] for the SFCW exciter used here, various sources of imperfections in the linear sweep produced an average sidelobe level 20 to 30 dB down from the peak.

There are offsetting disadvantages of this waveform. First, more complex equipment is required than with a conventional pulse system; however, recent progress in both analog and digital spectral-analysis techniques will make this difference less important. More important perhaps is the fact that with a delay-processed-only SFCW waveform, any Doppler shift from variable phase-path components is interpreted as a change in time delay. This effect is neglected in the present study since ionospheric Doppler is generally <1 Hz. This is a plausible upper

limit, for at a wavelength of 20 m, a 1-Hz Doppler implies a 72-km change in path length in one hour. Only during sizable disturbances and at dawn/sunset periods should this value be exceeded.[17,18] A Doppler spread, however, will deteriorate the quality of the effective pulse, not just move the pulse in the time-delay domain.

A final potential disadvantage of SFCW waveforms is that one must assume that the medium is stationary over the signal duration T (which varies from 0.1 to 1.0 s in this work). Time changes on a scale less than these values of T will not be observed. It is thought that this feature does not influence the results presented here.

Cesium-tube clocks were located at the transmitter and receiver sites to provide all timing and frequency standards. Stability was one part in 5×10^{-11}. Once these clocks were synchronized, absolute delay within 1 μs was available between these two sites. The delay uncertainty could shift 1 μs/day, and so these clocks were resynchronized periodically. The receiver had synthesized oscillators derived from the cesium standard and used an IF bandwidth of 6 kHz. A hybrid-type spectrum analyzer (Federal Scientific UA-7) produced a 500-line spectrum of the product-detector output. These 500 lines may be spread over bands ranging from 100 Hz to 10 kHz. Note that phase information is discarded in this type of spectrum analysis.

Forward-oblique soundings were available over the east-west Bearden-Los Banos path using the same SFCW modulation. Normally the Bearden 10-watt transmitter swept the 7-36 MHz band at 250 kHz/s. Sweeney[18] discusses the characteristics of oblique soundings as measured with the 1/2-degree-beamwidth antenna; particular attention is given to the azimuthal distribution of individual ionospheric modes. This distribution had implications for the discussion here of discrete echoes in backscatter data.

Backscatter soundings of the ionosphere are often hampered by inadequate calibration. Several calibration functions were provided for this experiment by a portable, single-antenna, delay-line repeater.[34] With it, one could place a known cross section at a known location on the earth's surface.

This device alternately switched between a receive and a transmit mode at a 10-kHz rate. While receiving, it stored energy in a 50-μs glass delay line, which was retransmitted during the following 50-μs period after a brief dead time to avoid oscillations. As long as the amplifiers in this device were not saturated, the device linearly repeated the same frequency components that it received. The 10-kHz chopping rate produced sidebands that were normally out of the receiver bandwidth of an SFCW receiver. A double balanced mixer was sometimes used to produce two sideband versions of the repeated signal, providing a convenient means of delay-shifting the repeater echo on SFCW backscatter data. Figure A-3 is a simplified schematic of this device.

When operating in the linear mode the repeater cross section σ_R may be calculated. For 1 watt m^2 incident power density, the antenna captures ($G_A^2 \lambda^2 / 4\pi$) watts. For a total repeater gain of G_S, the repeater delivers ($G_S G_A^2 \lambda^2 / 4\pi$) watts back to the antenna. Assuming the same gain applies for retransmission (i.e., a monostatic sounder and the same ionospheric mode of propagation both ways), then $G_S G_A^2 \lambda^2 / 4\pi$ watts are retransmitted. This is the repeater cross section where a matched system has been assumed and where G_S and G_A account for all gains and losses. This energy is reduced by the square of the duty cycle; for a 45-percent duty cycle (typical), the loss is 7 dB. When the repeater return is modulated, the energy in one sideband is down by 8 dB. Thus,

$$\sigma_R = \frac{G_S G_A^2 \lambda^2}{4\pi} - \begin{bmatrix} \text{duty} \\ \text{cycle} \\ \text{loss} \end{bmatrix} - \begin{bmatrix} \text{modulator} \\ \text{loss} \end{bmatrix}$$

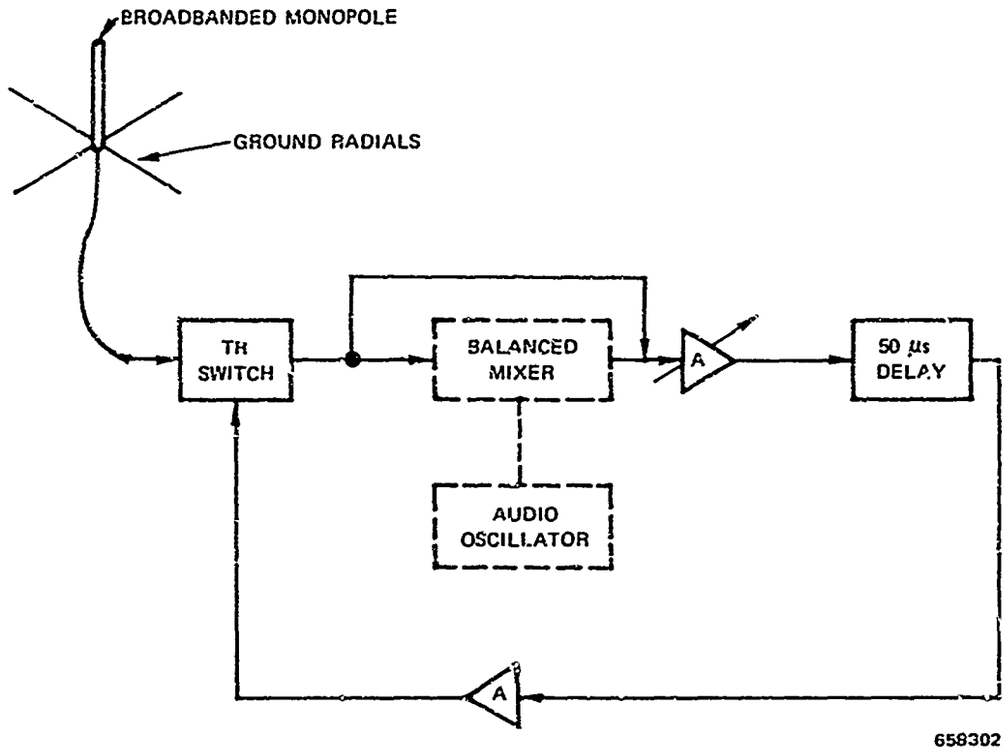

FIGURE A-3 BLOCK DIAGRAM OF THE PHILLIPS SINGLE-ANTENNA DELAY-LINE REPEATER. Also operates with car-mounted whip antenna.

and since G_S is variable, the cross section is variable. Since the repeater is broadband, interference may reduce the available cross section in that it may limit the value of G_S that may be used without saturating the amplifiers. Bandpass filters were helpful in reducing this limitation. The largest uncertainty lies in calibrating the antenna's performance, but it is known to within 3 dB.

This repeater was fully portable and was operated from a station wagon (see photographs in Figure A-4).

FIGURE A-4(a) THE PHILLIPS REPEATER IN OPERATION FROM A STATION WAGON IN NEW MEXICO

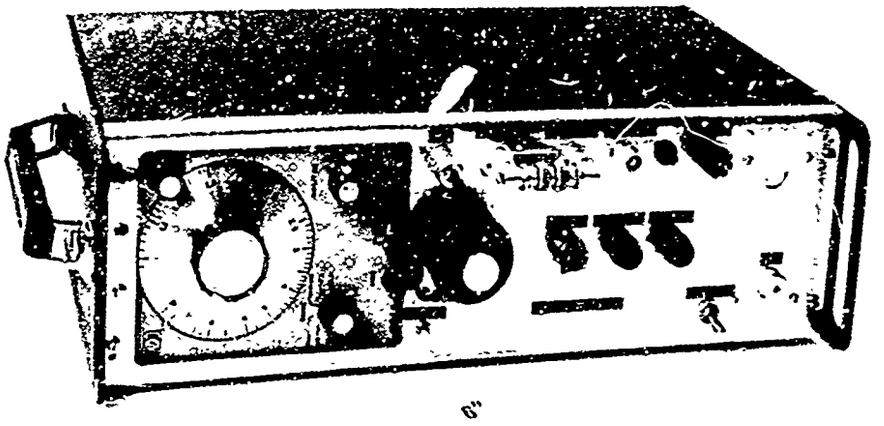

658317

FIGURE A-4(b) REPEATER PROTOTYPE

Appendix B

RESOLUTION IN TIME DELAY AND AZIMUTH

Appendix B

RESOLUTION IN TIME DELAY AND AZIMUTH

1. Interference Rejection

In order to assess the effect of a large time-bandwidth product on interference signals, consider an SFCW sounder sweeping over a bandwidth W Hz in T seconds (controlled by spectrum analysis integration time) at a rate of F_c Hz/s. The receiver bandwidth is W_r. A received SFCW signal is deramped and proceeds through the processing chain as a narrow-band spectrum. Fixed-frequency interference when deramped appears as a linearly sweeping signal as the sounder sweeps through its frequency. The receiver is operated so as to limit on any such signals that are larger than the desired SFCW signal; this has the result of spectrally spreading the interference. Thus, for this analysis consider SFCW signals to have the same amplitude as interference.

Now, impulsive noise ideally lasts $1/W_r$ (s) in the receiver while the interference signal persists the length of time required to sweep over the receiver bandwidth, W_r/F_c (s). Normally this is much longer than $1/W_r$ (s). The signal is integrated T s in the spectrum analyzer while an interfering signal lasts W_r/F_c (s); thus the ratio of signal-to-interference is TF_c/W_r. Furthermore, because the interference is spectrally spread (by assumption uniformly over the analyzer bandwidth), a further gain in signal-to-interference ratio is achieved. The signal lies in one resolution cell while interference is spread uniformly throughout all resolution cells. The time-bandwidth product of the spectrum analyzer is $T \cdot W_c$, where W_c is the frequency coverage of the analyzer. Thus,

$$\frac{\text{Signal}}{\text{Interference}} = \frac{T}{W_r/F_c} \cdot T\,W_c = T\,W\,\frac{W_c}{W_r} \quad .$$

W_c/W_r for the Los Banos sounder varied from 1 for normal use to 0.1 for very high resolution use, while TW varied from 2.5×10^3 to 5×10^5.

SFCW will thus provide nominally 40-dB interference rejection for a single interference signal (which can be tens of millivolts at the receiver input) encountered over the band W (varying from 25 kHz to 500 kHz). Each additional interference signal will decrease the interference rejection accordingly. Finally, it should be noted that the receiver used in this experiment did not react to interference in the "ideal" way. When very strong interference impulse was encountered, the receiver was essentially inoperable for periods on the order of milliseconds. The net result was that sizable time gaps occasionally appeared in the data, reducing the average signal available.

2. Evaluation of Time Delay and Azimuth Sidelobes

It is assumed that the τ and θ domains are independent, both in terms of power returned to the sounder and in terms of the subsequent processing of the data. This approximation is not strictly valid, but is permissible for the purposes at hand. Thus, $\sigma'(\tau,\theta) = \sigma'(\tau)\,\sigma'(\theta)$, where the primes denote the backscatter cross section of the earth-ionosphere combination. As far as processing is concerned, τ and θ are independent for a monostatic sounder and for sufficiently narrow-band systems for which the signal bandwidth is less than 10 to 20 percent of the carrier frequency.

Section II-A gave a description of the way a range-azimuth display was obtained by slowly scanning the antenna array (normally 1/4 degree per second) synchronously with repetitive SFCW sweeps. Azimuth information was obtained by comparing energy in a range gate for successive

sweeps (which were made at adjacent antenna steer positions). To the extent that the echoes remain fixed over the period of time it takes to generate an azimuth scan, the azimuth "processing" is independent of the SFCW processing. Thus the average power out of the sounder as a function of τ and θ may be described by a superposition of returns--namely (as given in Section II),

$$P_{\tau,\theta}(\tau,\theta) = \int \sigma'(\tau,\theta)\ h(\tau,\theta)\ d\tau\ d\theta \qquad \text{(B-1)}$$

where $h(\tau,\theta)$ describes the processing in delay and azimuth performed by the backscatter sounder (antenna effects included). Both $\sigma'(\tau,\theta)$ and $h(\tau,\theta)$ are separable functions by assumption; so

$$P_{\tau,\theta}(\tau,\theta) = P_{\tau}(\tau)\ P_{\theta}(\theta) \quad . \qquad \text{(B-2)}$$

It is a well known result in radar astronomy[35] that the average power as a function of delay and Doppler is the two-dimensional convolution of the target-scattering function and the radar-ambiguity function. By assumption, Doppler here is identically zero, and thus

$$P_{\tau}(\tau) = \int \sigma'(t)\ \psi^2(t - \tau, 0)\ dt \quad . \qquad \text{(B-3)}$$

The ambiguity function ψ^2 has been extensively studied for the type of waveforms used here.[14,15]

To evaluate the form of $P_{\theta}(\theta)$, consider a fixed delay gate and determine the output from a scattering element $\sigma'(\theta)$ when the transmit antenna is steered at θ_o and the receive antenna is steered at θ_1. For this incoherent azimuth processing, intensities add and the power received is proportional to $G_T(\theta - \theta_o)\ G_R(\theta - \theta_1)\ \sigma'(\theta)$. $G_T(\theta)$ and $G_R(\theta)$

are antenna power gains vs. azimuth. The total power received from all azimuths is obtained by integrating over θ. The transmit steer is usually kept as close as possible to the receive steer ($\theta_1 \approx \theta_o$), and thus

$$P_\theta(\theta_i) \propto \int G_R(\theta - \theta_1)\, G_T(\theta - \theta_1)\, \sigma'(\theta)\, d\theta \quad . \qquad \text{(B-4)}$$

The essential behavior is contained in a convolution of the combined antenna patterns with the modified scattering function $\sigma'(\theta)$. The sidelobe structure of $G_R(\theta)\, G_T(\theta)$ will indicate the self noise due to a scattering surface extended in azimuth.

For the purposes at hand the contribution of delay and azimuth sidelobes will be evaluated for two cases--first, the "close-in" behavior, and second, the average contribution of all sidelobes. The close-in sidelobe contribution within a few pulse widths and beamwidths of the peak may justly ignore the many loss factors in the radar equation, for they are essentially constant for small changes in τ and θ.

The function $\psi^2(\tau,o)$ is

$$\psi^2(\tau,o) = \left(1 - \frac{|\tau|}{T}\right)^2 \left(\frac{\sin b\tau[T - |\tau|]}{b\tau[T - |\tau|\,]}\right)^2 \qquad |\tau| \le T$$

and is identically zero for $|\tau| > T$. For a specific case of interest here, T = 1 s, and W = 5 X 10^5 Hz. In order to reduce the magnitude of the sidelobes of $\psi^2(\tau,o)$ at the expense of slight broadening of the peak, the data are weighted with a Hanning window.[14] The largest sidelobe is -32 dB, and the effective pulse width is 1.6/W (3.2 μs for this example). Figure 6 in the main text is a plot of the weighted function $\psi^2(\tau,o)$.

This plot of $\psi^2(\tau,o)$ is for an <u>ideal</u> linear SFCW waveform. The actual SFCW generators used were a step-wise approximation to a linear sweep. Phase discontinuities may increase the peak sidelobe level to

-25 dB,[36] although little broadening of the peak occurs. The actual sidelobe level varied depending on the frequency interval swept and the sweep rate.

Approximate evaluation of $G_T(\theta)$ and $G_R(\theta)$ may be accomplished analytically, although measured antenna patterns would be most desirable. It is assumed that the antennas are collocated and that the angle to which the array is steered is azimuth (in fact this angle is a combination of azimuth and elevation). The suboptimum phasing of the elements of the receive array when steered away from broadside is neglected; Sweeney[13] determined that little sidelobe enhancement occurs as long as the steer is less than 12 degrees from broadside. Close to the main lobe these approximations are certainly valid; far away from the main lobe, only the integrated sidelobe effects are of interest.

The receive-array gain pattern is readily calculated[37] with the modified Doiph taper installed at the 32-element subarray level. The power gain is

$$G_R(\theta) = \left| 2G_S(\theta) \sum_{i=0}^{\frac{n}{2}-1} \alpha_i \cos \frac{2i+1}{2} \psi_1 \right|^2 \qquad \text{(B-5)}$$

where $n = 8$, $\psi_1 = (2\pi d_1/\lambda) \sin\theta$, and $d_1 = 320$ m (subarray spacing). The taper coefficients are $\alpha_0 = 1.0$, $\alpha_1 = 0.794328$, $\alpha_2 = 0.562341$, $\alpha_3 = 0.354813$. The subarray voltage pattern is

$$G_S(\theta) = \frac{1}{k} \frac{\sin k \frac{\psi_2}{2}}{\sin \frac{\psi_2}{2}} \qquad \text{(B-6)}$$

where $k = 32$, $\psi_2 = (2\pi d_2/\lambda) \sin\theta$, and $d_2 = 10$ m (element spacing).

For this calculation the midband value of $\lambda = 20$ m is used.

$G_T(\vartheta)$ may also be calculated from Eq. (B-5) using the following parameters: $n = 18$, $\psi_i = (2\pi d_1/\lambda) \sin \vartheta$, $d_1 = 12$ m, $\alpha_9 = 1.0$, $\alpha_1 = \alpha_2 = 1.\sqrt{2}$, $\alpha_3 = \alpha_4 = 1.2$, $\alpha_5 = \alpha_6 = \alpha_7 = \alpha_8 = \sqrt{2.4}$, $\lambda = 20$ m. $G_S(\vartheta)$ for the transmit array is the element pattern for a single array element that has been derived from model range measurements. It should be noted that mutual-coupling effects are not taken into account even though they are thought to influence the radiation patterns. Finally the back-side behavior of the transmit array is approximated as the mirror image of the front-side pattern reduced by 20 dB. This front-to-back selectivity is provided by a backscreen. $G_R(\vartheta)$ and $G_T(\vartheta)$ have been calculated already in Figures 35 and 36. Here the interest is in the product $G_R(\vartheta)$ $G_T(\vartheta)$, which is plotted for $\lambda = 20$ m and $-5° \leq \vartheta \leq 5°$ in Figure 7.

Figures 6 and 7 are the respective delay and azimuth responses for $T = 1$ s, $W = 5 \times 10^5$ Hz, and $\lambda = 20$ m, at least within the few pulse widths and beamwidths from the origin that have been plotted. In order to ascertain the self clutter levels from <u>all</u> the sidelobes it is appropriate to take a different approach, while still considering the two domains separately.

First, very large TW-product SFCW waveforms have a knife-edge ambiguity function in the (τ,f) plane.[14] Because the (small) Doppler component is ignored, this function may be crudely approximated by the "thumb tack" ambiguity function sketched in Figure B-1. The average sidelobe level is found from the volume invariance condition to be $1/(4TW)$, which is not exact because the main peak is in fact broadened diagonally in the (τ,f) plane.

Following Rihaczek,[38] consider the scattering region of dimensions $\Delta\tau$ and Δf to have less extent than the pedestal of $\psi^2(\tau,f)$. Assume there are N discrete point scatterers in this space with total cross section σ_t and average cross section $\bar{\sigma} = \sigma_t/N$. The pedestal height must be scaled

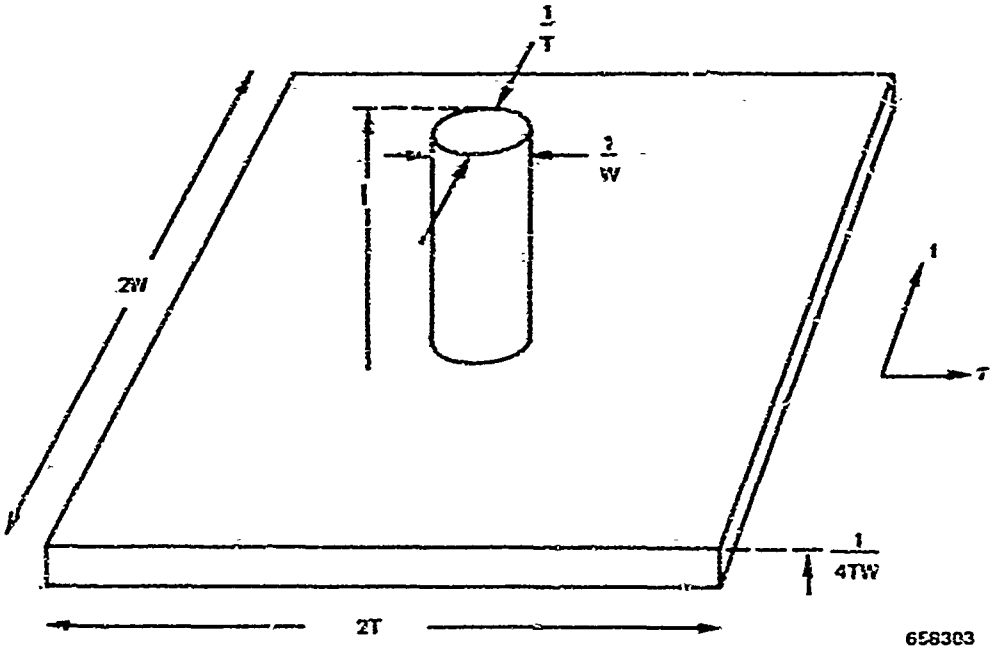

FIGURE B-1 THE THUMBTACK AMBIGUITY FUNCTION $\psi^2(\tau,f)$ USED IN ASSESSING INTEGRATED-DELAY SIDELOBE EFFECTS

by this cross section to evaluate the self clutter C. Thus,

$$C = \sum_{i=1}^{N} \frac{1}{4TW} \sigma_i = \frac{N\bar{\sigma}}{4TW} \quad .$$

The echo of interest has cross section σ; thus the ratio of signal to self clutter is

$$\frac{S}{C} = \frac{4\sigma TW}{N\bar{\sigma}} \quad .$$

Now consider a continuously spread echoing region as a set of point scatterers separated by the resolution-cell size. Thus N equals the number of these cells in the total scattering region; that is, $N = 4TW\Delta\tau\Delta f$. The echoing region is spread in the delay dimension only, and thus

$N = 2\Delta\tau W$ Substituting above,

$$\frac{S}{C} = \frac{\sigma}{\bar{\sigma}} \frac{2T}{\Delta\tau} \quad .$$

Adopting some acceptable value for S/C (say, 1 for simplicity), this relation says that $\sigma/\bar{\sigma} \geq \Delta\tau/2T$ must hold for observation of σ. Equivalently, for $\sigma = \bar{\sigma}$ one requires $T \geq \Delta\tau/2$. This places a restriction on the minimum acceptable signal duration (integration time) T Fisler,[39] through a somewhat different argument, also found that the ratio of signal to self clutter was proportional to T.

For the case at hand the echoing region in delay is that approximated by Figure 5 where $\Delta\tau \simeq 20$ ms. Since the effective cross section of the earth-ionosphere combination changes rapidly with τ, it is of interest to attach some meaning to $\bar{\sigma}$. One could simply let $\bar{\sigma}$ be the value of the effective cross section at the peak (the leading edge). Then one could assess the ability to observe σ relative to this peak. Alternatively, an average value of $\bar{\sigma}$ over the backscatter delay depth of 20 ms could be evaluated. (It is about 0.2 times the peak value for the example used here.)

For the processing done in this study, T was variously 0.1, 0.25, 0.5, and 1.0 second.

Turning to considerations of azimuth, there is a self-noise contribution from all the sidelobe region. However, treatment of its average effects cannot proceed as before. Generally speaking, the narrow beam was used to localize the azimuth from which backscatter energy was arriving. The signal-to-clutter ratio in the azimuth domain should vary as $G\,\sigma/\bar{\sigma}$, where σ and $\bar{\sigma}$ are now the azimuth counterparts of the echo cross section of interest and the average echo cross section. G in this case is the gain of the whole antenna system and can be evaluated for

specific cases by integrating the combined antenna gains over the whole sidelobe region.

Antenna sidelobes will degrade the ability to observe a desired σ in the presence of $\bar{\sigma}$. This is particularly true when one recalls that the earth-ionosphere combination of echo strengths in delay and azimuth are not only quite extended but are also extremely variable.

Numerical estimates of the contribution of self clutter require (1) knowledge of the ionospheric profile in all directions from the sounder, (2) measured antenna gains, (3) inclusion of elevation-angle effects, and (4) specific information as to the levels of cross section. The back-side response of this system is one particularly important factor. Backscatter to the west is from the Pacific Ocean, and it is thought that σ_o (ocean) $\approx 10\ \sigma_o$ (land) on the average (see Ref. 20 and references therein). Only by carefully choosing operating times, antenna steers and range gates could east-west ambiguity be avoided in backscatter returns.

A convenient means of measuring the self-clutter characteristics is available that does not require measurement of antenna patterns. If the repeater return is shifted out of the ground backscatter, a time-delay-vs.-azimuth data format will determine the point response in these two domains. Care should be taken to average out the various sources of fluctuation present. An experiment for measuring this point response is planned.

REFERENCES

1. A. M. Peterson, "The Mechanism of F-Layer Propagated Backscatter Echoes," J. Geophys. Res., Vol. 56, pp. 221-237 (June 1951).

2. W. Dieminger, "The Scattering of Radio Waves," Proc. Phys. Soc., Vol. 64B, pp. 142-158 (1951).

3. T. A. Croft, "Computation of HF Ground Backscatter Amplitude," Radio Science, Vol. 2, pp. 739-747 (July 1967).

4. T. A. Croft, "The Influence of Ionospheric Irregularities on Sweep Frequency Backscatter," J. Atm. Terr. Phys., Vol. 30, pp. 1051-1063 (1968).

5. T. M. Georges and J. J. Stephenson, "HF Radar Signatures of Travelling Ionospheric Irregularities, 3D Ray-Tracing Simulation," Radio Science, Vol. 4, pp. 679-696 (August 1969).

6. R. D. Hunsucker and L. H. Tveten, "Large Travelling Ionospheric Disturbances Observed at Midlatitudes Utilizing the High Resolution HF Backscatter Technique," J. Atm. Terr. Phys., Vol. 29, pp. 909-916 (1967).

7. L. H. Tveten and R. D. Hunsucker, "Remote Sensing of the Terrestrial Environment with an HF Radio High-Resolution Azimuthal Elevation Scan System," Proc. IEEE, Vol. 57, pp. 487-493 (April 1969).

8. E. D. R. Shearman, "The Technique of Ionospheric Investigation Using Ground Backscatter," Proc. IEE, Vol. 103E, pp. 210-221 (1956).

9. J. G. Steele, "High-Frequency Backscatter from Terrain with Trees," Proc. IEEE, Vol. 55, pp. 1583-1590 (September 1967).

10. J. R. Barnum, "High-Frequency Backscatter from Terrain with Buildings," Report SEL-67-002 (TR No. 130), Stanford Electronics Laboratories, Stanford, California (January 1967).

11. I. Ranzi, "Radiocommunication by Backscatter," Final Technical Report, Centro Radioelectrico Sperimentale "G. Marconi," Rome, Italy (1962).

12. R. Silberstein, "Sweep Frequency Backscatter--Some Observations and Deductions," IRE Trans. AP-2, pp. 56-63 (April 1954).

13. L. E. Sweeney, Jr., "Spatial Properties of Ionospheric Radio Propagation as determined with Half-Degree Azimuthal Resolution," Report SEL-70-034 (TR No. 155), Stanford Electronics Laboratories, Stanford, California (June 1970).

14. C. E. Cook and M. Bernfeld, Radar Signals An Introduction to Theory and Application (Academic Press, New York, N. Y., 1967).

15. R. S. Berkowitz, Modern Radar--Analysis, Evaluation, and System Design (John Wiley & Sons, New York, N. Y., 1965).

16. R. B. Fenwick and G. H. Barry, "HF Measurements Using Extended Chirp-Radar Techniques," Report SEL-65-058 (TR No. 103), Stanford Electronics Laboratories, Stanford, California (June 1965).

17. K. L. Chan and O. G. Villard, Jr., "Observation of Large-Scale Travelling Ionospheric Disturbances by Spaced-Path High-Frequency Instantaneous Frequency Measurements," J. Geophys. Res., Vol. 67, pp. 965-987 (March 1962).

18. T. M. Georges, "Ionospheric Effects of Atmospheric Waves," ESSA Technical Report IER 17-ITSA 54, U.S. Government Printing Office, Washington, D.C. (1967).

19. C. G. McCue, "High Frequency Backscatter Observations at Salisbury, South Australia," Austral. J. Phy., Vol. 9, pp. 454-470 (December 1956).

20. J. R. Barnum, "The Effect of Polarization Rotation on the Amplitude of Ionospherically Propagated Sea Backscatter," Report SEL-70-036 (TR No. 157), Stanford Electronics Laboratories, Stanford, Calif. (June 1970).

21. R. Silberstein, "The Use of Sweep-Frequency Backscatter Data for Determining Oblique-Incidence Ionospheric Characteristics," J. Geo. Res., Vol. 63, pp. 335-351 (June 1958).

22. A. C. Phillips, "Quasi-Linear Interference Suppressor," Report SEL-68-052 (TR No. 150), Stanford Electronics Laboratories, Stanford, Calif. (August 1968).

23. D. E. Kerr, Propagation of Short Radio Waves (Dover, New York, N. Y., 1951).

24. C. R. Gilliland, "Sweep-Frequency Backscatter with Calibrated Amplitude," Report SEL-65-095 (TR No. 111), Stanford Electronics Laboratories, Stanford, Calif. (October 1965).

25. R. M. Jones, "A Three-Dimensional Ray Tracing Computer Program," ESSA Technical Report IER 17-ITSA 17, U.S. Government Printing Office, Washington, D.C. (1966).

26. P. A. Fialer, "Irregularities in the Quiet Ionosphere and Their Effect on Propagation," Report SEL-70-037 (TR No. 156), Stanford Electronics Laboratories, Stanford, Calif. (June 1970).

27. J. T. Lynch, "Aperture Synthesis for HF Radio Signals Propagated via the F-Layer of the Ionosphere," Report SEL-70-066 (TR No. 161), Stanford Electronics Laboratories, Stanford, Calif. (September 1970).

28. J. T. Lynch, R. B. Fenwick and O. G. Villard, Jr., "Measurement of Maximum Time-Delay Resolution of Oblique Soundings on East-West and North-South Paths," Report SEL-68-048 (TR No. 146), Stanford Electronics Laboratories, Stanford, Calif. (June 1968).

29. T. A. Croft, "HF Radio Focussing Caused by the Electron Distribution Between Ionospheric Layers," J. Geophys. Res., Vol. 72, pp. 2343-2355 (May 1967).

30. M. R. Epstein, "Polarization of Ionospherically Propagated HF Radio Waves with Applications to Radio Communication," Radio Science, Vol. 4, pp. 53-67 (January 1969).

31. D. A. Hedlund and L. C. Edwards, "Polarization Fading Over an Oblique Incidence Path," IRE Trans. AP-6, pp. 21-25 (January 1958).

32. H. Kopka and H. G. Moller, "Interpretation of Anomalous Oblique Incidence Sweep-Frequency Records Using Raytracing," Radio Science, Vol. 3, pp. 43-51 (January 1968).

33. P. D. Welch, "The Use of Fast Fourier Transform for the Estimation of Power Spectra: A Method Based on Time Averaging Over Short, Modified Periodograms," IEEE Trans. AU-15, pp. 70-73 (June 1967).

34. A. C. Phillips, "A Single-Antenna Repeater for HF Radio Propagation Studies," Report SEL-69-064 (TR No. 154), Stanford Electronics Laboratories, Stanford, Calif. (October 1969).

35. J. V. Evans and T. Hagfors, Radar Astronomy (McGraw-Hill, New York, N. Y., 1968).

36. A. C. Phillips, Private Communication, 1970.

37. J. D. Kraus, Antennas (McGraw-Hill Book Co., Inc., New York, N. Y., 1950).

38. A. W. Rihaczek, Principles of High-Resolution Radar (McGraw-Hill Book Co., Inc., New York, N. Y., 1969).

39. P. A. Fialer, Private Communication, 1970.